Molecular changes in *Pink1* knockout mice – a model relevant to early-onset Parkinson's disease

Senior Practical Training

Period: October 26, 2020 – June 11, 2021

Sabrina Behuet
Student ID: i6224683

Department:
Forschungszentrum Jülich GmbH
Institute of Neuroscience and Medicine (INM-1)
Wilhelm-Jonen-Straße, 52425 Jülich, Germany

First institutional-UM supervisor:
Prof. Dr. Pilar Martinez-Martinez
Institutional-UM co-supervisor:
Msc. Daan van Kruining

External supervisors:
Dr. Hans-Jürgen Bidmon
PD Dr. Nicola Palomero-Gallagher

Abstract

Parkinson's disease (PD) is the second most common neurodegenerative disease, and is associated with the degeneration of dopaminergic neurons in the substantia nigra (SN). One of the most common genes causing early-onset PD is the mitochondrial serine/threonine kinase *PINK1* (PTEN-induced putative kinase 1). Neurotransmitter receptors, which are crucial for cell-to-cell communication in the brain, were shown to be altered in several neurodegenerative and psychiatric diseases and have been successful targets for therapeutic intervention. Because the effects of *Pink1*-associated gene mutations on neurotransmitter receptor expression are still largely unknown, the present study focused on *Pink1* knockout (*Pink1*$^{-/-}$) mice, a valuable mouse model for the prodromal phase of early-onset PD. Although previous approaches have focused mainly on the dopaminergic system, there is also evidence of non-dopaminergic receptor alterations in PD. We hypothesized that alterations in neurotransmitter receptors, including non-dopaminergic receptors, are already present in the prodromal phase of PD. Therefore, the present study aimed to investigate the density and regional distribution of functionally highly important dopaminergic and non-dopaminergic neurotransmitter receptors in the brains of *Pink1*$^{-/-}$ mice. Thereby, we focused on the motor and limbic systems to identify and discuss possible correlations between receptor alterations and functional or pathological changes. Quantitative *in vitro* receptor autoradiography of 19 receptor types of seven neurotransmitter systems was performed in 3-month-old *Pink1*$^{-/-}$ and age-matched control mice, followed by densitometric analysis of receptor densities in cytoarchitectonically-identified brain areas linked to the motor and limbic systems. Histological staining techniques were performed to facilitate the identification of brain areas. Immunohistochemistry experiments were performed to qualitatively analyze dopaminergic and GABAergic neurons as well as astrocytic glutamate recycling. We demonstrated several alterations in receptor densities between *Pink1*$^{-/-}$ and control mice. For instance, in the SN of *Pink1*$^{-/-}$ mice, decreased kainate receptor densities were in contrast to increased $mGlu_{2/3}$ receptor densities, which may be a compensatory mechanism to attenuate neurodegeneration. Whereas AMPA receptor densities were lower in the hippocampal CA1 region of *Pink1*$^{-/-}$ mice than in controls, $GABA_A$ receptor densities were higher, indicating an imbalance in the glutamatergic and GABAergic systems, which may also be related to cognitive impairments. The regional distribution in most neurotransmitter receptors examined was altered between the two groups. There was no evidence of changes in dopaminergic neurons between the two groups, but dopaminergic fibers tended to be thicker and were less dense in control than in *Pink1*$^{-/-}$ mice. Taken together, the observed neurotransmitter receptor alterations may be related to functional and pathological changes in *Pink1*$^{-/-}$ mice. In addition, novel data were presented highlighting the possible involvement of non-dopaminergic receptors in the functional and pathological changes in the prodromal phase of PD.

Table of contents

List of abbreviations

^{3}H	tritium
$5\text{-}HT_{1A}$, $5\text{-}HT_{2}$	5-hydroxytryptamin receptor subtype 1A, 2
α_1	adrenaline receptor subtype α1
A_1, A_{2A}	adenosine receptor subtypes 1, 2A
AD	Alzheimer's disease
AMPA	α-amino-3-hydroxy-5-methyl-4-isoxazol-propionic acid
ANOVA	analysis of variance
BZ	$GABA_A$-associated benzodiazepine binding site
BOS	base of support
CA	cornu ammonis
Cb	cerebellum
CNS	central nervous system
CPu	caudate putamen (striatum)
D_1, D_2, $D_{2/3}$	dopamine receptor subtypes 1, 2, 2 and 3
DG	dentate gyrus
DPX	dibutylphthalate polystyrene xylene
FRT	flip-recombinase target
GABA	γ-aminobutyric acid
$GABA_A$, $GABA_B$	GABA receptor subtypes A, B
GS	glutamine synthetase
L-DOPA	levodopa; L-3,4-dihydroxyphenylalanine
loxP	locus of X-over P1
M1	primary motor cortex
M_1, M_2, M_3	muscarinic acetylcholine receptor subtypes 1, 2, 3
MD	mean density
$mGlu_{2/3}$	metabotropic glutamate receptor subtypes 2 and 3
NMDA	N-methyl-D-aspartate
OB	olfactory bulb
PBS	phosphate-buffer solution
PD	Parkinson's disease
PFA	paraformaldehyde
PINK1 (human) or Pink1 (mice)	phosphatase and tensin homolog-induced kinase 1
Pink1 knockout mice	*Pink1*$^{-/-}$ mice
PRKN	parkin RBR E3 ubiquitin protein ligase
ROI	region of interest
RT	room temperature
S1	primary somatosensory cortex
SD	standard deviation
SN	substantia nigra
TH	tyrosine hydroxylase
V1	primary visual cortex

1. Introduction

1.1. Parkinson's disease

In 1817, James Parkinson was the first to describe Parkinson's disease (PD) in "An Essay on the Shaking Palsy", which was known as shaking palsy until 1872. PD is the most common neurodegenerative motor disease and the second most common neurodegenerative disease after Alzheimer's disease (AD). It affects more than 10 million people worldwide, of whom about 5 to 10% suffer from a monogenic form with Mendelian inheritance (1). Although not only aging but also environmental and genetic factors can influence the etiology of this multifactorial disease, the prevalence is approximately 1% for those over 60 years of age and 4% for those over 85 years of age (1). Patients with disease onset between the ages of 20 and 50 are classified as "early-onset", whereas patients with onset after the age of 50 are classified as "late-onset". Nevertheless, the cardinal motor symptoms of bradykinesia (slowness of movement), rigidity (stiffness), postural instability, resting tremor, as well as non-motor symptoms such as olfactory dysfunction are present in both onset subtypes (2). Motor-related symptoms are associated with severe degeneration of dopaminergic neurons in the substantia nigra (SN) of the mesencephalon, the neuropathological hallmark of PD (3). The SN belongs to the basal ganglia circuit that supplies the striatum with dopamine and plays a key role in modulating voluntary motor movements (4), thus dopamine levels in the striatum decrease upon the neurodegeneration (3). Moreover, due to the neurodegeneration, the activity of glutamate in the subthalamic nucleus increases, which exacerbates motor symptoms of PD (5).

Currently, it is assumed that PD develops in three stages (6). During the preclinical phase, no symptoms or signs of PD are recognized, although there is an onset of neurodegeneration. In the prodromal phase, patients show early motor and non-motor signs, such as gait and balance alterations (7), olfactory dysfunctions (8, 9), constipation, sleep disturbances, and depression (10), but these still do not meet the diagnostic criteria for PD. Finally, the diagnostic criteria in the clinical phase are reached when cardinal motor symptoms can be diagnosed according to the International Parkinson and Movement Disorder Society (MDS-PD) criteria. More specifically, the criteria are met when bradykinesia can be diagnosed in addition to resting tremor and/or rigidity. However, these symptoms are not clinically recognized until at least 60% of the dopaminergic neurons in the SN have degenerated (11), indicating a long prodromal (or presymptomatic) phase (12).

Neurotransmitters and their receptors are crucial for cell-to-cell communication and are known to be altered in various neurological and psychiatric diseases and their corresponding animal models (13, 14). As they are pharmacologically well accessible, they have proven to be successful targets for therapeutic applications. For instance, to compensate pharmacologically for the decrease in dopaminergic neurotransmission, levodopa (or L-DOPA), a precursor of the neurotransmitters dopamine, adrenaline (epinephrine), and noradrenaline (norepinephrine), is the most effective treatment for PD, particularly improving patients' motor symptoms (3,

15). However, the treatment does not stop the dopaminergic degeneration (2), its long-term use is associated with motor complications that can lead to involuntary movements known as L-DOPA induced dyskinesia (15, 16), and it is ineffective in treating non-motor symptoms (3). Non-motor symptoms, i.e. psychiatric disorders, fatigue, cognitive impairments, sleep deprivation, and olfactory dysfunctions, affect all Parkinson's patients, may contribute to severe disability, and increase as the disease progresses (6). For instance, late-stage PD patients suffer from about six to ten different non-motor symptoms (3), which represents an enormous burden for the patient and underlines the urgent need for clinical resources. Thus, to enhance the patient's quality of life, the management of PD has to be optimized to include both dopaminergic replacement therapy and treatment of non-motor symptoms. The latter could encompass both pharmacological and physical intervention, but also nutritional counseling, speech therapy, and psychotherapy for both the patient and closest relatives and/or carer (16). However, to find new promising treatment targets for PD, the crucial molecular mechanisms need to be understood.

1.2. PINK1 Parkinsonism

Approximately 15% of PD patients have a known family history of PD, and about 5 to 10% suffer from a monogenic form (1). The most common autosomal-recessive mutations that cause familial PD in descending order of frequency are parkin RBR E3 ubiquitin protein ligase *(PRKN),* phosphatase and tensin homolog (PTEN)-induced putative kinase 1 (*PINK1),* and Parkinsonism associated deglycase (*PARK7)* (17).

PINK1 is a mitochondrial serine/threonine kinase that plays a key role in at least three different processes that ensure mitochondrial health (18). First, it is involved in the modulation of the electron transport chain and thus in ATP production, as shown in a study in which complex I deficiency was rescued by wild type *PINK1* but not by *PINK1* with clinical mutations (19). Secondly, PINK1 regulates mitochondrial morphology and dynamics by affecting the fission and fusion process, as it has been shown that overexpression of *PINK1* promotes fission, whereas inhibition of *PINK1* causes exorbitant fusion (20). Finally, PINK1 accumulates on damaged mitochondria and recruits Parkin to induce mitophagy and thus mitochondrial degradation (21), which is essential for neuroprotection against oxidative stress (22). In contrast, mutations in *PINK1* have been shown to impair mitophagy, leading to the accumulation of damaged mitochondria and Ca^{2+}, which in turn results in reactive oxygen species production and apoptosis (23). These and other observations led to the suggestion that mitochondrial dysfunction contributes to neurodegeneration in PD (19, 21) and that dopaminergic neurons in the SN, in particular, are susceptible to imbalances in the mitochondrial dysfunction. Since *PINK1* is widely expressed in the brain, other non-dopaminergic systems are also considered to be involved in PD progression.

To date, 23 loci (*PARK1-PARK23*) and 19 genes (including ten autosomal dominant and nine autosomal recessive genes) have been identified for both early and late-onset PD (1). The autosomal-recessive mutations corresponding to the *PARK6* locus, chromosome 1p35-p36,

and includes the *PINK1* gene (*Pink1* in mus musculus). The *PINK1* gene consists of eight exons encoding 581 amino acid proteins and was first found in a large Sicilian family with early-onset levodopa-responsive Parkinsonism (24). PINK1-related PD is characterized by an early onset of disease with slow disease progression, high responsiveness to levodopa treatment, and frequent psychiatric issues (24, 25). So far, there is no evidence for an accumulation of Lewy bodies. Hyposmia, or olfactory dysfunction, and thus the impairment of the identification and discrimination of odors is a common feature in patients with homozygous PINK1 Parkinsonism and healthy individuals with heterozygous *PINK1* mutations (25). Interestingly, alterations in odor detection and distinction, but not in odor identification, were also observed in asymptomatic heterogeneous carriers, which the authors suggested as a possible underlying preclinical neurodegeneration (25).

1.3. *Pink1* knock-out mice

In the present study, we investigated the molecular changes in PINK1 Parkinsonism by using homozygous *Pink1* knockout (*Pink1*$^{-/-}$) mice. For this purpose, *Pink1*$^{-/-}$ mice were generated by our cooperation partner at the 'Institute of Developmental Genetics' of the 'Helmholtz Zentrum München' to analyze the underlying mechanisms of the disease development (26). The phenotype of these *Pink1*$^{-/-}$ mice showed that, although they did not show morphological changes in the dopaminergic system and thus no major motor dysfunctions, they developed visible gait alterations and olfactory dysfunctions (26). Since those are already present in the prodromal phase of PD, the *Pink1*$^{-/-}$ mice provide a valuable model for this early phase, in which compensatory mechanisms, such as synaptic adaptions (27), may still hinder the onset of neurodegeneration.

Concerning gait alterations, it was demonstrated that the base of support (BOS), i.e. the average distance between the centers of mass of the footprints at maximal contact, was significantly decreased in the hind paws of *Pink1*$^{-/-}$ mice (26). This was consistent with the narrowing BOS reported in PD patients (28). Moreover, *Pink1*$^{-/-}$ mice showed both reduced hind paw print lengths and stand duration (26), which is in line with the shortened and shuffling steps of PD patients. Finally, *Pink1*$^{-/-}$ mice showed altered levels of phase dispersion (26), which measures inter-limb coordination, that correspond well with the limping and decreased arm and leg swing during walking observed in the early stages of PD patients. Interestingly, these mild gait changes in early PD patients are not improved by L-DOPA treatment, suggesting that a neurotransmitter other than the dopaminergic system is responsible for these symptoms.

In terms of olfactory dysfunctions, *Pink1*$^{-/-}$ mice showed reduced olfactory discrimination and sensitivity between different odors (26), two crucial non-motor symptoms seen in PD patients (8). These alterations were shown to be independent of the memory function of *Pink1*$^{-/-}$ mice, coinciding with human PD studies, in which olfactory alterations were independent of cognitive, perceptual-motor manifestations, and memory manifestations (29).

1.4. Neurotransmitter receptors and quantitative receptor autoradiography

1.4.1. Neurotransmitters and receptors

Neurons can communicate with each other by releasing individual neurotransmitters, a process called synaptic transmission or neurotransmission. The neurotransmitters are synthesized by the neuron (e.g. from amino acid precursors) and are released from the synaptic vesicles of chemical synapses from the presynaptic neuron into the synaptic cleft upon activation (Fig. 1). There, they are received by their respective neurotransmitter receptor on the membrane of the postsynaptic neuron, causing either excitatory or inhibitory transmission, and thus a transient depolarization or hyperpolarization of the membrane potential, respectively. While depolarization results in a less negative or more positive charge compared to the resting potential within the neuron, hyperpolarization results in a more negative charge.

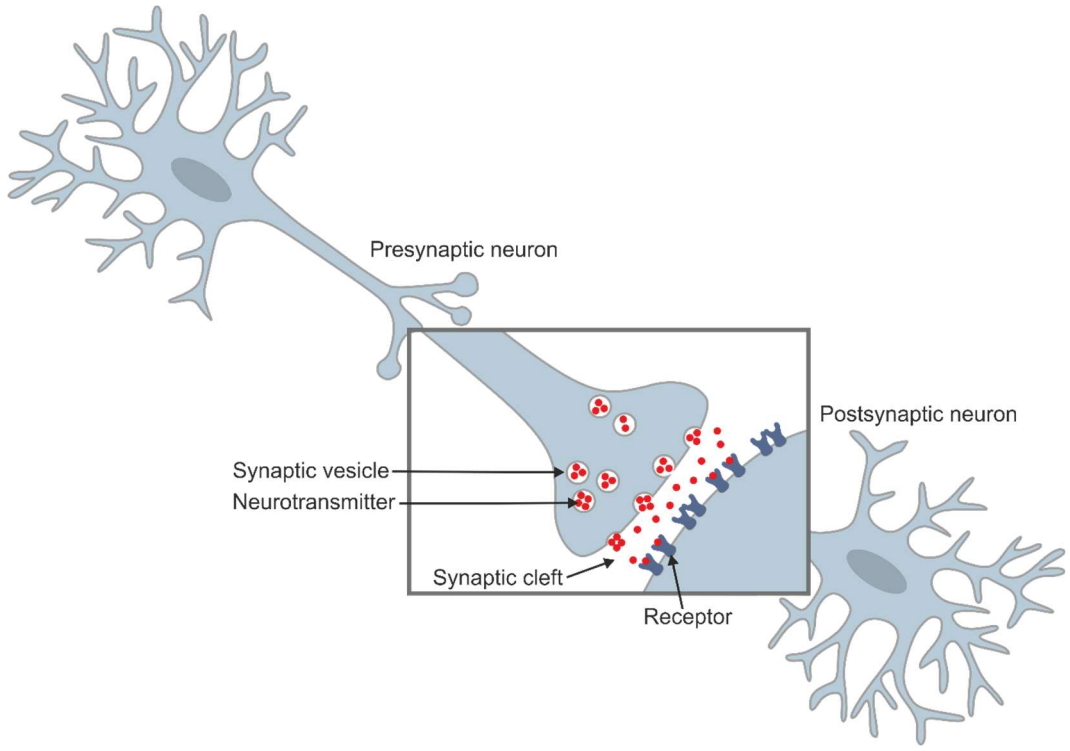

Fig. 1: Simplified scheme of neurotransmission.

Depending on the chemical structure of neurotransmitters, a distinction is made between amino acids (e.g. glutamate, GABA), monoamines (e.g. dopamine, serotonin, adrenaline), peptides (e.g. opioids), purines (e.g. adenosine), and acetylcholine. Moreover, neurotransmitter receptors are subdivided into either ionotropic or metabotropic (Fig. 2). Ionotropic receptors, such as the $GABA_A$, AMPA, kainate, and NMDA receptors, are also referred to as ligand-gated ion channels and are activated by the binding of their specific neurotransmitter (ligand) to a specific site on the channel, which then opens to the flow of cations (K^+, Na^+, and Ca^{2+}) and/or anions (Cl^-) across the cell membrane. This results in an immediate de- or hyperpolarization. Metabotropic receptors (or G-protein coupled receptors) such as the $GABA_B$ receptor do not form an ion channel pore itself but activate neighboring

ion channels or other intracellular events through signal transduction mechanisms (e.g. by G proteins) after a specific neurotransmitter binds to its respective binding site on the receptor. While activation of ionotropic receptors mediates fast transmission, metabotropic receptors produce much slower and long-lasting responses.

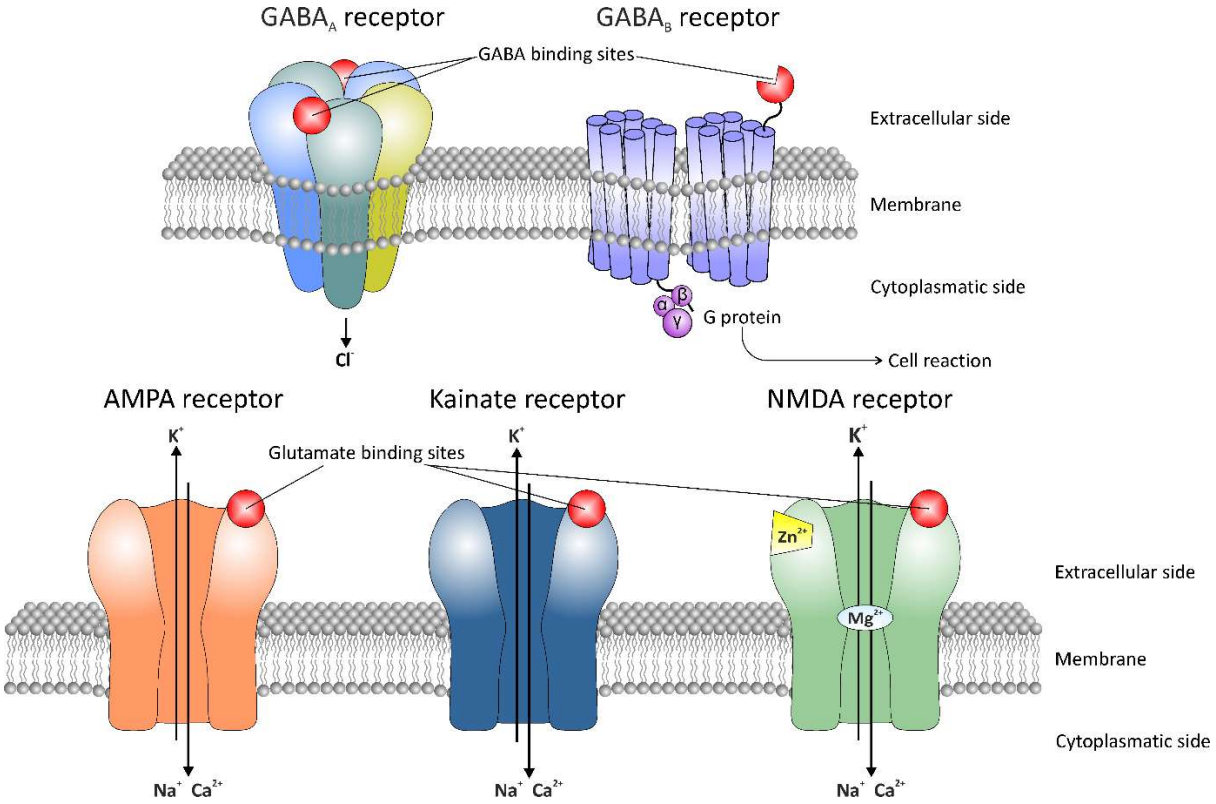

Fig. 2: Schematic structure of ionotropic $GABA_A$, AMPA, kainate, and NMDA receptor and metabotropic $GABA_B$ receptor.

In the present study, we examined alterations in 19 receptor types of seven neurotransmitter systems, i.e. GABA, glutamate, acetylcholine, adrenaline, dopamine, serotonin, and adenosine, of *Pink1*$^{-/-}$ mice compared with control mice that may be associated with PD.

GABA is the most prominent inhibitory neurotransmitter in the central nervous system (CNS). GABA receptors play an important role in brain physiology and can be divided into ionotropic $GABA_A$, including benzodiazepine (BZ) that binds to an allosteric binding site on the $GABA_A$ receptor, and metabotropic $GABA_B$ receptors (30). A recent non-invasive magnetic resonance spectroscopy study demonstrated increased GABA levels in the basal ganglia of PD patients that correlated with gait alterations (31).

Glutamate is the most prominent excitatory neurotransmitter in the mouse brain. The glutamate receptors can be divided into the ionotropic AMPA, kainate, and NMDA receptors, and metabotropic receptors, which are classified into three groups: Group I (mGlu1 and 5), Group II (mGlu2 and 3), and Group III (mGlu4, 6, 7, and 8) (32). They play an important role in synaptic plasticity, which is the ability of synapses to change in strength, and are thus

associated with the modulation of memory and learning (32, 33). In PD, alterations in neurotransmission within the basal ganglia were shown to affect glutamatergic receptors (34).

The neurotransmitter acetylcholine plays a crucial role in neurotransmission in both the CNS and peripheral nervous system, which is mediated by two classes of receptors: ionotropic nicotinic acetylcholine receptors and metabotropic muscarinic acetylcholine receptors (35). In the CNS, the former consists of a combination of different subunits (α_4, α_5, α_6, α_7, α_9, α_{10}, and β_2), and for the latter, there are five subtypes (M_1-M_5). Early in the study of PD, it was discovered that degeneration of dopaminergic neurons disturbs the balance between dopamine and acetylcholine levels in the brain (15). Interestingly, the first drugs used in PD therapy to restore this balance were antagonists of the cholinergic receptor (15), which are now mainly replaced by L-DOPA therapy. Moreover, several motor and non-motor symptoms of PD, e.g. gait alterations, cognitive impairments, psychosis, and olfactory dysfunctions, have been associated with altered cholinergic levels or degeneration of cholinergic terminals (35).

The catecholamines adrenaline (epinephrine) and noradrenaline (norepinephrine) are neurotransmitters in the CNS that activate the G-protein-coupled adrenergic receptors, which are subdivided into α receptors ($\alpha_{1(A, B, D)}$ and $\alpha_{2(A-C)}$) and β receptors (β_{1-3}) (36). They play an important role in attention and stress response and may contribute to learning and memory processes as well as motor control (37). In PD, neurodegeneration of the locus coeruleus results in lower levels of noradrenaline that have been associated with various motor and non-motor symptoms of PD (37, 38).

Dopamine is a neurotransmitter synthesized from the precursor L-DOPA in the SN and ventral tegmental area. In the CNS, it plays a crucial role in motor control, cognitive processes, and motivation (39). It activates G-protein-coupled dopamine receptors, which are divided into two families: The D1-like family includes the D_1 and D_5 receptor subtypes that are excitatory, and the D2-like family includes the D_2, D_3, and D_4 receptor subtypes that are inhibitory (39). PD is associated with the degeneration of dopaminergic neurons in the SN leading to a deficiency of dopamine levels in the striatum (3).

The monoamine serotonin, also known as 5-hydroxytryptamine (5-HT), is a neurotransmitter that is primarily synthesized in the CNS in the dorsal raphe nuclei of the brainstem (40). There are seven 5-HT receptor families (5-HT_{1-7}) including at least 15 receptor subtypes. Several non-motor symptoms of PD such as depression, anxiety, and dementia, are associated with a dysfunctional serotonergic system (40, 41).

Adenosine acts as a neuromodulator in the brain, where it activates G-protein-coupled adenosine receptors, of which there are four subtypes: A_1, A_{2A}, A_{2B}, and A_3. The adenosinergic system influences various processes, such as control of sleep and motor function, and is involved in PD (42).

In general, neurotransmitter receptors can be visualized, and their densities absolutely quantified using the experimental method of quantitative *in vitro* receptor autoradiography,

thus enabling comparisons between different experimental groups. Therefore, a comprehensive study of the described neurotransmitter receptor systems using quantitative *in vitro* receptor autoradiography may lead to a better understanding of the molecular mechanisms underlying the clinical manifestations of Parkinson's disease.

1.4.2. Quantitative *in vitro* receptor autoradiography

Quantitative *in vitro* receptor autoradiography is a method based on the principle that radiolabeled ligands (in our case tritium [^{3}H] is used as the radioactive agent) will bind to specific receptor binding sites in unfixed brain sections, allowing quantification and visualization of active neurotransmitter receptor binding sites. Furthermore, this enables the analysis of regional and/or laminar distribution patterns of neurotransmitter receptor binding sites (13, 14, 43, 44). Because pathological conditions are often associated with changes in more than just one receptor type, a major advantage of this method is the possibility to analyze multiple receptor subtypes (e.g. the glutamatergic AMPA, kainate, and NMDA receptors) or different co-localized receptor systems (e.g. GABA, dopamine, and acetylcholine receptors) simultaneously within the same brain tissue. In addition, various transmembrane receptors for neurotransmitters and neuromodulators are located in only one neuron, and as cyto- and receptor-based architectonic methods showed, receptors link the anatomical structure and their function (45). From this, a conclusion may be drawn about functional interactions or influences between different receptor systems. In PD, for example, a complex interdependence between the adrenergic, cholinergic, and dopaminergic receptor systems was previously indicated (46).

In our previous study that focused on *Parkin* and *DJ-1* knockout mice, which are valuable models for monogenic PD-causing genes, we already demonstrated by using *in vitro* receptor autoradiography that non-dopaminergic receptors, such as the kainate and $GABA_B$ receptors, were upregulated in several brain areas (14). Moreover, AMPA receptors in hippocampal regions were downregulated in *Parkin* knockout mice (14). This provides further proof that the dopaminergic system is not the only receptor system affected in PD. However, to our knowledge, there is no previous comprehensive study focusing on neurotransmitter receptor alterations in mouse models of PINK1 Parkinsonism and thus in the prodromal phase of PD.

1.5. Objectives and experimental approach

To find new therapeutic applications, especially for non-motor symptoms, it is crucial to understand the relationship between PD, in our case PINK1 Parkinsonism, and the expression of different neurotransmitter receptors. Since the consequences of *PINK1* gene mutations on the expression of neurotransmitter receptors are still unknown, we aimed to identify how the expression of different neurotransmitter receptor binding sites, including non-dopaminergic receptors, is altered in *PINK1*-related early-onset PD. We hypothesized that alterations of neurotransmitter receptors in functional systems are already present in the prodromal phase of PD. Thus, this study aimed to perform a comparative analysis of neurotransmitter receptor

densities and their regional distribution in *Pink1*$^{-/-}$ mice and to discuss the possible link between receptor alterations and functional or pathological changes.

Since it was previously shown that pathological states are often associated with changes in more than just one receptor type, we analyzed 19 different receptor types of seven functionally highly important neurotransmitter systems simultaneously and, importantly, in the same brain tissue of ten *Pink1*$^{-/-}$ mice and ten control mice by using quantitative *in vitro* receptor autoradiography. Specially, we focused on the following receptors: GABAergic $GABA_A$, $GABA_A$-associated benzodiazepine (BZ) binding sites, and $GABA_B$; glutamatergic AMPA, kainate, NMDA, and $mGlu_{2/3}$, cholinergic M_1, M_2, M_3, and nicotinic $\alpha_4\beta_2$; adrenergic α_1; dopaminergic D_1, D_2, and $D_{2/3}$; serotonergic 5-HT_{1A}, and 5-HT_2; and finally adenosinergic A_1, A_{2A}. We then qualitatively analyzed the regional distribution of neurotransmitter densities in ten different brain areas associated with the olfactory, somatosensory, limbic, motor, and visual systems. Because *Pink1*$^{-/-}$ mice showed gait and olfactory changes in previous behavioral studies, the receptor densities of these neurotransmitter receptors were additionally quantitatively analyzed in seven different brain areas associated with the motor and limbic systems (including the olfactory bulb for olfaction). To facilitate the localization and analysis of the different brain regions, we also visualized the neuronal structure in adjacent sections to those used for receptor autoradiography by using two different staining techniques: Nissl staining with cresyl violet acetate and Nissl staining by Merker (47). In addition, qualitative analysis of dopaminergic neurons, astrocytic glutamate recycling, and GABAergic neurons was performed by immunohistochemistry experiments using primary antibodies against tyrosine hydroxylase, glutamine synthetase, and GABA, respectively. With this approach, we aimed to complement the currently predominant dopamine-related approaches in Parkinson's research and to present novel data concerning the role of non-dopaminergic receptors in PD.

2. Material and Methods

2.1. Generation of *Pink1* knock-out mice

Pink1$^{-/-}$ mice were generated by our cooperation partner at the Institute of Developmental Genetics of the Helmholtz Center Munich (26). Briefly, the generation was based on the deletion of exons 2 and 3 of the *Pink1* locus. A more detailed overview of the genetic background is given below.

First, a polymerase chain reaction was used to amplify 129/ola genomic DNA fragments, which were subsequently inserted into the targeting Psk62-easyflox vector. The construct consisted of a neomycin resistance cassette flanked by flip-recombinase target (FRT) sites inserted in front of exon 2 (Fig. 3). Exons 2 and 3 and the FRT-flanked neomycin resistance cassette were also flanked with locus of X-over P1 (loxP) sites. The vector was then electroporated into embryonic stem cells, followed by injection of those cell clones into blastocysts of C57BL/6J mice, which were transferred into pseudopregnant foster mothers. The male offspring were then mated to female C57BL/6J mice, resulting in offspring that are conditionally floxed (*Pink1*$^{l/+}$). Heterozygous *Pink1* mice (*Pink1*$^{-/+}$) were born after Cre deleter mice were mated to the *Pink1*$^{l/+}$ mice, resulting in Cre recombination, i.e. binding of Cre recombinase to loxP targets on the chromosome, removing the FRT sites, the neomycin resistance cassette, and both exons 2 and 3. The single active loxP site in between exons 1 and 4 generated a frameshift in the *Pink1* RNA coding sequence, which then created a stop codon shortly behind exon 1. At the protein level, a truncated form of *Pink1* is produced, consisting exclusively of those amino acids encoded by the first of the eight exons. To generate complete *Pink1* knockout mice (*Pink1*$^{-/-}$), heterozygous male *Pink1*$^{-/+}$ were crossed with female Cre deleter mice. Correct insertions were verified as previously described (26).

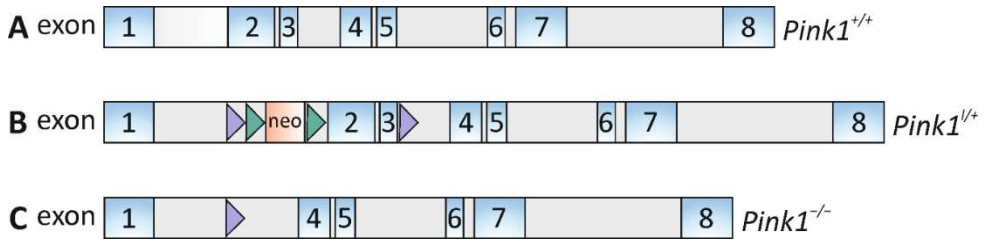

Fig. 3: Generation of *Pink1*$^{-/-}$ mice (adapted from (26)). **A**: The exon of the *Pink1* locus is shown. **B**: Neomycin resistance cassette (orange box) was flanked by FRT sites (green triangle), while the neomycin resistance cassette and both exons 2 and 3 were additionally flanked by loxP sites (violet triangle). **C**: After mating conditional *Pink1* mice with Cre deleter mice, Cre recombination and the removal of FRT flanked neo, exons 2 and 3 occurred, while the loxP site between exon 1 and 4 remained active, creating a stop codon behind exon 1 and finally to a truncated protein form of *Pink1*. Heterozygous male *Pink1*$^{-/+}$ mice were mated with female Cre deleter mice, leading to complete *Pink1* knockout (*Pink1*$^{-/-}$) offspring. Abbreviations: *FRT*, flip-recombinase target; *loxP*, locus of X-over P1; *neo*, neomycin resistance cassette

2.2. Animals

Male, 12-week-old *Pink1*$^{-/-}$ mice (C57BL/6J$^{3.5CreDel_KO}$) and age-matched control mice (C57BL/6J) were kept under specific pathogen-free conditions with ad libitum access to food and water at the Institute of Developmental Genetics (Helmholtz Center Munich, Germany). They were generously provided by Prof. Dr. med. Wolfgang Wurst for autoradiographic, histological, and immunohistochemical analyses. All experiments were performed according to the German animal welfare act and approved by the responsible governmental agency, LANUV NRW (Landesamt für Natur, Umwelt und Verbraucherschutz NRW).

For the autoradiographic and histological analyses, ten male *Pink1*$^{-/-}$ mice and ten control mice were sedated by carbon dioxide (CO_2) inhalation and subsequently decapitated. The brains were immediately removed and then deep-frozen in isopentane at -50°C for approximately 2 min. Subsequently, they were placed and delivered on dry ice to the Research Center Jülich, where they were finally stored at -80°C until further use.

For immunohistochemical analyses, five male *Pink1*$^{-/-}$ mice and five control mice were deeply anesthetized followed by intracardiac perfusion, first with phosphate-buffered saline (PBS) to flush the vessels and then with 4% paraformaldehyde in PBS (PFA/PBS; pH 7.5). Brains were immediately removed and post-fixed in 4% PFA/PBS for 24 h. Subsequently, all brains were transferred to a 15% sucrose solution for cryoprotection and transported to the Research Center Jülich on refrigerated packs. Directly thereafter, they were transferred to a 25% sucrose solution, frozen at -40°C in precooled isopentane, and stored at -80°C until further use.

2.3. Preparation of tissues and sections

For autoradiographic and histological analyses, tissue was taken from the -80°C storage and acclimatized in the cryostat microtome (Leica CM3050, Leica Biosystems GmbH, Germany) for at least 30 min at -14°C. Subsequently, the brains were fixed on a specimen holder by embedding them in Tissue-Tek® (Sakura Finetek Germany GmbH, Germany), after which they were serially sectioned (10 µm section thickness) at -14°C in the coronal plane at five different rostro-caudal levels encompassing the olfactory bulb, striatum, hippocampus, SN, and cerebellum (Fig. 4) using the cryostat microtome. For each animal and region of interest (ROI), three sections were prepared for total binding and one additional section for each animal at the striatum level for unspecific binding. Each section was thaw-mounted on pre-cooled, silanized glass slides (76x26 mm, Starfrost, Germany) and dried on a heating plate at 37°C for at least 30 min. The sections were stored in plastic boxes at -80°C until they were used for either receptor autoradiography experiments or histological staining.

For immunohistochemical analyses, brains were taken from the -80°C storage on the day of sectioning and mounted on the pre-cooled sample holder (-35°C) of the Frigomobil (Leica Biosystems GmbH, Germany) with Tissue-Tek®, covered with an aluminum cap. After increasing the temperature to -16°C the whole setup was left for 15 min in order to adapt to

the cutting temperature. The brains were serially sectioned (section thickness: 50 µm; object temperature: -16°C; knife temperature: RT) in the coronal plane at the same rostro-caudal levels as mentioned above, and sections were collected in 0.1M PBS (pH 7.4).

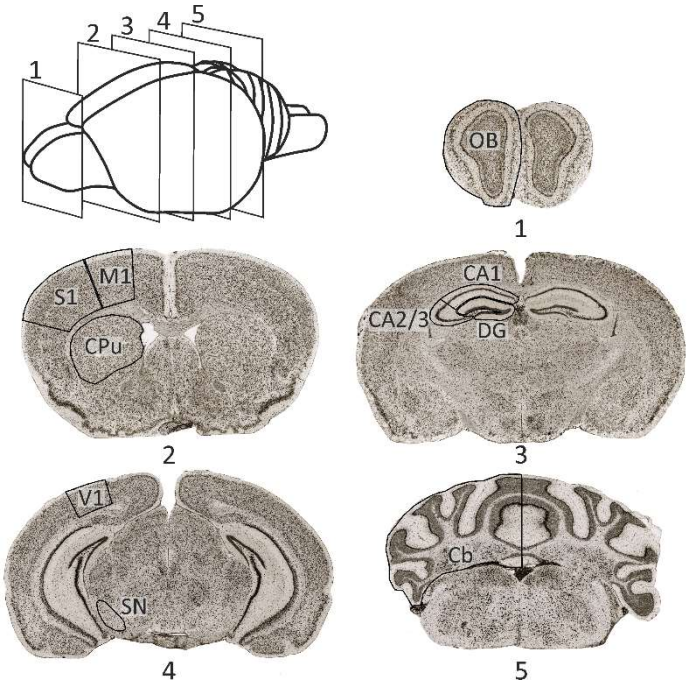

Fig. 4: Top left: Example of the five section planes: olfactory bulb (1), striatum (2), hippocampus (3), SN (4), and cerebellum (5), that were sectioned for each brain. **1-5:** The exemplary Nissl stained sections (by Merker) correspond to the five section planes and show delineated ROIs that were analyzed either qualitatively and/or quantitatively: olfactory bulb (OB), motor cortex (M1), somatosensory cortex (S1), striatum (CPu), hippocampal regions CA1, CA2/3, and DG, visual cortex (V1), SN, and cerebellum (Cb).

2.4. Histological staining

2.4.1. Nissl staining

To identify cytoarchitectonic ROIs, two different staining procedures were performed according to established protocols on sections adjacent to those used for receptor autoradiography: Nissl staining by using cresyl violet acetate and Nissl staining by Merker (47). The procedure for the Nissl staining using cresyl violet acetate is summarized in Table A1 (see Supplemental Material and Methods, Section 8.1.10.), while the procedure for the Nissl staining by Merker is summarized in Table A2 (see Supplemental Material and Methods, Section 8.1.10.). Nissl stained coverslipped sections were scanned and visualized using a Zeiss AxioScan.Z1 scanning microscope (Carl Zeiss Microscopy GmbH, Germany) with a 20x objective at a final resolution of 0.325µm/pixel.

2.4.2. Immunohistochemical staining

To analyze tyrosine hydroxylase (TH) for the dopaminergic receptor system and astrocytic glutamine synthetase (GS) for glutamate recycling, immunohistochemical experiments were performed. 50µm sections were rinsed 3 x 20 min under gentle 0.1M PBS (pH 7.4) to remove

the fixative. Afterward, sections were incubated in 5% blocking serum (normal goat serum, Vector Laboratories, USA) dissolved in 0.1M PBS containing 0.3% saponin (Sigma-Aldrich Chemie GmbH, Germany) for 1h at RT. The sections were then incubated for 48h in primary antibodies [anti-TH-chicken, Abcam, United Kingdom, #ab76442 (diluted 1:1000) and anti-GS-rabbit, Sigma-Aldrich Chemie GmbH, Germany, #G2781 (diluted 1:500)] dissolved in 0.1M PBS + 0.1% saponin + 1% blocking serum at +4°C under gentle shaking. Sections were rinsed for 3 x 30min in 0.1M PBS at RT followed by an incubation with secondary antibodies [goat-anti-chicken Alexa-Fluor 488, Jackson ImmunoResearch Laboratories, USA (diluted 1:200) and goat-anti-rabbit-Cy-3 conjugated, Jackson ImmunoResearch Laboratories, USA, (diluted 1:200)] dissolved in 0.1M PBS + 0.1% saponin + 1% blocking serum for 48h at +4°C. Sections were rinsed for 3 x 30 min in 0.1M PBS followed by incubation in DAPI - Hoechst (Thermo Fisher Scientific GmbH, Germany, #33342 (diluted 1:2000)), rinsed for 3 times, mounted on glass slides, and coverslipped with Fluoromount G (SouthernBiotec, USA).

For the co-localization of TH and GABA, the same immunohistochemical procedures were performed as described above but with the primary antibody combination of anti-TH-chicken and anti-GABA-rabbit [Sigma-Aldrich Chemie GmbH, Germany, #A2052 (diluted 1:500)] and for anti-GABA-rabbit visualization goat-anti-rabbit-Cy3 conjugated second antibody was used as described above.

For an overview, staining was visualized by scanning the section with a fluorescence Zeiss AxioScan.Z1 scanning microscope (Carl Zeiss Microscopy GmbH, Germany) with a 20x objective at a final resolution of 0.325µm/pixel. For more detail, a confocal laser scanning microscope Zeiss LSM 880 (Carl Zeiss, Germany) was used with an Plan-Apochromate 40x/1,4 Oil DIC oil-immersion objective and immersion oil type 518F/24°C (Carl Zeiss Microscopy GmbH, Germany) with a final resolution of 0.221µm/pixel. Images were acquired and processed using ZEN 2.0 software (Carl Zeiss Microscopy GmbH, Germany).

2.5. Quantitative *in vitro* receptor autoradiography

To visualize and measure neurotransmitter receptor densities, quantitative *in vitro* receptor autoradiography was performed for 19 different receptor binding sites from seven different neurotransmitter systems. In detail, experiments were performed according to previously described protocols (48-50) for the following receptors: GABAergic $GABA_A$, $GABA_A$-associated BZ binding sites, and $GABA_B$; glutamatergic AMPA, kainate, NMDA, and $mGlu_{2/3}$; cholinergic M_1, M_2, M_3, and nicotinic $\alpha_4\beta_2$; adrenergic α_1; dopaminergic D_1, D_2, and $D_{2/3}$; serotonergic $5\text{-}HT_{1A}$, and $5\text{-}HT_2$; adenosinergic A_1, A_{2A}. All experimental protocols for receptor autoradiography are summarized in Table A3 (see Supplemental Material and Methods, Section 8.1.11.) and consisted of three main steps: a pre-incubation, a main incubation, and a rinsing step.

In the pre-incubation, sections were incubated in a buffer solution that rehydrated the sections, adapted the pH, and led to the washout of endogenous ligands. Two different

protocols were used for the main incubation: one for identification of the total number of binding sites, and one for the nonspecific binding. The main incubation protocol for total binding involved the labeling of sections in a buffer solution with the respective [^{3}H]-labeled receptor ligand alone, whereas in the protocol for nonspecific binding, an at least 1000-fold higher concentration of a specific nonradioactive displacer was also added. The high-affinity displacer competes for the receptor binding site and displaces the [^{3}H]ligand, representing the nondisplaceable binding, which is usually less than 10% of the total binding. When the nonspecific binding is greater than 10% of the total binding, the specific binding is calculated as follows: **total binding – nonspecific binding = specific binding**

The final concentration of the [^{3}H]ligand in buffer solution was calculated from the measurements of triplicates of the respective sample in the Liquid Scintillation Counter Hidex 300 SL (Hidex, Finland). The main incubation lasted between 40 and 120 min, depending on the [^{3}H]ligand, and the sections were light protected throughout this step. Finally, during the rinsing step, the binding process was stopped in buffer solution by removing the excess [^{3}H]ligands. Subsequently, the sections were rinsed in distilled water to wash out salts of the buffer solutions, except for the AMPA and kainate receptor protocols, where the sections were fixated in 2.5% glutaraldehyde/acetone. After the experiments, the sections were dried under a fan and stored at RT until their exposure against β^--sensitive films.

2.6. Film exposition and development

To visualize and quantify the radiolabeled neurotransmitter receptor densities in brain sections, all sections must first be prepared for film exposition. Thus, the dried sections were trimmed and fixed on white paper sheets with double-sided adhesive tape. The sections were exposed together with self-established microscales with known [^{3}H]-concentrations against β^--sensitive films (Carestream BioMax MR Film, Sigma-Aldrich Chemie GmbH, Germany). This was performed in a photography laboratory under red light by placing sections and microscales between plastic plates that were shut tightly with metal clips and then stored in light-protected boxes for nine to 15 weeks. The exposure time for each [^{3}H]ligand is summarized in Table A4 (see Supplemental Material and Methods, Section 8.1.12.). After the respective exposure time, β^--sensitive films were developed in a photography laboratory under red light by using [^{3}H]-sensitive emulsion (GBX-Developer and DBX-Fixer, Sigma-Aldrich Chemie GmbH, Germany) and a semi-automatic Hyperprocessor (Amersham Biosciences Europe GmbH, Germany).

2.7. Digitalization of autoradiographic films

To generate images of each radiolabeled brain section, the autoradiographic films were digitalized using the high-end microscope camera AxioCam HRc (Carl Zeiss Microscopy GmbH, Germany) that was connected to the AxioVision Rel. 4.8.2. software (Carl Zeiss Microscopy GmbH, Germany). The digitalization was performed in darkness with a pre-warmed camera (at least 20min before the start) and on a homogeneously illuminated light table. At first, a shading correction was performed to ensure that the measured areas of the film had a

homogeneous light intensity. For each film, gray values of the background were checked and, if necessary, the brightness was then adjusted to a defined range. To guarantee that all images (autoradiograms) were comparable, settings were not changed during the digitalization process. All images were saved 8-bit coded in 256 gray values (0=black; 255=white) and a spatial resolution of 4164x3120 pixel.

2.8. Calibration and color coding

To visualize the regional distribution of neurotransmitter receptors in brain sections, all radiolabeled brain sections were color-coded. First, non-linear transformation curves of co-exposed microscales of each autoradiographic film were computed for calibration, representing the correlation between [^{3}H]-concentration in the tissue and gray values in the digitalized autoradiogram (Fig. 5). By using MATLAB®-software (MathWorks, USA), gray values of each pixel in the autoradiogram were converted into [^{3}H]-concentrations and corresponding receptor densities (fmol/mg protein), resulting in linearized autoradiograms. The linearized autoradiograms, in which gray values correlate to receptor densities as a linear function, were subsequently contrast-enhanced and color-coded for optimal visualization of regional neurotransmitter receptor distribution. A color scale, which is equally spaced into eleven density ranges, corresponds to the assigned 256 gray values of the linearized autoradiogram. While red-colored pixels correspond to high receptor densities (fmol/mg protein), the blue-colored pixels correspond to low receptor densities.

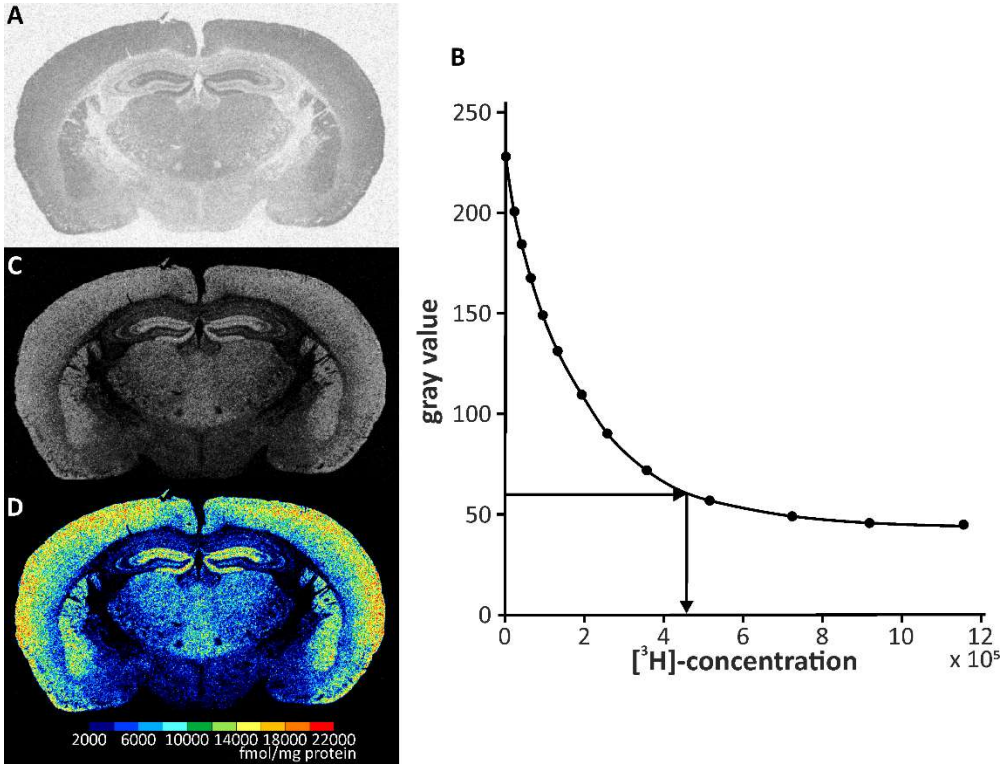

Fig. 5: The original [^{3}H]LY 341495 autoradiogram (A) was converted to a linearized image (C) using a non-linear calibration curve (B) representing the correlation between gray values and [^{3}H]-concentrations and corresponding receptor densities (48). Neurotransmitter receptor distribution was then visualized in a color-coded image (D).

To allow direct comparison of the regional distribution pattern between *Pink1*$^{-/-}$ and control mice, all brain sections of a neurotransmitter receptor were color-coded with the same lower limits (always 0) and upper limits (depending on the receptor). Because not all brain sections can be displayed, one color-coded image per group (*Pink1*$^{-/-}$ mice and control mice) and per rostro-caudal level (olfactory bulb, striatum, hippocampus, SN, and cerebellum) was selected as an example for each neurotransmitter receptor and are shown in Figs. 7-13 (see Results, Sections 3.2.1.-3.2.7.). The qualitative analysis of the regional distribution of neurotransmitter receptors focused on the olfactory bulb (OB), motor cortex (M1), somatosensory cortex (S1), visual cortex (V1), hippocampal regions cornu ammonis (CA) CA1 and CA2/3, and dentate gyrus (DG), SN, and cerebellum (CB) (Fig. 4). Thereby, low densities were described for densities that were approximately in the blue to green range of the color scale, while intermediate described the green to yellow range, and high described the yellow to red range.

2.9. Densitometric analysis

To quantify the neurotransmitter receptor densities, densitometric analysis was performed for each receptor binding site using the image analyzer software AxioVision 4.8.2. (Carl Zeiss Microscopy GmbH, Germany) by delineating the ROIs in both hemispheres and comparing the delineation with the defined areas in "The Mouse Brain in Stereotaxic Coordinates" (51) and with the histological staining. Thereby, the quantitative analysis focused on the following ROIs: OB, M1, CPu, hippocampal regions CA1, CA2/3, and DG, as well as SN (Fig. 4). Three sections were delineated for each ROI, animal, and receptor binding site to determine the average of receptor densities.

2.10. Statistical analysis

Mean receptor densities (MD) ± standard deviation (SD) were calculated for each of the 19 different receptor binding sites of the seven neurotransmitter systems GABA, glutamate, acetylcholine, dopamine, adrenaline, serotonin, and adenosine in *Pink1*$^{-/-}$ and control mice (each group represented with n=10) and brain areas of the limbic (OB, and hippocampal regions CA1, CA2/3, and DG) and motor systems (M1, CPu, and SN) (see Supplemental Data, Section 8.2.1., Tables A5 – A42). Interhemispheric differences in receptor densities were tested by analysis of variance (ANOVA, linear mixed-effects models; R version 4.0.4). Because they were not significantly different, data from the left and right hemispheres were pooled. In the next step differences between control and *Pink1*$^{-/-}$ mice were statistically determined for each brain area using ANOVA, and if significant, a post hoc t-test was performed for each neurotransmitter receptor to test for significant differences between control and *Pink1*$^{-/-}$ mice. The results are presented in bar charts that depict the MD ± SD (expressed in fmol/mg protein) of each receptor subtype in *Pink1*$^{-/-}$ and control mice (see Figs. 14-19 and Supplemental Data, Section 8.2.3., Figs. A5-A11). Significant changes between the two groups are indicated with asterisks (*$p<0.05$ or **$p<0.01$).

3. Results

3.1. Immunohistochemical staining

So far, qualitative evaluation of the immunohistochemical localization of dopaminergic neurons by TH within the SN and other cerebral regions showed no differences between the 3-month-old *Pink1*$^{-/-}$ and control mice (see Supplemental Data, Section 8.2.2., Fig. A1). However, at higher magnification, changes were observed between *Pink1*$^{-/-}$ and control mice, indicating differences in the distribution of TH-positive fibers and terminals in the striatum. In particular, fibers in control mice tended to be thicker than in *Pink1*$^{-/-}$ mice, where they also tended to be denser (Fig. 6). This observation deserves further evaluation with additional antibody combinations towards target neurons and synaptic boutons (axon terminals) with antibodies directed towards synaptic proteins. Regarding immunohistochemical localization of GS, astrocytes within the SN and striatum indicated no signs of activation or other changes. In contrast to GS, GABA immunoreactivity was clearly co-localized with TH-positive neurons within the SN and other regions (see Supplemental Data, Section 8.2.2., Figs. A2-A3). Finally, overall GABA staining intensity appeared to be slightly reduced in the striatum of *Pink1*$^{-/-}$ mice compared with age-matched control mice (see Supplemental Data, Section 8.2.2., Fig. A4).

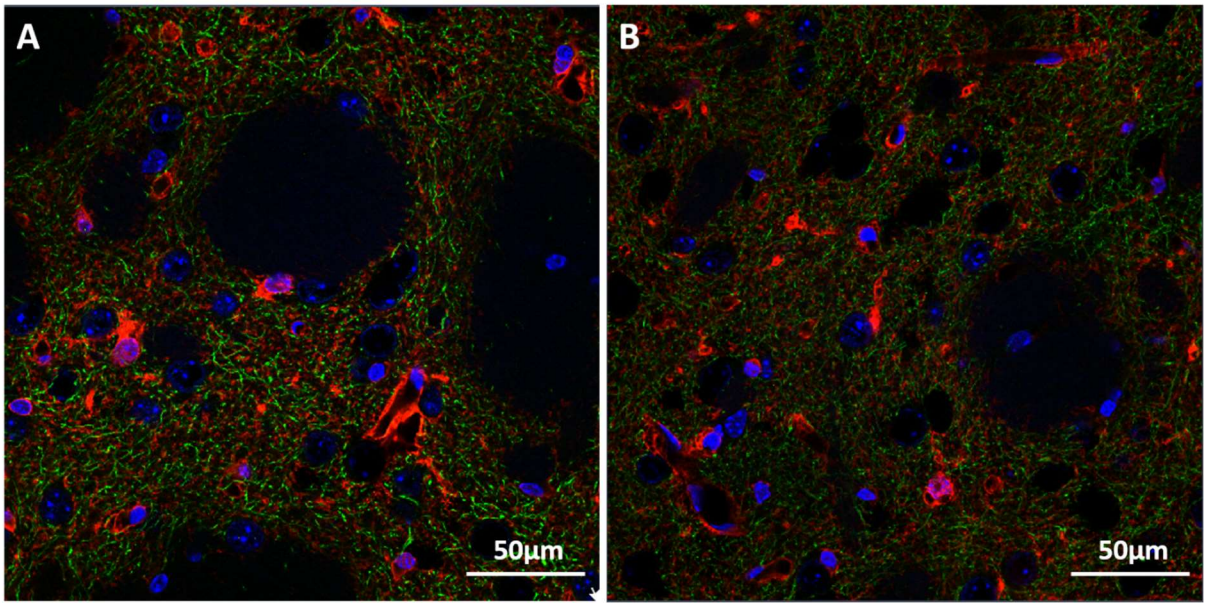

Fig. 6: Exemplary immunohistochemical staining against TH (green) and GS (red) in the striatum of control mice (A) and *Pink1*$^{-/-}$ mice (B) indicating differences in the distribution of TH-positive fibers and terminals. The fibers in control mice are thicker than in *Pink1*$^{-/-}$ mice, where they were also denser. Cell nuclei are stained blue. Magnification: 40x objective at a final resolution of 0.221µm/pixel. Scale bar = 50µm

3.2. Regional distribution of neurotransmitter receptors

3.2.1. GABA receptors

$GABA_A$ receptors

In both groups, low $GABA_A$ receptor densities were found in the CA2/3 region of the hippocampus, striatum, and SN, whereas high densities were found in the olfactory bulb and cerebellum (Fig. 7A). All other brain areas examined showed intermediate densities. Comparing the two groups, *Pink1*$^{-/-}$ mice showed a tendency toward lower densities in the olfactory bulb and cerebellum, whereas they tended to be higher in the motor, somatosensory, and visual cortex, striatum, and hippocampus (CA1, CA2/3, and DG).

$GABA_A$-associated BZ binding sites

Compared with the other GABA receptor subtypes examined, BZ binding site densities were generally highest (Fig. 7B). They were very low in the striatum, low in the cerebellum, and intermediate in the CA2/3 region of the hippocampus, while in the other brain areas examined, densities were high (Fig. 7B). Comparing the two groups, densities in *Pink1*$^{-/-}$ mice tended to be higher in the motor cortex and lower in the visual cortex than in control mice.

$GABA_B$ receptors

$GABA_B$ receptor densities were low in the olfactory bulb, striatum, and SN, whereas other ROIs showed intermediate to high densities (Fig. 7C). Between the two groups, in all brain regions, $GABA_B$ receptor densities were higher in the control group than in *Pink1*$^{-/-}$ mice.

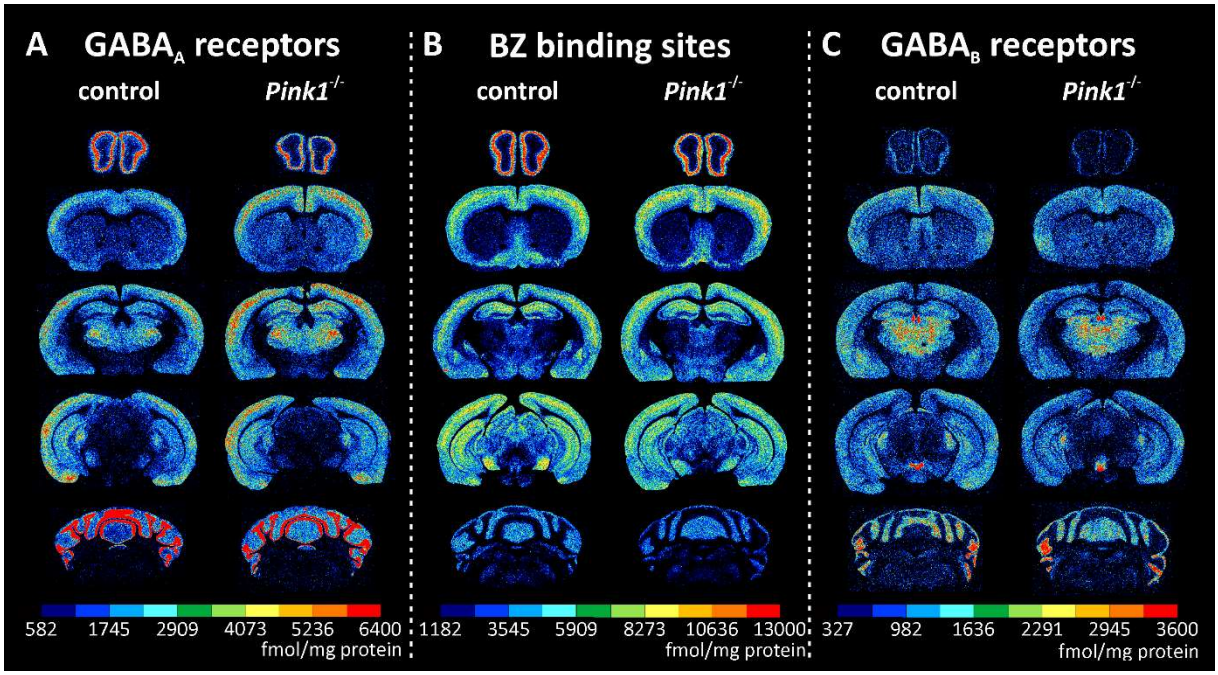

Fig. 7: Color-coded images showing the distribution pattern of GABAergic receptor densities in different brain regions of control and *Pink1*$^{-/-}$ mice. Color scales code receptor densities in fmol/mg protein. **A**: Ligand: [^{3}H]Muscimol; **B:** Ligand: [^{3}H]Flumazenil; **C**: Ligand: [^{3}H]CGP 54626

3.2.2. Glutamate receptors

AMPA receptors

The lowest AMPA receptor densities were found in the SN, followed by the olfactory bulb, motor, somatosensory, and visual cortex, striatum, and cerebellum (Fig. 8A). While densities were intermediate in the hippocampal regions CA2/3 and DG, they were highest in its CA1. Comparing the densities between the two groups, control mice showed higher densities in the hippocampus (CA1, CA2/3, and DG) and visual cortex than *Pink1*$^{-/-}$ mice.

Kainate receptors

Kainate receptor densities were lowest compared with the other glutamate receptor subtypes analyzed (Fig. 8B). In the hippocampal region CA1, SN, and cerebellum, densities were low, whereas in the motor, somatosensory, and visual cortex, and in the hippocampal regions CA2/3 and DG, densities were found to be intermediate. The highest densities were found in the olfactory bulb and striatum. *Pink1*$^{-/-}$ mice showed a tendency toward lower kainate receptor densities in the SN, whereas they were evenly distributed in all other ROIs.

NMDA receptors

NMDA receptor densities were below the detection limit in the cerebellum (Fig. 8C). They were very low in the SN, and low in the olfactory bulb and striatum. While intermediate densities were found in the motor, somatosensory, and visual cortex, as well as in the hippocampal CA2/3 region, densities were higher in the hippocampal DG region and exceptionally high in its CA1 region. In the comparison between *Pink1*$^{-/-}$ and control mice, NMDA receptor densities were homogeneously distributed.

mGlu$_{2/3}$ receptors

Of all glutamate receptor subtypes analyzed in the present study, mGlu$_{2/3}$ receptor densities were highest (Fig. 8D). The densities were low in the olfactory bulb, CA1 and CA2/3 region of the hippocampus, SN, and cerebellum. They were high in all cortical areas, in the striatum, and the hippocampal region DG. Except for the cerebellum, where densities were homogeneously distributed, all brain areas showed higher densities in *Pink1*$^{-/-}$ mice compared to control mice.

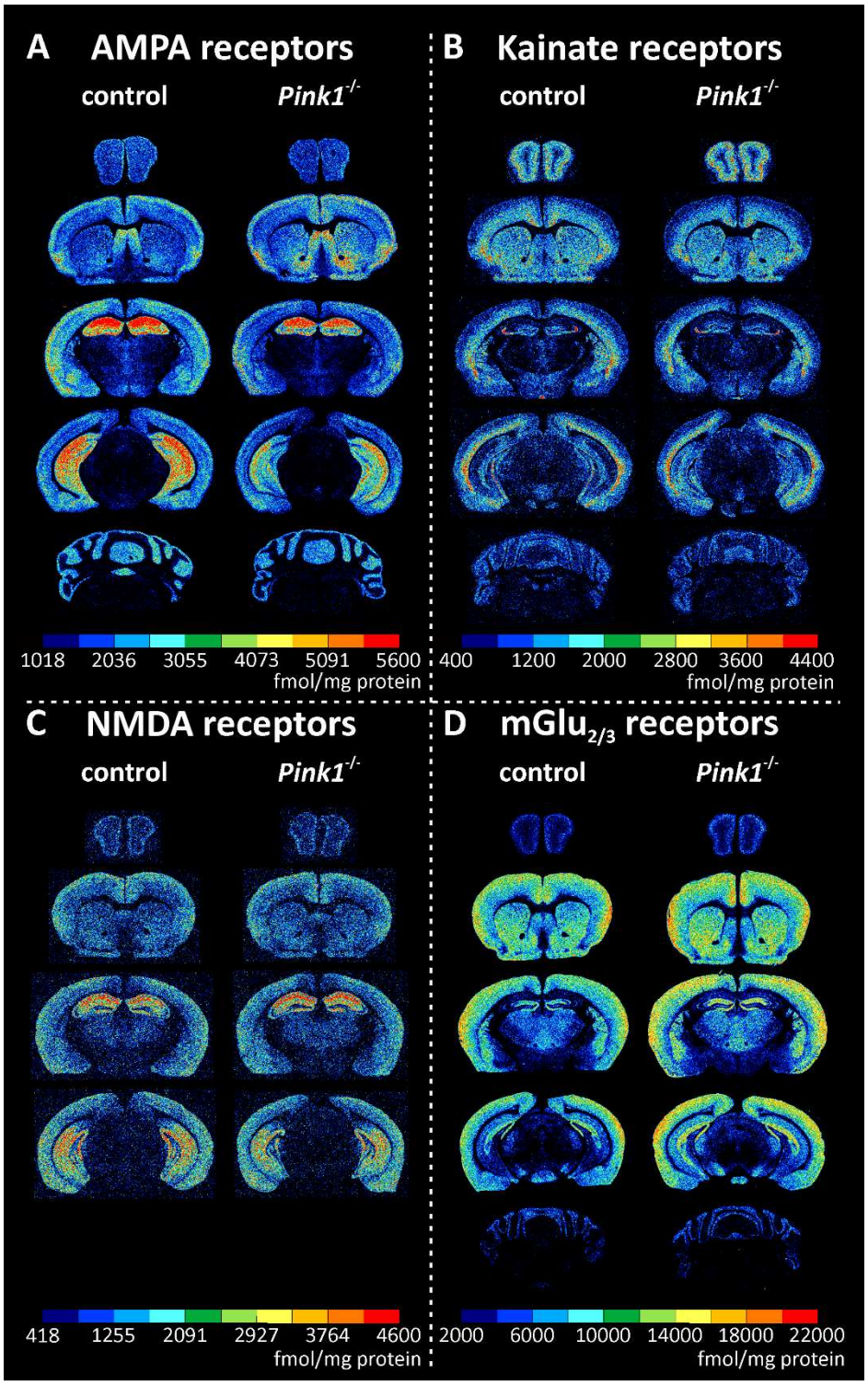

Fig. 8: Color-coded images showing the distribution pattern of glutamatergic receptor densities in different brain regions of control and *Pink1*$^{-/-}$ mice. Color scales code receptor densities in fmol/mg protein. **A**: Ligand: [^{3}H]AMPA; **B:** Ligand: [^{3}H]Kainic acid; **C**: Ligand: [^{3}H]MK-801; **D**: Ligand: [^{3}H]LY 341495

3.2.3. Acetylcholine receptors

M_1 receptors

M_1 receptor densities were below the detection limit in the cerebellum (Fig. 9A). They were low in the olfactory bulb and especially in the SN, whereas intermediate densities were found in the motor, somatosensory, and visual cortex, and in the CA2/3 region of the hippocampus. The highest densities were found in the striatum and in the hippocampal regions CA1 and DG. In general, M_1 receptor densities were higher in control mice than in *Pink1*$^{-/-}$ mice.

M_2 receptors

The muscarinic M_2 receptor was the only cholinergic receptor subtype found in the cerebellum, although densities were very low (Fig. 9B). Densities were low in all hippocampal regions and in the SN, while they were intermediate in the motor, somatosensory, and visual cortex, and highest in the olfactory bulb and striatum. Comparing both groups, M_2 receptor densities were more or less homogeneously distributed.

M_3 receptors

M_3 receptor densities were below the detection limit in the cerebellum (Fig. 9C). In general, the M_3 receptors showed the highest densities of all cholinergic receptors and their regional distribution was comparable to that of the M_1 receptor subtype. Thus, the lowest densities were found in the SN, followed by the olfactory bulb. The densities increased in the following order: hippocampal CA2/3 region, motor cortex, somatosensory cortex, visual cortex, hippocampal regions DG and then CA1, and finally striatum. In all ROIs, M_3 receptor density distribution was similar when comparing the two groups.

Nicotinic $\alpha_4\beta_2$ receptors

The nicotinic $\alpha_4\beta_2$ receptor densities were below the detection limit in the cerebellum (Fig. 9D). Densities were generally very low in both groups and showed the lowest densities of all cholinergic receptor subtypes. Whereas very low densities were found in the olfactory bulb and hippocampal regions CA1 and CA2/3, slightly higher densities were found in the SN and in the DG region of the hippocampus. Intermediate densities were found in the motor, somatosensory, and visual cortex, whereas the highest densities were found in the striatum. In all brain regions examined, densities were slightly higher in control mice than in *Pink1*$^{-/-}$ mice.

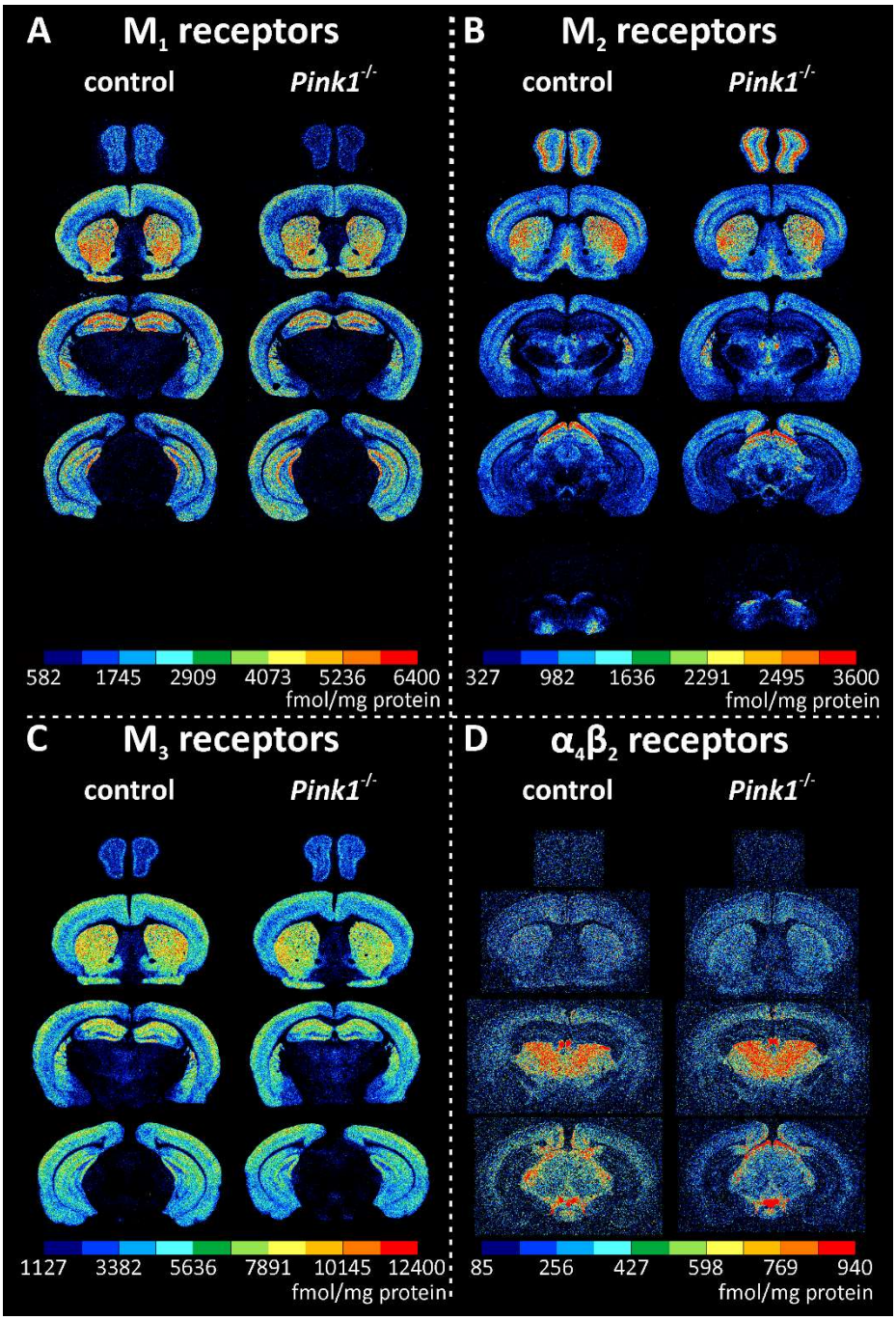

Fig. 9: Color-coded images showing the regional distribution pattern of cholinergic receptor densities in different brain regions of control and *Pink1*$^{-/-}$ mice. Color scales code receptor densities in fmol/mg protein. **A**: Ligand: [^{3}H]Pirenzepine; **B:** Ligand: [^{3}H]Oxotremorine-M; **C:** Ligand: [^{3}H]4-DAMP; **D:** Ligand: [^{3}H]Epibatidine

3.2.4. Adrenaline receptors

α_1 receptors

While α_1 receptor densities were low in the striatum, all hippocampal regions (CA1, CA2/3, and DG), SN, and cerebellum, they were comparatively higher in the olfactory bulb, and in the somatosensory and visual cortex (Fig. 10). The highest densities were found in the motor cortex. The α_1 receptor densities in *Pink1*$^{-/-}$ mice tended to be higher in the motor cortex and slightly lower in the striatum compared with control mice. All other brain areas examined appeared to show similar densities between the two groups.

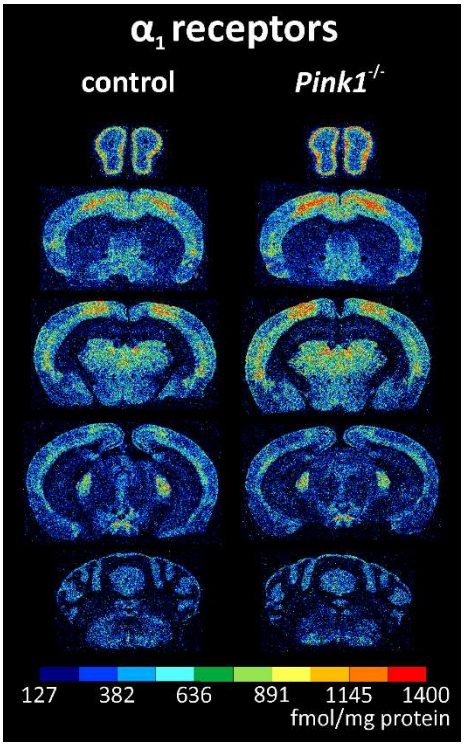

Fig. 10: Color-coded images showing the distribution pattern of α_1 receptor densities in different brain regions of control and *Pink1*$^{-/-}$ mice. Color scale codes receptor densities in fmol/mg protein. Ligand**:** [^{3}H]Prazosin

3.2.5. Dopamine receptors

D_1 receptors

D_1 receptor densities were below the detection limit in the hippocampus (Fig. 11A). Densities in the striatum were much higher than in other brain areas examined and tended to be higher in *Pink1*$^{-/-}$ than in control mice. The SN showed the second-highest D_1 receptor densities and tended to be lower in *Pink1*$^{-/-}$ than in control mice. In the olfactory bulb, motor, somatosensory, and visual cortex, and in the cerebellum, densities were very low and similar.

D_2 receptors

Because the striatum was the only brain region in which D_2 receptor densities were detectable, only exemplary color-coded images of the striatum are shown in Fig. 11B, where densities were similar between the two groups.

$D_{2/3}$ receptors

The densities of the dopaminergic $D_{2/3}$ receptor subtype were very low in the olfactory bulb, motor cortex, and somatosensory cortex, while they were much higher in the striatum (Fig. 11C). The densities were below the detection limit in all other ROIs. $D_{2/3}$ receptor densities were comparable between *Pink1*$^{-/-}$ and control mice.

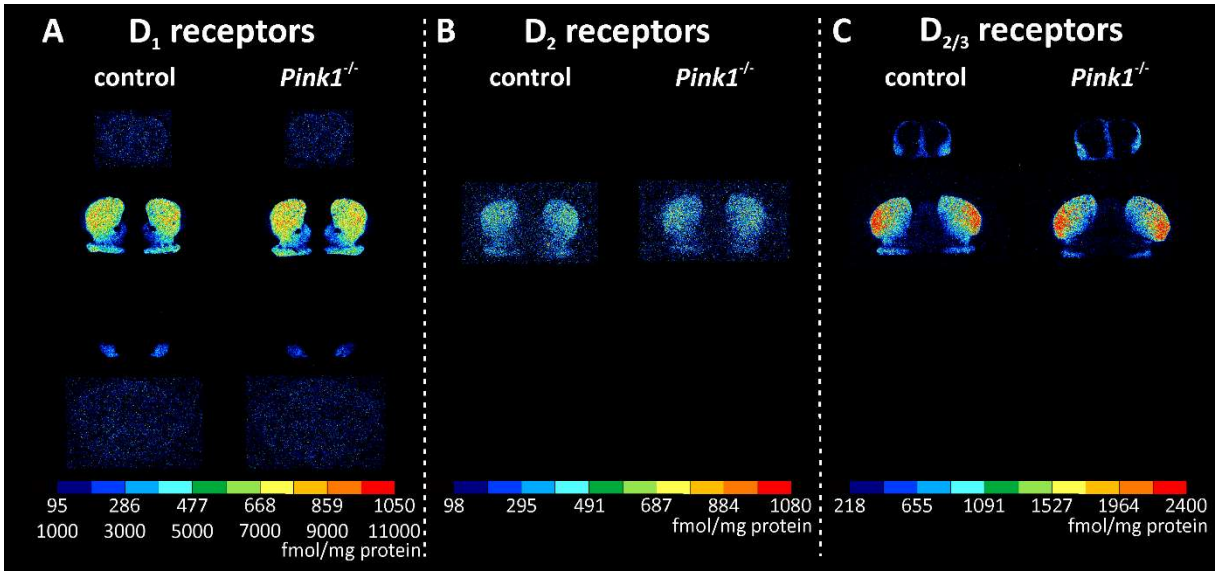

Fig. 11: Color-coded images showing the distribution pattern of dopaminergic receptor densities in different brain regions of control and *Pink1*$^{-/-}$ mice. Color scales code receptor densities in fmol/mg protein. Note that in **A** coding of color scales is shown separately for the striatum and SN (lower numbers) and other brain areas (upper numbers) due to the large difference in regional densities. **A**: Ligand: [^{3}H]SCH 23390; **B:** Ligand: [^{3}H]Raclopride; **C**: Ligand: [^{3}H]Fallypride.

3.2.6. Serotonin receptors

5-HT$_{1A}$ receptors

5-HT$_{1A}$ receptor densities were below the detection limit in the olfactory bulb and cerebellum. The densities were generally very low, except in the CA1 region of the hippocampus, where densities were much higher compared with the other ROIs (Fig. 12A). In all ROIs, densities tended to be higher in *Pink1*$^{-/-}$ than in corresponding control mice.

5-HT$_2$ receptors

As observed previously for the 5-HT$_{1A}$ receptor, the densities were generally very low (Fig. 12B). Compared with the other ROIs, slightly higher densities were found in the motor cortex, somatosensory cortex, and striatum. In all brain regions examined, there was a tendency toward higher 5-HT$_2$ receptor densities in *Pink1*$^{-/-}$ than in control mice.

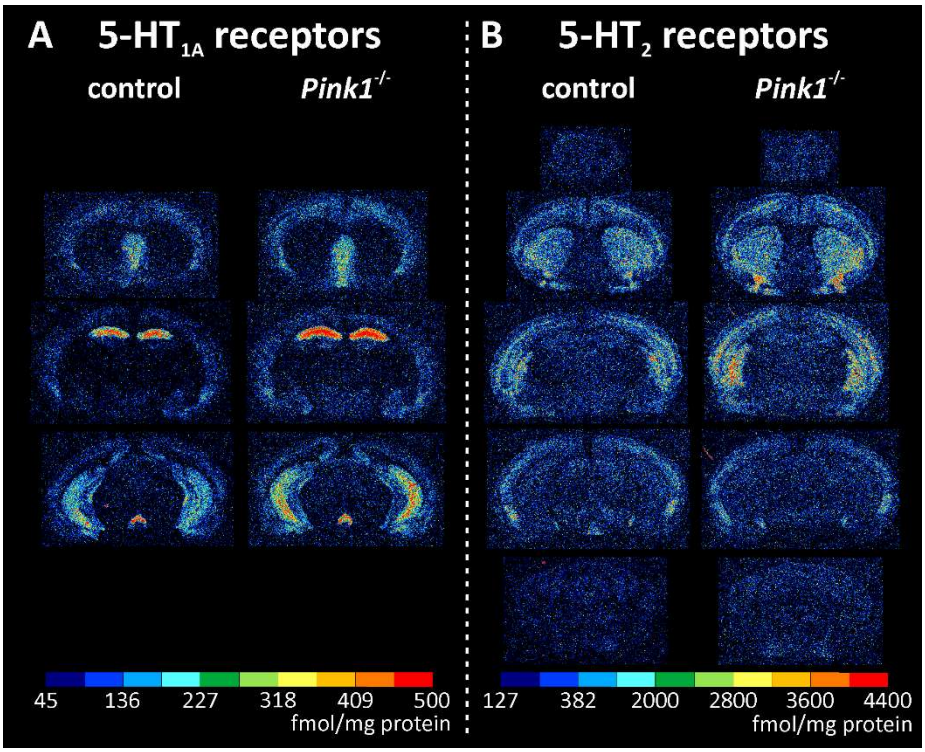

Fig. 12: Color-coded images showing the distribution pattern of serotonergic receptor densities in different brain regions of control and *Pink1*$^{-/-}$ mice. Color scales code receptor densities in fmol/mg protein. **A**: Ligand: [^{3}H]8-OH-DPAT; **B:** Ligand: [^{3}H]Ketanserin

3.2.7. Adenosine receptors

A_1 receptors

Low adenosine A_1 receptor densities were found in the olfactory bulb, which tended to be higher in *Pink1*$^{-/-}$ mice than control mice (Fig. 13A). In the motor cortex, striatum, hippocampal DG region, visual cortex, and cerebellum, similar and intermediate densities were found in both groups, whereas they were slightly higher in the somatosensory cortex. A_1 receptor densities in the SN were intermediate and tended to be lower in *Pink1*$^{-/-}$ mice. The highest densities were found in hippocampal regions CA1 and CA2/3, where densities tended to be higher in *Pink1*$^{-/-}$ than in control mice.

A_{2A} receptors

Comparable to the previously described D_2 receptor, the only brain area where A_{2A} receptors were detectable was the striatum, where densities were slightly higher in *Pink1*$^{-/-}$ mice than in control mice (Fig. 13B).

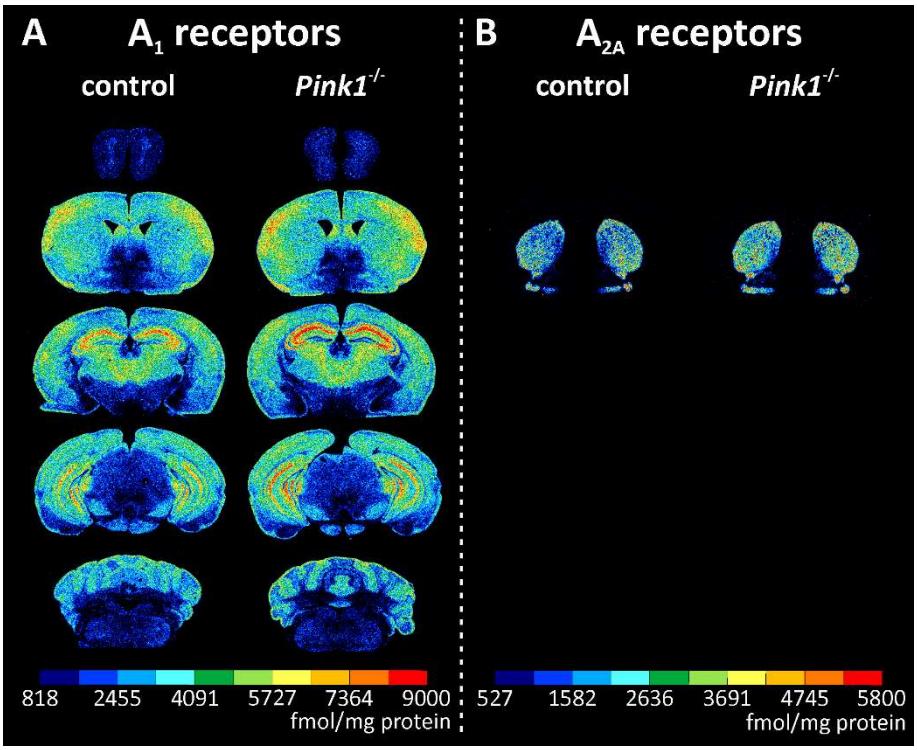

Fig. 13: Color-coded images showing the distribution pattern of adenosinergic receptor densities in different brain regions of control and *Pink1*$^{-/-}$ mice. Color scales code receptor densities in fmol/mg protein. **A**: Ligand: [^{3}H]DPCPX; **B:** Ligand: [^{3}H]ZM 241385

3.3. Quantification of neurotransmitter receptor densities

The receptor densities, mean densities ± standard deviations for each receptor subtype, animal group, and brain area (in the left and right hemisphere) are presented in Tables A5 – A42 (see Supplemental Data, Section 8.2.1.). The percentage differences that indicate increases or decreases in receptor densities between *Pink1*$^{-/-}$ and control mice are shown in Table 1.

Table 1: Percentage differences indicating a trend toward upregulated (positive percentages) or downregulated (negative percentages) mean receptor densities in *Pink1*$^{-/-}$ mice compared to control mice. Significant changes ($p<0.05$) are marked in green. Blank boxes (-) correspond to receptor densities that could not be evaluated in the respective brain area because they were below the detection limit.

		Brain areas						
		OB	**CA1**	**CA2/3**	**DG**	**M1**	**CPu**	**SN**
Neurotransmitter receptors	**M_1**	-13.4%	-7.3%	-11.3%	-8.8%	-8.9%	-7.4%	-3.6%
	M_2	2.9%	-1.5%	1.4%	1.0%	4.4%	2.8%	6.6%
	M_3	0.5%	-0.2%	-1.2%	-1.2%	-2.4%	-1.4%	-4.8%
	$\alpha_4\beta_2$	-5.2%	-3.5%	-7.1%	-5.1%	-2.0%	-1.4%	-2.7%
	A_1	7.2%	1.3%	3.0%	1.0%	2.8%	1.4%	-4.8%
	A_{2A}	-	-	-	-	-	4.0%	-
	α_1	1.8%	-2.1%	-2.7%	-2.6%	4.9%	-5.4%	-2.3%
	D_1	1.7%	-	-	-	0.2%	5.0%	-13.8%
	D_2	-	-	-	-	-	-1.9%	-
	$D_{2/3}$	-7.5%	-	-	-	-2.0%	2.1%	-
	$GABA_A$	-4.8%	19.1%	15.3%	15.7%	10.2%	11.8%	1.3%
	BZ	-1.1%	2.3%	1.1%	1.0%	6.1%	4.1%	0.7%
	$GABA_B$	-5.8%	-11.1%	-10.9%	-8.4%	-4.3%	-6.5%	-7.4%
	AMPA	-0.9%	-7.8%	-9.1%	-10.2%	3.4%	1.1%	-4.4%
	Kainate	3.2%	-1.1%	-2.3%	1.6%	-1.0%	-1.9%	-8.4%
	NMDA	1.2%	-0.5%	-0.1%	0.4%	1.9%	4.3%	2.1%
	$mGlu_{2/3}$	12.8%	16.3%	12.9%	10.3%	2.7%	6.6%	16.2%
	5-HT_{1A}	-	5.4%	4.5%	3.7%	6.9%	7.9%	3.7%
	5-HT_2	10.7%	6.6%	5.2%	0.8%	4.6%	5.2%	3.0%

3.3.1. GABA receptors

$GABA_A$ receptors

$GABA_A$ receptor densities varied from 832 fmol/mg protein (CA2/3, control) to 2640 fmol/mg protein (OB, *Pink1*$^{-/-}$). Statistical tests revealed significantly higher densities in the hippocampal CA1 region (19.1%; control: 1885 ± 386 fmol/mg protein; *Pink1*$^{-/-}$: 2245 ± 397 fmol/mg protein; $p<0.05$) of *Pink1*$^{-/-}$ mice compared to control mice. Although not statistically significant, there was a tendency for upregulated densities in the striatum (11.8%), the motor cortex (10.2%), and in the hippocampal regions CA2/3 (15.3%) and DG (15.7%) in *Pink1*$^{-/-}$ mice. Moreover, *Pink1*$^{-/-}$ mice exhibited a tendency of lower densities in the olfactory bulb (-4.8%). The results are summarized in Fig. 14 and Table 1.

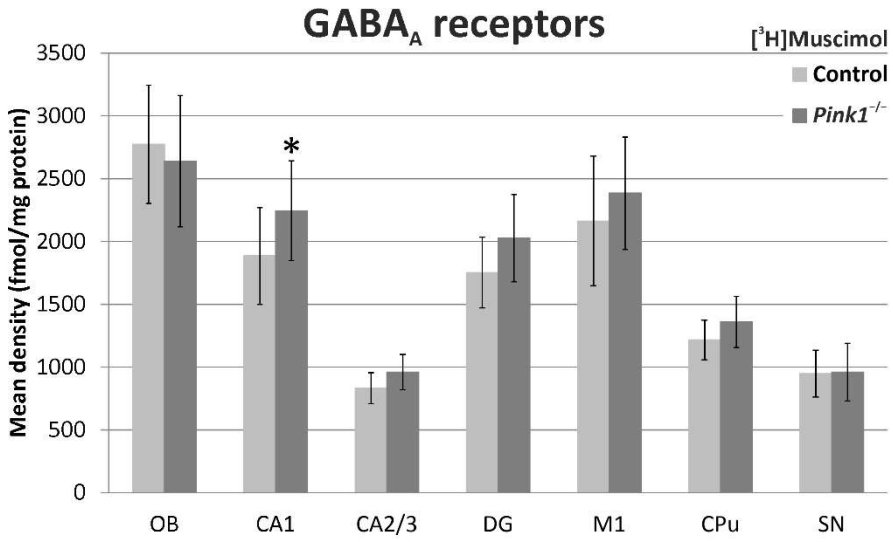

Fig. 14: Bar charts of mean $GABA_A$ receptor densities (fmol/mg protein) including standard deviation in brain regions of the limbic (OB, hippocampal regions CA1, CA2/3, and DG) and motor systems (M1, CPu, SN) of control (light gray) and *Pink1*$^{-/-}$ mice (dark gray). Significant differences are indicated by asterisks (*p<0.05 or **p<0.01). Ligand: [^{3}H]Muscimol

$GABA_A$-associated BZ binding sites

Mean $GABA_A$-associated BZ binding site densities ranged between 1006 fmol /mg protein (CPu, control) and 4963 fmol/mg protein (CA1, *Pink1*$^{-/-}$). No significant alterations in BZ binding site densities were found between *Pink1*$^{-/-}$ and control mice. However, the mean densities in the motor cortex tended to be upregulated by 6.1% in *Pink1*$^{-/-}$ mice. The results are summarized in Fig. A5A (see Supplemental Data, Section 8.2.3) and Table 1.

$GABA_B$ receptors

The mean $GABA_B$ receptor densities extended from 407 fmol/mg protein (OB, *Pink1*$^{-/-}$) to 1192 fmol/mg protein (DG, control). Statistical tests did not reveal significant alterations of $GABA_B$ receptor densities between *Pink1*$^{-/-}$ and control mice, although, in all ROIs, densities showed a trend toward downregulated densities in *Pink1*$^{-/-}$ mice (from -4.3% in the motor cortex to -11.1% in the hippocampal CA1 region). The results are summarized in Fig. A5B (see Supplemental Data, Section 8.2.3) and Table 1.

3.3.2. Glutamate receptors

AMPA receptors

Mean AMPA receptor densities were the lowest in SN (control: 453 fmol/mg protein; *Pink1*$^{-/-}$: 433 fmol/mg protein) and the highest in hippocampal region CA1 (control: 6034 fmol/mg protein; *Pink1*$^{-/-}$: 5564 fmol/mg protein). *Pink1*$^{-/-}$ mice exhibited a significant decrease in receptor densities in the hippocampal region CA1 (-7.8%; control: 6034 ± 991 fmol/mg protein; *Pink1*$^{-/-}$: 5564 ± 805 fmol/mg protein; p<0.01) compared to control mice. Although not significant, there was a trend toward downregulated densities in *Pink1*$^{-/-}$ mice in the hippocampal regions CA2/3 (-9.1%) and DG (-10.2%). The results are summarized in Fig. 15 and Table 1.

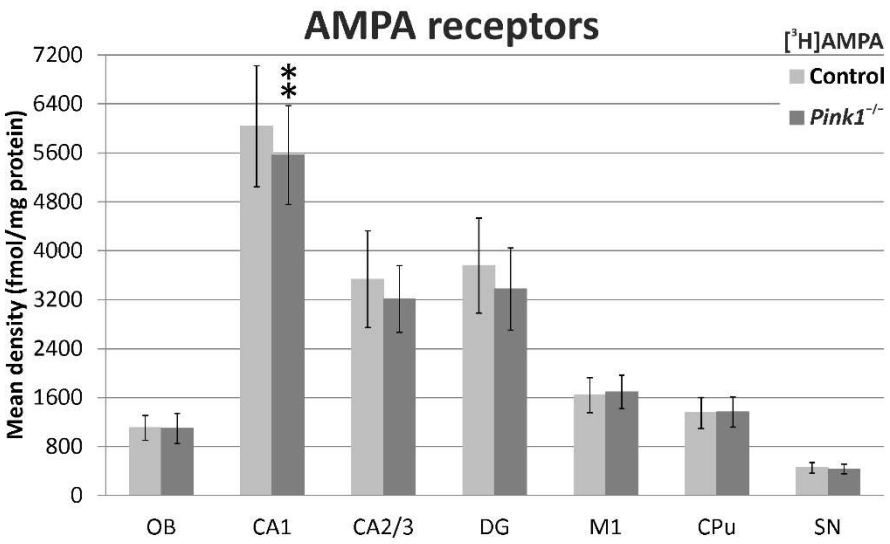

Fig. 15: Bar charts of mean AMPA receptor densities (fmol/mg protein) including standard deviation in brain regions of the limbic (OB, hippocampal regions CA1, CA2/3, and DG) and motor systems (M1, CPu, SN) of control (light gray) and *Pink1*$^{-/-}$ mice (dark gray). Significant differences are indicated by asterisks (*p<0.05 or **p<0.01). Ligand: [^{3}H]AMPA

Kainate receptors

The range of kainate receptor densities extended from 299 fmol/mg protein (SN, *Pink1*$^{-/-}$) to 1797 fmol/mg protein (OB, *Pink1*$^{-/-}$). Statistical tests revealed a significant decrease in the SN (-8.4%; control: 3264 ± 394 fmol/mg protein; *Pink1*$^{-/-}$: 2991 ± 365 fmol/mg protein; p<0.01) of *Pink1*$^{-/-}$ mice compared to control mice. The results are summarized in Fig. 16 and Table 1.

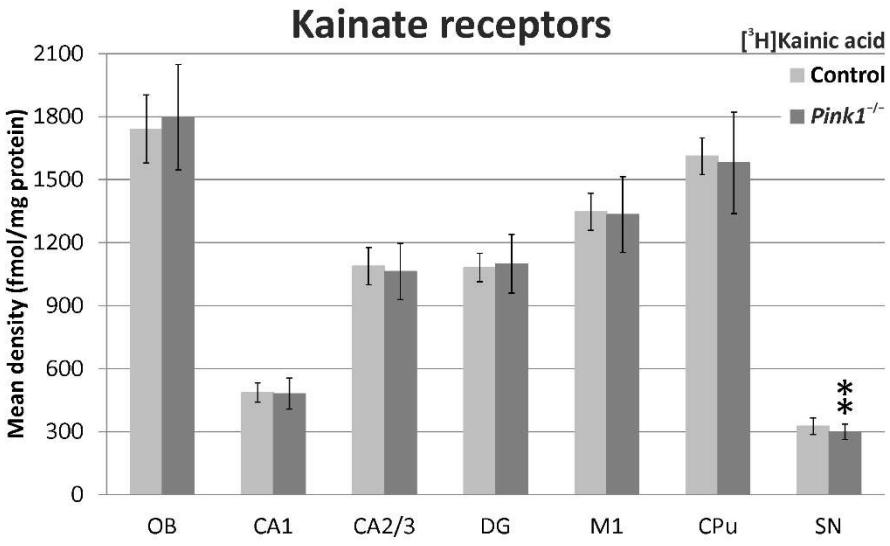

Fig. 16: Bar charts of mean kainate receptor densities (fmol/mg protein) including standard deviation in brain regions of the limbic (OB, hippocampal regions CA1, CA2/3, and DG) and motor systems (M1, CPu, SN) of control (light gray) and *Pink1*$^{-/-}$ mice (dark gray). Significant differences are indicated by asterisks (*p<0.05 or **p<0.01). Ligand: [^{3}H]Kainic acid

NMDA receptors

The lowest NMDA receptor densities were found in the SN (control: 291 fmol/mg protein; *Pink1*$^{-/-}$: 297 fmol/mg protein) and the highest in hippocampal region CA1 (control: 4229

fmol/mg protein; *Pink1*$^{-/-}$: 4208 fmol/mg protein). There were no significant alterations between the NMDA receptor densities of *Pink1*$^{-/-}$ mice and control mice. The results are summarized in Fig. A6 (see Supplemental Data, Section 8.2.3) and Table 1.

mGlu$_{2/3}$ receptors

Mean mGlu$_{2/3}$ receptor densities varied from 2101 fmol/mg protein (CA2/3, control) to 9638 fmol/mg protein (M1, *Pink1*$^{-/-}$). Statistical tests showed a significant increase of mGlu$_{2/3}$ receptor densities in *Pink1*$^{-/-}$ mice compared to the corresponding control mice in hippocampal regions CA1 (16.3%; control: 3105 ± 513 fmol/mg protein; *Pink1*$^{-/-}$: 3611 ± 551 fmol/mg protein; p<0.01) and DG (10.3%; control: 8583 ± 959 fmol/mg protein; *Pink1*$^{-/-}$: 9468 ± 1019 fmol/mg protein; p<0.01), and in the SN (16.2%; control: 3525 ± 580 fmol/mg protein; *Pink1*$^{-/-}$: 4096 ± 587 fmol/mg protein; p<0.01). Although no statistical significances were found in the other ROIs, all tended to be upregulated in *Pink1*$^{-/-}$ mice. The results are summarized in Fig. 17 and Table 1.

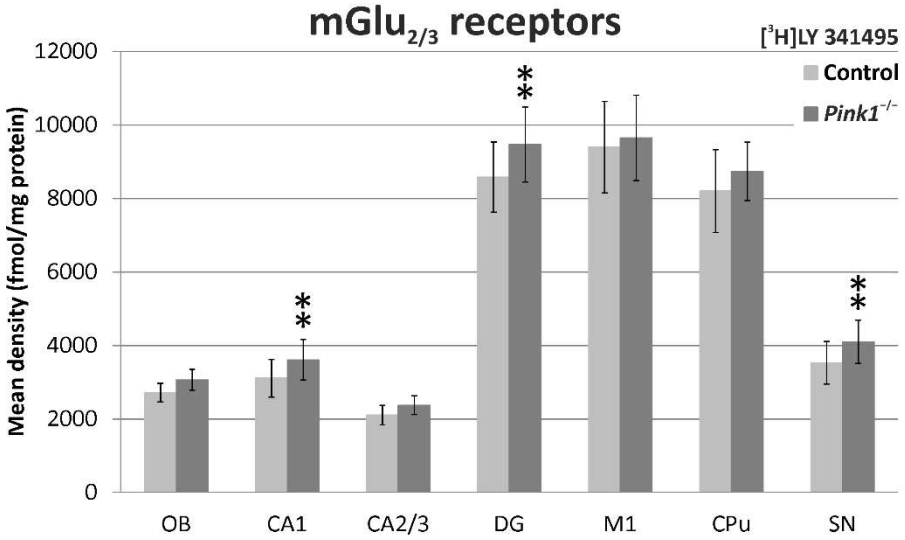

Fig. 17: Bar charts of mean mGlu$_{2/3}$ receptor densities (fmol/mg protein) including standard deviation in brain regions of the limbic (OB, hippocampal regions CA1, CA2/3, and DG) and motor systems (M1, CPu, SN) of control (light gray) and *Pink1*$^{-/-}$ mice (dark gray). Significant differences are indicated by asterisks (*p<0.05 or **p<0.01). Ligand: [^{3}H]LY 341495

3.3.3. Acetylcholine receptors

M$_1$ receptors

Mean muscarinic M$_1$ receptor densities ranged from 358 fmol/mg protein (SN, *Pink1*$^{-/-}$) to 5248 fmol/mg protein (DG, control). Significant decreases in receptor densities were found in the hippocampal CA1 (-7.3%; control: 4698 ± 1167 fmol/mg protein; *Pink1*$^{-/-}$: 4354 ± 1458 fmol/mg protein; p<0.05) and DG (-8.8%; control: 5248 ± 1295 fmol/mg protein; *Pink1*$^{-/-}$: 4789 ± 1636 fmol/mg protein; p<0.05) regions of *Pink1*$^{-/-}$ mice compared to control mice. In all regions analyzed, M$_1$ receptor densities tended to be lower in *Pink1*$^{-/-}$ mice than in control mice. The results are summarized in Fig. 18 and Table 1.

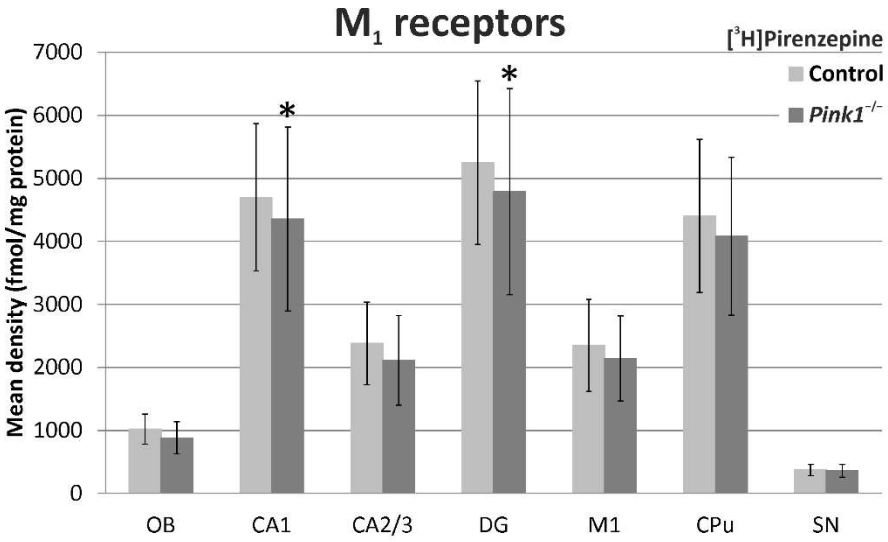

Fig. 18: Bar charts of mean M_1 receptor densities (fmol/mg protein) including standard deviation in brain regions of the limbic (OB, hippocampal regions CA1, CA2/3, and DG) and motor systems (M1, CPu, SN) of control (light gray) and *Pink1*$^{-/-}$ mice (dark gray). Significant differences are indicated by asterisks (*p<0.05 or **p<0.01). Ligand: [^{3}H]Pirenzepine

M_2 receptors

The range of M_2 receptor densities extended from 417 fmol/mg protein (DG, control) to 2804 fmol/mg protein (CPu, *Pink1*$^{-/-}$). Within the brain regions analyzed, densities were more or less homogeneously distributed between the two groups. Thus, no significant alterations in M_2 receptor densities were found between *Pink1*$^{-/-}$ and control mice. The results are summarized in Fig. A7A (see Supplemental Data, Section 8.2.3) and Table 1.

M_3 receptors

M_3 receptor densities ranged from 607 fmol/mg protein (SN, *Pink1*$^{-/-}$) to 8585 fmol/mg protein (CPu, control). Statistical tests did not reveal significant differences between densities of *Pink1*$^{-/-}$ and control mice in the investigated brain regions. The results are summarized in Fig. A7B (see Supplemental Data, Section 8.2.3) and Table 1.

Nicotinic $\alpha_4\beta_2$ receptors

The mean densities of the nicotinic $\alpha_4\beta_2$ receptor ranged from 106 fmol/mg protein (CA2/3, control) to 325 fmol/mg protein (CPu, control). In contrast to other cholinergic receptors, nicotinic $\alpha_4\beta_2$ receptor densities were generally low. In all ROIs, the mean densities were lower in *Pink1*$^{-/-}$ than in control mice. Nevertheless, statistical tests revealed no significant difference between the two groups. The results are summarized in Fig. A7C (see Supplemental Data, Section 8.2.3) and Table 1.

3.3.4. Adrenaline receptors

α_1 receptors

Mean α_1 receptor densities ranged from 122 fmol/mg protein (CA2/3, *Pink1*$^{-/-}$) to 567 fmol/mg protein (OB, *Pink1*$^{-/-}$). No significant differences in α_1 receptor densities were observed in the brain regions examined of *Pink1*$^{-/-}$ mice compared to control mice. However, when comparing

the two groups, a tendency for higher densities was found in the motor cortex (4.9%), while they tended to be lower in the striatum (-5.4%) of *Pink1*$^{-/-}$ mice. In all other ROIs, densities were approximately equal. The results are summarized in Fig. A8 (see Supplemental Data, Section 8.2.3) and Table 1.

3.3.5. Dopamine receptors

D_1 receptors

D_1 receptor densities were below the detection limit in the hippocampus. The mean densities extended from 103 fmol/mg protein (OB, control) to 5994 fmol/mg protein (CPu, *Pink1*$^{-/-}$). Statistical tests revealed a significant decrease of D_1 receptor densities in the SN (-13.8%; control: 2292 ± 483 fmol/mg protein; *Pink1*$^{-/-}$: 1976 ± 344 fmol/mg protein; $p<0.01$) of *Pink1*$^{-/-}$ mice compared to control mice. Although no other significant differences were found, there was a trend toward higher densities in the striatum (5%) of *Pink1*$^{-/-}$ compared to control mice. In general, densities in the striatum were up to 58 times higher than in other brain areas examined. The results are summarized in Fig. 19 and Table 1.

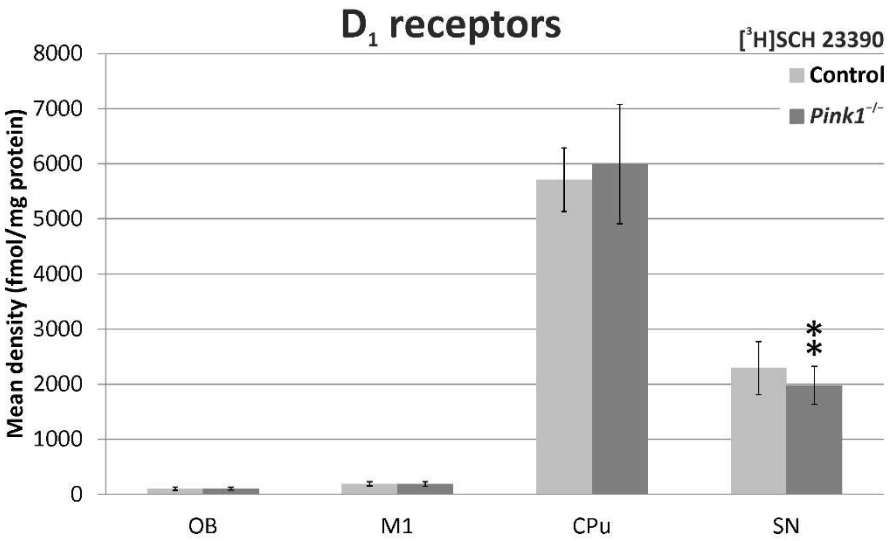

Fig. 19: Bar charts of mean D_1 receptor densities (fmol/mg protein) including standard deviation in brain regions of the limbic (OB) and motor systems (M1, CPu, SN) of control (light gray) and *Pink1*$^{-/-}$ mice (dark gray). Significant differences are indicated by asterisks (*p<0.05 or **p<0.01). Ligand: [^{3}H]SCH 23390

D_2 receptors

D_2 receptor densities were only detectable in the striatum, where densities were similar between *Pink1*$^{-/-}$ mice (408 fmol/mg protein) and control mice (416 fmol/mg protein). Hence, statistical tests revealed no significant differences in the D_2 receptor densities between the two groups. The results are summarized in Fig. A9A (see Supplemental Data, Section 8.2.3) and Table 1.

$D_{2/3}$ receptors

The $D_{2/3}$ receptor densities were below the detection limit in the hippocampal regions CA1, CA2/3, and DG, and in the SN. Mean densities were exceptionally higher in the striatum than in the olfactory bulb and motor cortex. There was no significant difference in densities

between *Pink1*$^{-/-}$ and control mice, although densities in the olfactory bulb tended to be downregulated by -7.5% in *Pink1*$^{-/-}$ mice. $D_{2/3}$ receptor densities in the striatum were up to 20 times higher compared with the other brain regions. The results are summarized in Fig. A9B (see Supplemental Data, Section 8.2.3) and Table 1.

3.3.6. Serotonin receptors

5-HT$_{1A}$ receptors

5-HT$_{1A}$ receptor densities were below the detection limit in the olfactory bulb. Densities were generally below 83 fmol/mg protein, except in the hippocampal region CA1 (control: 383 fmol/protein; *Pink1*$^{-/-}$:403 fmol/mg protein). No significant differences were found in the brain regions analyzed between *Pink1*$^{-/-}$ mice and control mice, although densities tended to be slightly higher in *Pink1*$^{-/-}$ mice in all ROIs. The results are summarized in Fig. A10A (see Supplemental Data, Section 8.2.3) and Table 1.

5-HT$_2$ receptors

The mean 5-HT$_2$ receptor densities extended from 157 fmol/mg protein (OB, control) to 570 fmol/mg protein (CPu, *Pink1*$^{-/-}$). In all brain areas analyzed, mean densities tended to be slightly higher in *Pink1*$^{-/-}$ than in control mice, however, statistical tests revealed no significant alterations. The results are summarized in Fig. A10B (see Supplemental Data, Section 8.2.3) and Table 1.

3.3.7. Adenosine receptors

A$_1$ receptors

The mean A_1 receptor densities ranged from 976 fmol/mg protein (OB, control) to 7217 fmol/mg protein (CA1, *Pink1*$^{-/-}$). Statistical tests revealed no significant differences in densities between *Pink1*$^{-/-}$ and control mice in the brain regions examined. However, a tendency of higher mean densities was found in the olfactory bulb (7.2%) of *Pink1*$^{-/-}$ mice, while they tended to be lower in the SN (-4.8%). The results are summarized in Fig. A11A (see Supplemental Data, Section 8.2.3) and Table 1.

A$_{2A}$ receptors

Regarding A_{2A} receptors, all ROIs were below the detection limit, with the sole exception of the striatum, where no significant alterations were observed between *Pink1*$^{-/-}$ mice and control mice. However, there was a trend toward higher densities in *Pink1*$^{-/-}$ mice (4%; control: 2420 fmol/mg protein; *Pink1*$^{-/-}$: 2517 fmol/mg protein). The results are summarized in Fig. A11B (see Supplemental Data, Section 8.2.3) and Table 1.

4. Discussion

The present study focused on the molecular mechanisms of PD by investigating alterations of 19 different receptor binding sites of seven neurotransmitter systems (GABA, glutamate, acetylcholine, dopamine, serotonin, and adenosine) by means of quantitative *in vitro* receptor autoradiography in an established mouse model of the prodromal phase of early-onset PD, *Pink1*$^{-/-}$ mice, and in corresponding control mice. Several significant alterations or tendencies for down- and upregulated receptors in different brain areas of the limbic (olfactory bulb, hippocampal regions CA1, CA2/3, and DG) and motor systems (motor cortex, striatum, and SN) were found in the neurotransmitter receptors investigated.

4.1. GABA receptors

$GABA_A$ receptor densities were significantly increased by 19.1% in the hippocampal CA1 region of *Pink1*$^{-/-}$ mice. The hippocampus is involved in episodic memory (the what, where, and when memory) and possibly in their long-term storage, which is thought to be mediated at least partly by synaptic plasticity (52). In general, $GABA_A$ receptors mediate fast hyperpolarization by inhibition of neuronal excitability via their Cl^- channels and are involved in memory processes, anxiety, and induction of seizures (53). Recently, a magnetic resonance spectroscopy study demonstrated a correlation between decreased GABA levels in the hippocampus and cognitive impairments of patients with relapsing-remitting multiple sclerosis (54). As cognitive impairments have also been observed in PD patients (55), which affects approximately 20 to 50% of PD patients and varies from subtle cognitive changes to dementia (55), there may be an association with the changes in $GABA_A$ receptor densities observed in the present study. Thus, we propose that the increased receptor densities in this mouse model of the prodromal phase of PD may be a compensatory mechanism for potentially decreased GABA levels. Therefore, it would be interesting for a future study to analyze both GABA levels and active GABA receptors in 3-month-old but also in aged *Pink1*$^{-/-}$ mice, e.g. by microdialysis, a method to study extracellular neurotransmitter levels, and receptor autoradiography, respectively, because reduced inhibition could enhance overall excitability which goes along with increased oxidative stress and neuronal functional impairment. In addition, behavioral tests should be considered to test correlations between GABA levels and GABA receptor densities with memory impairments. Depending on the modulation of GABA action, memory can be either impaired or improved (56). Thus, treatment options that modulate GABA neurotransmission may be appropriate for cognitively impaired PD patients.

$GABA_B$ receptor densities using the antagonist [^{3}H]CGP 54626 tended to be downregulated in all ROIs (between -4.3% in the motor cortex and -11.1% in the hippocampal region CA1) of *Pink1*$^{-/-}$ mice. This is in contrast to our previous results in the PD models of *Parkin*, *DJ-1*, and *Pitx3*^{ak} mice (13, 14), where significantly increased densities were found in several brain regions. Although these decreased densities were not statistically significant, this may be an indication that *Pink1* and its loss or disturbance may affect $GABA_B$ receptors in a way that has

not yet been described in the literature, but would be interesting to investigate in future studies.

4.2. Glutamate receptors

AMPA receptor densities were significantly decreased in the CA1 region of the hippocampus (-7.8%) of *Pink1*$^{-/-}$ mice and tended to be decreased in its CA2/3 (-9.1%) and DG region (-10.2%). This is in accordance with our previous study, in which these brain regions were significantly decreased in *Parkin* knockout mice (14). AMPA receptors mediate fast excitatory neurotransmission in the CNS and are involved in synaptic plasticity, particularly in the long-term potentiation that strengthens synapses (57). A balance between the most prominent inhibitory neurotransmitter GABA and the most prominent excitatory neurotransmitter glutamate is crucial for normal brain function (58). The decreased AMPA receptor densities contrast with the described increased $GABA_A$ receptor densities in the hippocampus of *Pink1*$^{-/-}$ mice, indicating an imbalance in the GABA-glutamate system. Therefore, we hypothesize that similar to the increased $GABA_A$ receptor densities, the decreased AMPA receptor densities might be related to the cognitive impairments of PD patients. In this case, treatment of cognitively impaired PD patients with AMPA receptor potentiators that bind to allosteric sites on AMPA receptors to slow the desensitization, which in turn increases AMPA receptor signaling, may be beneficial. However, to restore the balance between GABA and glutamate, new treatments must be found that take both systems into account.

Kainate receptor densities were significantly downregulated by -8.4% in the SN of *Pink1*$^{-/-}$ mice compared to control mice. In contrast, in our previous study, *Parkin* and *DJ-1* knockout mice showed significantly increased kainate receptor densities in several cortical areas, which was thought to reflect kainate-mediated excitotoxicity (14). However, kainate receptors promote not only excitotoxicity but also microglial activation, synaptic stripping, and neuroinflammation, all of which are known in PD to contribute to the progression of neurodegeneration in the SN (4, 59). We hypothesize that the decreased kainate receptor densities in *Pink1*$^{-/-}$ mice, as a model for the prodromal phase of PD in which neurodegeneration in the SN may not yet be profound, is kept low here by compensatory mechanisms, e.g. by upregulation of $mGlu_{2/3}$ receptors (4). However, it is important to note that kainate receptors differ functionally depending on whether they are located presynaptically, postsynaptically, or at extrasynaptic sites. Whereas presynaptic kainate receptors play a modulatory role in both excitatory and inhibitory neurotransmission, postsynaptic ones play a role in excitatory neurotransmission, and extrasynaptic ones are involved in determining the excitability of neurons (60). Because our chosen method, *in vitro* receptor autoradiography, cannot distinguish between presynaptic, postsynaptic, and extrasynaptic receptors, a different experimental approach, e.g. by electrophysiological studies, must be performed in a future study to prove our hypothesis.

Pink1$^{-/-}$ mice exhibited significant increases in **$mGlu_{2/3}$ receptor** densities in the hippocampal CA1 and DG regions and in the SN. In general, $mGlu_{2/3}$ receptors are involved in spatial memory

formation in the hippocampus by modulating synaptic plasticity, specifically by stimulating long-term depression of excitatory synaptic transmission (33). They also play a key role in reducing glutamate-mediated excitotoxicity by inhibiting glutamate release from axon terminals (4). Therefore, the increase in $mGlu_{2/3}$ receptor densities may reflect a mechanism that attempts to reduce the activation of ionotropic glutamate receptors (i.e. AMPA, kainate, and NMDA) and thereby reducing their excitotoxic effects. LY 341,495, which was used in the present study, is a competitive $mGlu_{2/3}$ receptor antagonist that binds to the same binding site as agonists without activating the receptor, thereby blocking the action of the agonist (61). As previously shown, LY 341,495 can be displaced by the orthosteric agonist LY-354,740, both of which bind with high affinity to the $mGlu_{2/3}$ receptor (61). Recently, activation of the $mGlu_{2/3}$ receptor with the agonist LY-354,740 (or eglumegad) was shown to reduce both L-DOPA-induced dyskinesia and psychosis-like behaviors in an animal model of PD (62). This makes the $mGlu_{2/3}$ receptor a promising target for novel therapeutic applications that may help alleviate motor and non-motor symptoms in PD patients.

4.3. Acetylcholine receptors

Lower densities of the **nicotinic $\alpha_4\beta_2$ receptor** were previously found in the cortex, hippocampus, SN, and striatum of PD patients using *in vitro* receptor autoradiography on postmortem brain tissue (63, 64). It was hypothesized that decreased nicotinic receptors, which are frequently found in PD patients with cognitive and depressive symptoms, correlate with nigrostriatal neurodegeneration. For instance, it was demonstrated that smoking reduces the risk of developing PD and that nicotine treatment has neuroprotective effects (65). In addition, dopaminergic neurons in the putamen (part of the striatum) were demonstrated to be partially activated by nicotinic cholinergic neurons via the β_2-subunit of their receptor (10). Thus, nicotinic acetylcholine receptors could be potential targets for new treatment strategies of PD, for example, by investigating the therapeutic benefit of agonists of the β_2-containing nicotinic receptors. Because the present study found no statistically significant changes in *Pink1*$^{-/-}$ mice, a mouse model known to lack neurodegeneration in SN, our results may further support the aforementioned hypothesis.

Muscarinic M_1 receptors are highly expressed in the hippocampus and are crucial for neuronal excitability, synaptic plasticity, and cognitive function (e.g. attention and information processing) (66, 67). Consequently, M_1 receptor dysfunction is associated with mild cognitive impairments in PD patients and other neurodegenerative diseases such as Alzheimer's (67). Our results are consistent with these observations, as *Pink1*$^{-/-}$ mice exhibited a significant decrease in M_1 receptor densities in the hippocampal CA1 (-7.3%) and DG (-8.8%) regions. As previously shown, activation of M_1 receptors with the selective allosteric agonist GSK1034702 may improve memory encoding, presumably due to modulation of hippocampal function, which may be a treatment strategy for cognitively impaired AD and PD patients (66, 68). However, more studies are needed to confirm the benefit of M_1 receptor activation. M_1 receptor densities in the olfactory bulb of *Pink1*$^{-/-}$ mice, although not significantly altered, tended to be downregulated by -13.4% (1021 ± 238 fmol/mg protein in control mice versus

884 ± 251 fmol/mg protein in *Pink1*$^{-/-}$ mice). The olfactory bulb is a brain area potentially involved in olfactory dysfunction, a non-motor symptom that was found in aged *Pink1*$^{-/-}$ mice (26) and PD patients (9). Olfactory dysfunction is often the first (non-motor) feature of PD that affects approximately 50 to 90% of patients and is associated with altered acetylcholine levels. This in turn is related to the nucleus basalis of Meynert, which is usually rich in acetylcholine but is affected by neurodegeneration in PD (9). Thus, the described tendency of downregulated M_1 receptor densities in the olfactory bulb may indicate an association with olfactory dysfunction.

4.4. Adrenaline receptors

The α_1 receptor plays important roles in olfaction, cognitive functions (e.g. regulating synaptic plasticity and memory), and in the regulation of dopaminergic neurotransmission (36). Noradrenaline is mainly synthesized in the locus coeruleus, which is impaired by neurodegeneration in PD patients, consequently leading to lower levels of noradrenaline (37, 38). This loss was associated with several motor and non-motor symptoms of PD. Interestingly, α_1 receptor densities tended to be slightly upregulated in the motor cortex (4.9%), whereas they tended to be slightly downregulated in the striatum (-5.4%) of *Pink1*$^{-/-}$ mice, although statistical tests found no significances. Nevertheless, while the reduced expression of α_1 receptors may be in line with depression, psychosis, and motor deficits in PD, the higher expression may be a compensatory mechanism in this prodromal phase of PD for reduced noradrenergic innervation in the motor cortex (69), a brain region involved in planning and control of voluntary movements.

4.5. Dopamine receptors

D_1 receptor densities were significantly decreased by -13.8% in the SN of *Pink1*$^{-/-}$ mice. In general, dopaminergic D_1 receptors are involved in locomotor activity, thus the motion and movement needed to change places, and in learning and memory (39). One of the pathological hallmarks of PD is the progressive degeneration of dopaminergic neurons in the SN, resulting in decreased levels of dopamine in the striatum, which causes major motor symptoms (12). However, dopamine levels in PD patients not only decrease in the striatum but also in the SN as previously demonstrated by Gröger et al. (2014), using magnetic resonance spectroscopy (70), which also supports our findings of decreased D_1 receptor densities. By using immunohistochemical staining for TH as a marker of dopaminergic neurons, a decrease of 25% and 50% was observed in the SN of 6- and 8-month-old *Pink1* knockout rats, respectively, which was accompanied by impairments in motor behavior (71). In contrast, immunohistochemical staining for TH in the SN of *Pink1*$^{-/-}$ mice showed no differences in the number of TH-positive neurons in 3-month-old (present study), as well as in 6- and 19-month-old mice (26). It was hypothesized that rats with *Pink1* deficiency are more susceptible to age-related oxidative stress than mice as a result of impaired mitochondrial dynamics (71). Indeed, the lack of significant degeneration of dopamine-producing neurons in our mouse model is in line with other knockout mouse models of *Pink1* (72, 73) and may also account for their lack

of major motor symptoms, although subtle gait impairments were found in aged mice (26). Even if neurodegeneration in *Pink1*$^{-/-}$ mice is not significant, the alterations in D_1 receptor densities highlight that the dopaminergic receptor system is already changing in the prodromal phase of PD, independent of the extent of neurodegeneration.

4.6. Serotonin receptors

In *Pink1*$^{-/-}$ mice, both **5-HT$_{1A}$ receptor** and **5-HT$_2$ receptor** densities tended to be higher than in control mice in all brain regions analyzed, however, statistical tests did not reveal any significance. Both receptor subtypes are involved in the modulation of glutamatergic and dopaminergic neurotransmission and are altered in various diseases such as anxiety, depression, and schizophrenia (41). Regarding PD, both increased and decreased 5-HT$_{1A}$ and 5-HT$_2$ receptor levels were found in PD patients, which also depended in part on whether they were already treated, on their respective symptoms, and the brain areas analyzed (41). Moreover, immunohistochemical staining showed that aged *Pink1*$^{-/-}$ mice (19 months) had reduced density of serotonergic fibers in the glomerular layer of the olfactory bulb, which may be related to the observed olfactory dysfunctions of aged *Pink1*$^{-/-}$ mice (26). Taken together, these data highlight a potentially important role of both receptor subtypes in PD and suggest the possibility that their densities may change significantly in aged *Pink1*$^{-/-}$ mice. Therefore, the 3-month-old *Pink1*$^{-/-}$ mice analyzed in the present study may have been too young to develop significant alterations. Whether there is a link between altered serotonergic receptors to olfactory dysfunction and mood changes, could be analyzed in aged *Pink1*$^{-/-}$ mice in a future study.

4.7. Adenosine receptors

Pink1$^{-/-}$ mice showed a tendency toward downregulated **A_1 receptor** densities in the SN (-4.8%), although no significances were found (p=0.0733). Inhibitory A_1 receptors were associated with neuroprotective effects, but their sustained activation is thought to promote neurodegeneration by cross-talk with excitatory A_{2A} receptors (42). Whether the decreased densities in the SN are due to possible degenerations of adenosinergic neurons or due to compensatory mechanisms to counteract neurodegeneration cannot be interpreted from the present data but would be an interesting subject for a future study.

5. Conclusion and Synthesis

Parkinson's disease is the second most common neurodegenerative disease. The progression of PD is linked to the ongoing degeneration of neurons and consequently with the continuing loss of synapses and neurotransmitters (74). Neurodegeneration and some non-motor symptoms occur before the onset of cardinal motor symptoms and thus before the clinical diagnosis of PD. To date, no treatment is known to halt the progression of the disease, and those that are available mostly alleviate the motor but not the non-motor symptoms. The majority of studies in the past focused on alterations in the dopaminergic system, although recent studies suggested an association between both motor and non-motor symptoms of PD and alterations in non-dopaminergic systems. However, there is still a large gap of knowledge in understanding the underlying mechanisms between non-dopaminergic receptor alterations and the pathogenesis of PD.

Therefore, the present study aimed to perform a comparative analysis of neurotransmitter receptor densities of seven neurotransmitter systems as well as their regional distribution in an established mouse model of the prodromal phase of early-onset PD*, Pink1*$^{-/-}$ mice, and corresponding control mice. We also aimed to discuss the possible link between receptor alterations and functional or pathological changes. We hypothesized that alterations in neurotransmitter receptors in functional systems are already present in the prodromal phase of PD.

The present study found evidence for this hypothesis by describing alterations in both dopaminergic and non-dopaminergic receptors in 3-month-old *Pink1*$^{-/-}$ mice compared to corresponding control mice. Most notably, $GABA_A$ receptor densities were significantly increased, whereas AMPA receptor densities were significantly decreased in the hippocampal CA1 region. These changes may be associated with cognitive impairments seen in PD patients, due to the role of the receptors in synaptic plasticity. The balance between GABA and glutamate in the brain is crucial for normal brain functioning, and imbalances have been reported for several neurological and psychiatric diseases (58). Therefore, new treatment options need to be found to restore the balance between GABA and glutamate in PD. Regarding the kainate receptor, densities were significantly downregulated in the SN of *Pink1*$^{-/-}$ mice, whereas $mGlu_{2/3}$ receptor densities were significantly upregulated in this brain area. It was suggested that compensatory mechanisms in the brain might protect from the progression of neurodegenerative diseases, such as Alzheimer's and Parkinson's (75). Since kainate receptors promote excitotoxicity, microglial activation, synaptic stripping, and neuroinflammation (4), all of which contribute to the neurodegeneration in PD, we hypothesize that in this early stage of PD, compensatory mechanisms such as the described upregulation of $mGlu_{2/3}$ receptors could attenuate kainate-mediated neurotoxic effects. The present study also demonstrated that dopaminergic D_1 receptor densities were significantly reduced in the SN of *Pink1*$^{-/-}$ mice, which is in line with decreased dopamine levels in the SN of PD patients (70). Although immunohistochemical stainings showed no differences in TH-positive neurons in both adult (present study) and aged (26) *Pink1*$^{-/-}$ mice, alterations in

dopaminergic receptors highlight that the system is already changing in the absence of apparent neurodegeneration. Taken together, these alterations in (non-) dopaminergic receptors highlight the importance of further investigations in order to find new treatment strategies for both non-motor and motor symptoms.

Neurotransmitter levels or densities of neurotransmitter receptors may alter differently depending on the cause (in the case of Mendelian inherited forms), stressor, stage of disease, age, and/or symptomatology of PD patients (13, 14, 31, 64, 74). In the case of Mendelian inherited forms of PD, the function of disease-causing genes and their mutations need to be investigated in physiological and pathological conditions. Moreover, ontogenetic studies of already established or newly tested PD animal models, which would investigate receptor alterations in the progression of PD, would be helpful in order to find new disease-halting treatments, treatment options for non-motor symptoms, or even biomarkers for an early diagnosis of PD. However, the challenge would be the translation of knowledge from these studies into developing new treatment interventions or diagnostic tools. Therefore, a collaboration between different departments such as animal science, neuroscience, biochemistry, toxicology, and pharmacology would be important in order to find and test new therapy targets as promising and fast as possible.

6. Valorization

Parkinson's disease is a complex, multifactorial disease in which age, environment, and genetic factors may influence etiology. Treatment options remain limited, especially for the non-motor symptoms of patients with PD, but these symptoms further limit patients' quality of life. Because the present data will be made available to the scientific community through an open-access publication and will also be presented at an international neuroscience conference, our data can be applied to a broad range of interests, e.g. in neuroscience, biochemistry, toxicology, and pharmacology communities. This provides an opportunity for others, in addition to our laboratory, to develop new treatment strategies by identifying and/or verifying appropriate agonists or antagonists of the respective neurotransmitter receptors in animal models. In addition, our fundamental research on neurotransmitter receptor alterations in mouse models of PD could lead to collaborations with biomedical and neuroscience institutes or pharmacological companies to further investigate neurotransmitter receptor alterations and potential treatment candidates. Together, this could lead to clinical trials in which the new treatment options could be tested in PD patients, eventually leading to patenting and commercialization of the respective treatment options. Ultimately, new therapeutic interventions that are made available will benefit Parkinson's patients and significantly improve their quality of life, which will also benefit society.

7. References

1. Deng H, Wang P, Jankovic J. The genetics of Parkinson disease. Ageing Res Rev. 2018;42:72-85.
2. Fahn S. Description of Parkinson's disease as a clinical syndrome. Ann N Y Acad Sci. 2003;991:1-14.
3. Dexter DT, Jenner P. Parkinson disease: from pathology to molecular disease mechanisms. Free Radic Biol Med. 2013;62:132-44.
4. Ambrosi G, Cerri S, Blandini F. A further update on the role of excitotoxicity in the pathogenesis of Parkinson's disease. J Neural Transm. 2014;121(8):849-59.
5. DeLong MR, Wichmann T. Basal ganglia circuits as targets for neuromodulation in Parkinson disease. JAMA Neurol. 2015;72(11):1354-60.
6. Marsili L, Rizzo G, Colosimo C. Diagnostic criteria for Parkinson's disease: from James Parkinson to the concept of prodromal disease. Front Neurol. 2018;9:156-.
7. Baltadjieva R, Giladi N, Gruendlinger L, Peretz C, Hausdorff JM. Marked alterations in the gait timing and rhythmicity of patients with de novo Parkinson's disease. Eur J Neurosci. 2006;24(6):1815-20.
8. Haehner A, Hummel T, Hummel C, Sommer U, Junghanns S, Reichmann H. Olfactory loss may be a first sign of idiopathic Parkinson's disease. Mov Disord. 2007;22(6):839-42.
9. Fullard ME, Morley JF, Duda JE. Olfactory dysfunction as an early biomarker in Parkinson's disease. Neurosci Bull. 2017;33(5):515-25.
10. Werner F-M, Coveñas R. Classical neurotransmitters and neuropeptides involved in major depression in a multi-neurotransmitter system: a focus on antidepressant drugs. Curr Med Chem.2013;20(38):4853-8.
11. Lee FJS, Liu F. Genetic factors involved in the pathogenesis of Parkinson's disease. Brain Res Rev. 2008;58(2):354-64.
12. Braak H, Ghebremedhin E, Rüb U, Bratzke H, Del Tredici K. Stages in the development of Parkinson's disease-related pathology. Cell Tissue Res. 2004;318(1):121-34.
13. Cremer JN, Amunts K, Graw J, Piel M, Rösch F, Zilles K. Neurotransmitter receptor density changes in Pitx3ak mice – A model relevant to Parkinson's disease. Neuroscience. 2015;285(0):11-23.
14. Cremer JN, Amunts K, Schleicher A, Palomero-Gallagher N, Piel M, Rosch F, et al. Changes in the expression of neurotransmitter receptors in Parkin and DJ-1 knockout mice--A quantitative multireceptor study. Neuroscience. 2015;311:539-51.
15. Zahoor I, Shafi A, Haq E. Pharmacological treatment of Parkinson's disease. In: Stoker TB, Greenland JC, editors. Parkinson's disease: pathogenesis and clinical aspects. Brisbane (AU): Codon Publications; 2018.
16. Brooks DJ. Optimizing levodopa therapy for Parkinson's disease with levodopa/carbidopa/entacapone: implications from a clinical and patient perspective. Neuropsychiatr Dis Treat. 2008;4(1):39-47.
17. Valente EM, Salvi S, Ialongo T, Marongiu R, Elia AE, Caputo V, et al. PINK1 mutations are associated with sporadic early-onset parkinsonism. Ann Neurol. 2004;56(3):336-41.
18. Park J-S, Davis RL, Sue CM. Mitochondrial dysfunction in Parkinson's disease: new mechanistic insights and therapeutic perspectives. Curr Neurol Neurosci Rep. 2018;18(5):21-.
19. Morais VA, Verstreken P, Roethig A, Smet J, Snellinx A, Vanbrabant M, et al. Parkinson's disease mutations in PINK1 result in decreased complex I activity and deficient synaptic function. EMBO Mol Med. 2009;1(2):99-111.
20. Yang Y, Ouyang Y, Yang L, Beal MF, McQuibban A, Vogel H, et al. Pink1 regulates mitochondrial dynamics through interaction with the fission/fusion machinery. Proc Natl Acad Sci USA. 2008;105(19):7070-5.
21. Narendra DP, Jin SM, Tanaka A, Suen D-F, Gautier CA, Shen J, et al. PINK1 Is selectively stabilized on impaired mitochondria to activate parkin. PLOS Biol. 2010;8(1):e1000298.
22. Pickrell AM, Youle RJ. The roles of PINK1, parkin, and mitochondrial fidelity in Parkinson's disease. Neuron. 2015;85(2):257-73.
23. Scott L, Dawson VL, Dawson TM. Trumping neurodegeneration: targeting common pathways regulated by autosomal recessive Parkinson's disease genes. Exp Neurol. 2017;298:191-201.
24. Valente EM, Abou-Sleiman PM, Caputo V, Muqit MMK, Harvey K, Gispert S, et al. Hereditary early-onset Parkinson's disease caused by mutations in PINK1. Science. 2004;304(5674):1158-60.
25. Ferraris A, Ialongo T, Passali GC, Pellecchia MT, Brusa L, Laruffa M, et al. Olfactory dysfunction in Parkinsonism caused by PINK1 mutations. Mov Disord. 2009;24(16):2350-7.
26. Glasl L, Kloos K, Giesert F, Roethig A, Di Benedetto B, Kühn R, et al. Pink1-deficiency in mice impairs gait, olfaction and serotonergic innervation of the olfactory bulb. Exp Neurol. 2012;235(1):214-27.
27. de la Fuente-Fernández R, Schulzer M, Kuramoto L, Cragg J, Ramachandiran N, Au WL, et al. Age-specific progression of nigrostriatal dysfunction in Parkinson's disease. Ann Neurol. 2011;69(5):803-10.

28. Morris ME, Huxham F, McGinley J, Dodd K, Iansek R. The biomechanics and motor control of gait in Parkinson disease. Clin Biomech. 2001;16(6):459-70.
29. Doty RL, Riklan M, Deems DA, Reynolds C, Stellar S. The olfactory and cognitive deficits of Parkinson's disease: evidence for independence. Ann Neurol. 1989;25(2):166-71.
30. Ben-Ari Y, Gaiarsa JL, Tyzio R, Khazipov R. GABA: a pioneer transmitter that excites immature neurons and generates primitive oscillations. Physiological reviews. 2007;87(4):1215-84.
31. O'Gorman Tuura RL, Baumann CR, Baumann-Vogel H. Beyond dopamine: GABA, glutamate, and the axial symptoms of Parkinson disease. Front Neurol. 2018;9(806).
32. Riedel G, Platt B, Micheau J. Glutamate receptor function in learning and memory. Behav Brain Res. 2003;140(1–2):1-47.
33. Altinbilek B, Manahan-Vaughan D. A specific role for group II metabotropic glutamate receptors in hippocampal long-term depression and spatial memory. Neuroscience. 2009;158(1):149-58.
34. Zhang Z, Zhang S, Fu P, Zhang Z, Lin K, Ko JK-S, et al. Roles of glutamate receptors in Parkinson's disease. Int J Mol Sci. 2019;20(18):4391.
35. Perez-Lloret S, Barrantes FJ. Deficits in cholinergic neurotransmission and their clinical correlates in Parkinson's disease. npj Parkinson's Disease. 2016;2(1):16001.
36. Perez DM. α1-adrenergic receptors in neurotransmission, synaptic plasticity, and cognition. Front Pharmacol. 2020;11(1563).
37. Benarroch EE. The locus ceruleus norepinephrine system - functional organization and potential clinical significance. Neurology. 2009;73(20):1699-704.
38. Tohgi H, Abe T, Takahashi S, Takahashi J, Nozaki Y, Ueno M, et al. Monoamine metabolism in the cerebrospinal fluid in Parkinson's disease: relationship to clinical symptoms and subsequent therapeutic outcomes. J Neural Transm. 1993;5(1):17-26.
39. Mishra A, Singh S, Shukla S. Physiological and functional basis of dopamine receptors and their role in neurogenesis: possible implication for Parkinson's disease. J Exp Neurosci. 2018;12:1179069518779829.
40. Muñoz A, Lopez-Lopez A, Labandeira CM, Labandeira-Garcia JL. Interactions between the serotonergic and other neurotransmitter systems in the basal ganglia: role in Parkinson's disease and adverse effects of L-DOPA. Front Neuroanat. 2020;14(26).
41. Huot P, Fox SH. The serotonergic system in motor and non-motor manifestations of Parkinson's disease. Exp Brain Res. 2013;230(4):463-76.
42. Stockwell J, Jakova E, Cayabyab FS. Adenosine A1 and A2A receptors in the brain: current research and their role in neurodegeneration. Molecules. 2017;22(4):676.
43. Palomero-Gallagher N, Zilles K. Cortical layers: cyto-, myelo-, receptor- and synaptic architecture in human cortical areas. NeuroImage. 2019;197:716-41.
44. Behuet S, Cremer JN, Cremer M, Palomero-Gallagher N, Zilles K, Amunts K. Developmental changes of glutamate and GABA receptor densities in wistar rats. Front Neuroanat. 2019;13(100).
45. Amunts K, Lenzen M, Friederici AD, Schleicher A, Morosan P, Palomero-Gallagher N, et al. Broca's region: novel organizational principles and multiple receptor mapping. PLoS biology. 2010;8(9).
46. Xu Y, Yan J, Zhou P, Li J, Gao H, Xia Y, et al. Neurotransmitter receptors and cognitive dysfunction in Alzheimer's disease and Parkinson's disease. Prog Neurobiol. 2012;97(1):1-13.
47. Merker B. Silver staining of cell bodies by means of physical development. J Neurosci Methods. 1983;9(3):235-41.
48. Zilles K, Palomero-Gallagher N, Grefkes C, Scheperjans F, Boy C, Amunts K, et al. Architectonics of the human cerebral cortex and transmitter receptor fingerprints: reconciling functional neuroanatomy and neurochemistry. Eur Neuropsychopharmacol. 2002;12(6):587-99.
49. Palomero-Gallagher N, Zilles K. Chapter 24 - Cyto- and receptor architectonic mapping of the human brain. In: Huitinga I, Webster MJ, editors. Handbook of Clinical Neurology. 150: Elsevier; 2018. p.355-87.
50. Zilles K, Palomero-Gallagher N, Schleicher A. Transmitter receptors and functional anatomy of the cerebral cortex. J Anat. 2004;205(6):417-32.
51. Paxinos G, Franklin KB. The mouse brain in stereotaxic coordinates: Academic press; 2001.
52. Neves G, Cooke SF, Bliss TVP. Synaptic plasticity, memory and the hippocampus: a neural network approach to causality. Nat Rev Neurosci. 2008;9(1):65-75.
53. Fritschy J-M, Panzanelli P. GABAA receptors and plasticity of inhibitory neurotransmission in the central nervous system. Eur J Neurosci. 2014;39(11):1845-65.
54. Cao G, Edden RAE, Gao F, Li H, Gong T, Chen W, et al. Reduced GABA levels correlate with cognitive impairment in patients with relapsing-remitting multiple sclerosis. Eur Radiol. 2018;28(3):1140-8.

55. Goldman JG, Vernaleo BA, Camicioli R, Dahodwala N, Dobkin RD, Ellis T, et al. Cognitive impairment in Parkinson's disease: a report from a multidisciplinary symposium on unmet needs and future directions to maintain cognitive health. npj Parkinson's Disease. 2018;4(1):19.
56. Chapouthier G, Venault P. GABA-A receptor complex and memory processes. Curr Top Med Chem. 2002;2(8):841-51.
57. Henley JM, Wilkinson KA. Synaptic AMPA receptor composition in development, plasticity and disease. Nat Rev Neurosci. 2016;17(6):337-50.
58. Steel A, Mikkelsen M, Edden RAE, Robertson CE. Regional balance between glutamate+glutamine and GABA+ in the resting human brain. NeuroImage. 2020;220:117112.
59. Zhang X-M, Zhu J. Kainic acid-induced neurotoxicity: targeting glial responses and glia-derived cytokines. Curr Neuropharmacol. 2011;9(2):388-98.
60. Evans AJ, Gurung S, Henley JM, Nakamura Y, Wilkinson KA. Exciting times: new advances towards understanding the regulation and roles of kainate receptors. Neurochem Res. 2019;44(3):572-84.
61. Johnson BG, Wright RA, Arnold MB, Wheeler WJ, Ornstein PL, Schoepp DD. [3H]-LY341495 as a novel antagonist radioligand for group II metabotropic glutamate (mGlu) receptors: characterization of binding to membranes of mGlu receptor subtype expressing cells. Neuropharmacology. 1999;38(10):1519-29.
62. Frouni I, Hamadjida A, Kwan C, Bédard D, Nafade V, Gaudette F, et al. Activation of mGlu2/3 receptors, a novel therapeutic approach to alleviate dyskinesia and psychosis in experimental parkinsonism. Neuropharmacology. 2019;158:107725.
63. Aubert I, Araujo DM, Cécyre D, Robitaille Y, Gauthier S, Quirion R. Comparative alterations of nicotinic and muscarinic binding sites in Alzheimer's and Parkinson's diseases. Journal of neurochemistry. 1992;58(2):529-41.
64. Pimlott SL, Piggott M, Owens J, Greally E, Court JA, Jaros E, et al. Nicotinic acetylcholine receptor distribution in Alzheimer's disease, dementia with lewy bodies, Parkinson's disease, and vascular dementia: in vitro binding study using 5-[125I]-A-85380. Neuropsychopharmacology.2004;29(1):108-16.
65. Kas A, Bottlaender M, Gallezot JD, Vidailhet M, Villafane G, Grégoire MC, et al. Decrease of nicotinic receptors in the nigrostriatal system in Parkinson's disease. J Cereb Blood Flow Metab. 2009;29(9):1601-8.
66. Dennis SH, Pasqui F, Colvin EM, Sanger H, Mogg AJ, Felder CC, et al. Activation of muscarinic M1 acetylcholine receptors induces long-term potentiation in the hippocampus. Cereb Cortex. 2016;26(1):414-26.
67. Konar A, Gupta R, Shukla RK, Maloney B, Khanna VK, Wadhwa R, et al. M1 muscarinic receptor is a key target of neuroprotection, neuroregeneration and memory recovery by i-Extract from Withania somnifera. Sci Rep. 2019;9(1):13990.
68. Nathan PJ, Watson J, Lund J, Davies CH, Peters G, Dodds CM, et al. The potent M1 receptor allosteric agonist GSK1034702 improves episodic memory in humans in the nicotine abstinence model of cognitive dysfunction. Int J Neuropsychopharmacol. 2013;16(4):721-31.
69. Paredes-Rodriguez E, Vegas-Suarez S, Morera-Herreras T, De Deurwaerdere P, Miguelez C. The noradrenergic system in Parkinson's disease. Front Pharmacol. 2020;11:435-.
70. Gröger A, Kolb R, Schäfer R, Klose U. Dopamine reduction in the substantia nigra of Parkinson's disease patients confirmed by in vivo magnetic resonance spectroscopic imaging. PloS one. 2014;9(1):e84081-e.
71. Dave KD, De Silva S, Sheth NP, Ramboz S, Beck MJ, Quang C, et al. Phenotypic characterization of recessive gene knockout rat models of Parkinson's disease. Neurobiol Dis. 2014;70:190-203.
72. Kitada T, Pisani A, Porter DR, Yamaguchi H, Tscherter A, Martella G, et al. Impaired dopamine release and synaptic plasticity in the striatum of PINK1-deficient mice. Proc Natl Acad Sci USA. 2007;104(27):11441-6.
73. Gispert S, Ricciardi F, Kurz A, Azizov M, Hoepken H-H, Becker D, et al. Parkinson phenotype in aged PINK1-deficient mice is accompanied by progressive mitochondrial dysfunction in absence of neurodegeneration. PloS one. 2009;4(6):e5777.
74. Creed RB, Menalled L, Casey B, Dave KD, Janssens HB, Veinbergs I, et al. Basal and evoked neurotransmitter levels in Parkin, DJ-1, PINK1 and LRRK2 knockout rat striatum. Neuroscience. 2019;409:169-79.
75. Bobkova N, Vorobyov V. The brain compensatory mechanisms and Alzheimer's disease progression: a new protective strategy. Neural Regen Res. 2015;10(5):696-7.

8. Supplemental Information

8.1. Supplemental Material and Methods

8.1.1. Preparation of sections

- Cryostat Leica CM3050 (Leica Biosystems Vertrieb GmbH, Wetzlar, Germany)
- Isopentane (Honeywell GmbH, Seelze, Germany)
- Silan-coated glass slides (76x26 mm, Starfrost, Germany)
- Tissue-Tek® (Sakura Finetek Germany GmbH, Staufen im Breisgau, Germany)

8.1.2. Receptor autoradiography: measurement of [^{3}H] concentration

- Liquid Scintillation Counter Hidex 300 SL (Hidex, Turku, Finland)
- Liquid Scintillation Counter Cocktail AquaLight Beta (Hidex, Turku, Finland)

8.1.3. Receptor autoradiography: buffers and solutions

- Adenosine deaminase (Sigma-Aldrich Chemie GmbH, Steinheim, Germany)
- Ascorbic acid (Sigma-Aldrich Chemie GmbH, Steinheim, Germany)
- Acetone (VWR International, Langenfeld, Germany)
- Calcium acetate (Ca-acetate) (Sigma-Aldrich Chemie GmbH, Steinheim, Germany)
- Calcium chloride dihydrate ($CaCl_2$ x 2 H_2O) (Merck KGaA, Darmstadt, Germany)
- Citric acid (VWR International, Langenfeld, Germany)
- D-Glucose (VWR International, Langenfeld, Germany)
- Ethylenediaminetetraacetic acid dihydrate (EDTA x 2 H_2O) (Sigma-Aldrich Chemie GmbH, Steinheim, Germany)
- Glutamic acid (Sigma-Aldrich Chemie GmbH, Steinheim, Germany)
- Glutaraldehyde (Sigma-Aldrich Chemie GmbH, Steinheim, Germany)
- Glycine (Sigma-Aldrich Chemie GmbH, Steinheim, Germany)
- Guanosine 5'-[β,γ-imido]triphosphate trisodium salt hydrate (Gpp(NH)p) (Sigma-Aldrich Chemie GmbH, Steinheim, Germany)
- HEPES (Sigma-Aldrich Chemie GmbH, Steinheim, Germany)
- Magnesium chloride hexahydrate ($MgCl_2$ x 6 H_2O) (VWR International, Langenfeld, Germany)
- Magnesium sulfate ($MgSO_4$) (Sigma-Aldrich Chemie GmbH, Steinheim, Germany)
- Manganese(II) chloride tetrahydrate ($MnCl_2$ x 4 H_2O) (Sigma-Aldrich Chemie GmbH, Steinheim, Germany)
- Mianserin (Sigma-Aldrich Chemie GmbH, Steinheim, Germany)
- Phenylmethanesulfonyl fluoride (PMSF) (Sigma-Aldrich Chemie GmbH, Steinheim, Germany)
- Potassium bromide (KBr) (Sigma-Aldrich Chemie GmbH, Steinheim, Germany)
- Potassium chloride (KCl) (Sigma-Aldrich Chemie GmbH, Steinheim, Germany)

- Potassium phosphate monobasic (KH_2PO_4) (VWR International, Langenfeld, Germany)
- Potassium thiocyanate (KSCN) (Sigma-Aldrich Chemie GmbH, Steinheim, Germany)
- Sodium bicarbonate ($NaHCO_3$) (VWR International, Langenfeld, Germany)
- Sodium chloride (NaCl) (VWR International, Langenfeld, Germany)
- Sodium phosphate dibasic dihydrate (Na_2HPO_4 x 2 H_2O) (VWR International, Langenfeld, Germany)
- Spermidine (Sigma-Aldrich Chemie GmbH, Steinheim, Germany)
- Tris (Sigma-Aldrich Chemie GmbH, Steinheim, Germany)
- Tris-acetate (Sigma-Aldrich Chemie GmbH, Steinheim, Germany)
- Tris-HCl (Sigma-Aldrich Chemie GmbH, Steinheim, Germany)

8.1.4. Receptor autoradiography: [^{3}H]ligands

- AMPA (Perkin Elmer, Rodgau, Germany)
- CGP 54626 (Biotrend Chemikalien GmbH, Köln, Germany)
- 4-DAMP (Perkin Elmer, Rodgau, Germany)
- DPCPX (Perkin Elmer, Rodgau, Germany)
- Epibatidine (Perkin Elmer, Rodgau, Germany)
- Fallypride (Institute for Nuclear Chemistry, Johannes Gutenberg Universität Mainz, Mainz, Germany)
- Flumazenil (Perkin Elmer, Rodgau, Germany)
- Kainic acid (Perkin Elmer, Rodgau, Germany)
- Ketanserin (Perkin Elmer, Rodgau, Germany)
- LY 341495 (Biotrend Chemikalien GmbH, Köln, Germany)
- MK-801 (Perkin Elmer, Rodgau, Germany)
- Muscimol (Perkin Elmer, Rodgau, Germany)
- 8-OH-DPAT (Perkin Elmer, Rodgau, Germany)
- Oxotremorine-M (Perkin Elmer, Rodgau, Germany)
- Pirenzepine (Perkin Elmer, Rodgau, Germany)
- Prazosin (Perkin Elmer, Rodgau, Germany)
- Raclopride (Perkin Elmer, Rodgau, Germany)
- SCH 23390 (Perkin Elmer, Rodgau, Germany)
- ZM 241385 (Biotrend Chemikalien GmbH, Köln, Germany)

8.1.5. Receptor autoradiography: displacers

- Atropine sulphate (Sigma-Aldrich Chemie GmbH, Steinheim, Germany)
- (+)Butaclamol hydrochloride (Sigma-Aldrich Chemie GmbH, Steinheim, Germany)
- Carbamyolcholine chloride (Carbachol) (Sigma-Aldrich Chemie GmbH, Steinheim, Germany)
- CGP 55845 (Biotrend Chemikalien GmbH, Köln, Germany)
- 2-Chloroadenosine (Sigma-Aldrich Chemie GmbH, Steinheim, Germany)

- Clonazepam (Sigma-Aldrich Chemie GmbH, Steinheim, Germany)
- GABA (Biotrend Chemikalien GmbH, Köln, Germany)
- Haloperidol (Sigma-Aldrich Chemie GmbH, Steinheim, Germany)
- L-Glutamic acid (Sigma-Aldrich Chemie, Steinheim, Germany)
- Mianserin HCl (Sigma-Aldrich Chemie GmbH, Steinheim, Germany)
- (+)MK 801 (Biotrend Chemikalien GmbH, Köln, Germany)
- Nicotine-di-d-tartrate (Sigma-Aldrich Chemie GmbH, Steinheim, Germany)
- Phentolamine mesylate (Biotrend Chemikalien GmbH, Köln, Germany)
- Pirenzepine dihydrochloride (Sigma-Aldrich Chemie GmbH, Steinheim, Germany)
- R-phenyl-iso-propyl-adenosine (R-(-)-PIA) (Sigma-Aldrich Chemie GmbH, Steinheim, Germany)
- Serotonin HCl (5-HT) (Sigma-Aldrich Chemie GmbH, Steinheim, Germany)
- SKF 83566 (Sigma-Aldrich Chemie GmbH, Steinheim, Germany)
- SYM 2081 (Sigma-Aldrich Chemie GmbH, Steinheim, Germany)
- (+)Quisqualate (Biotrend Chemikalien GmbH, Köln, Germany)

8.1.6. Film exposition and development

- BioMax MR Film (Carestream, Sigma-Aldrich Chemie GmbH, Steinheim, Germany)
- GBX-Developer (Kodak, Sigma-Aldrich Chemie GmbH, Steinheim, Germany)
- GBX-Fixer (Kodak, Sigma-Aldrich Chemie GmbH, Steinheim, Germany)
- Hyperprocessor SRX-101A (Amersham Biosciences, GE Healthcare Europe GmbH, Freiburg im Breisgau, Germany)
- Radioactive microscales (self-made in November 2011, Research Center Jülich, Jülich, Germany)

8.1.7. Digital processing of autoradiographic films

- AxioVision image analyzing software Rel. 4.8.2 (Carl Zeiss Microscopy GmbH, Oberkochen, Germany)
- Digital camera AxioCam HRm (Carl Zeiss Microscopy GmbH, Oberkochen, Germany)

8.1.8. Histological staining: solutions

- Acetic acid (CH_3COOH) (VWR International, Langenfeld, Germany)
- Ammonium nitrate (NH_4NO_3) (VWR International, Langenfeld, Germany)
- Cresyl violet acetate (Sigma-Aldrich Chemie GmbH, Steinheim, Germany)
- DPX (dibutylphthalate polystyrene xylene) mountant for histology (Fluka, Sigma-Aldrich Chemie GmbH, Steinheim, Germany)
- 4% Formaldehyde solution (w/v) (VWR International, Langenfeld, Germany)
- Formic acid (VWR International, Langenfeld, Germany)
- Hydrogen peroxide (H_2O_2) (VWR International, Langenfeld, Germany)
- 2-Propanol (VWR International, Langenfeld, Germany)

- Sodium acetate ($NaCH_3COO$) (VWR International, Langenfeld, Germany)
- Sodium carbonate (Na_2CO_3) (VWR International, Langenfeld, Germany)
- Silver nitrate ($AgNO_3$) (VWR International, Langenfeld, Germany)
- Tungstosilicic acid hydrate (VWR International, Langenfeld, Germany)
- T-MAX (Kodak, Sigma-Aldrich Chemie GmbH, Steinheim, Germany)
- Xylene (VWR International, Langenfeld, Germany)

8.1.9. Immunohistochemical staining

- Antibodies & Fluorescent Dyes
    - anti-GABA-rabbit (Sigma-Aldrich Chemie GmbH, Steinheim, Germany)
    - anti-glutamine synthetase, rabbit (Sigma-Aldrich Chemie GmbH, Steinheim, Germany)
    - anti-tyrosine hydroxylase, chicken (abcam, Cambridge, United Kingdom)
    - goat-anti-chicken Alexa-Fluor 488 (Jackson ImmunoResearch Laboratories, West Grove, USA)
    - goat-anti-rabbit-Cy-3 conjugated (Jackson ImmunoResearch Laboratories, West Grove, USA)
    - DAPI - Hoechst (Thermo Fisher Scientific GmbH, Dreieich, Germany)
- Solutions
    - Fluoromount G (SouthernBiotec, Birmingham, USA)
    - Normal goat serum (Vector Laboratories, Burlingame, USA)
    - Phosphate-buffered saline (PBS) (VWR International, Langenfeld, Germany)
    - Saponin (Sigma-Aldrich Chemie GmbH, Steinheim, Germany)

8.1.10. Standard protocols: histological staining

Table A1: Procedure of Nissl staining using cresyl violet acetate. The cresyl violet acetate solution was filtered before use. It is long lasting if prepared in a tinted glass bottle and can be used multiple times.

Procedure	**Solution**	**Preparation for 500ml:**	**Conditions**
Fixation	4% Formalin		At least 30min
Rinsing	Distilled water		15min
Staining (regressive)	Cresyl violet acetate	Cresyl violet acetate solution: 500ml Distilled water + 2.7g Sodium acetate (CH_3COONa) + 4.7ml 100% Acetic acid + 0.5g Cresyl violet acetate	2 – 12min; depending on the tissue
Rinse off excess dye with distilled water squeeze bottle.			
Rinsing	Distilled water		Dip for approx. 5sec
Differentiation (1)	70% 2-Propanol	150ml 100% 2-Propanol + 350ml Distilled water	1min, 3 dips
Differentiation (2)	70% 2-Propanol	see above	1min, 3 dips
Differentiation (3)	96% 2-Propanol	20ml 100% 2-Propanol + 480ml Distilled water	1 – 20min; check sections regularly under microscope
Dehydration (1)	100% 2-Propanol		
Dehydration (2)	100% 2-Propanol		
Intermedium	Xylene		At least 10min
Mounting	DPX		

Table A2: Procedure of Nissl staining by Merker (47). All solutions were prepared the week before the experiment. Performic acid and stock solution A were stored at 4°C, while the other solutions were stored at 22°C. All stock solutions (A, B, and C) were prepared in tinted glass bottles. The development solution was used only once per batch and was always mixed immediately before the procedure. All other solutions were used for every batch (6 in total).

Procedure	**Solution**	**Preparation for 500ml:**	**Conditions**
Fixation	4% Formalin		At least 30min
Rinsing	Running demineralized water		20 – 30min
Acid cleaning (1)	4% Formic acid	480ml Distilled water + 20ml 100% Formic acid	20min; protected from light
Acid cleaning (2)	Performic acid	350ml Distilled water + 112.5ml 30% Hydrogen peroxide + 37.5ml 100% Formic acid	40min; protected from light
Rinsing	Running demineralized water		20 – 30min
Incubation	1% Acetic acid	445ml Distilled water + 5ml ~100% Acetic acid	2 x 5min
Development	A+B+C	250ml Stock solution A + 75ml Stock solution B + 175ml Stock solution C <u>For stock solution A:</u> 500ml Distilled water + 25g Sodium carbonate (Na_2CO_3)	10 – 30min; dip every 30sec; keep sections under light (lamp); as soon as sections get darker check

		<u>For stock solution B:</u> 500ml Distilled water + 1g Ammonium nitrate (NH_4NO_3) + 1g Silver nitrate ($AgNO_3$) + 5g Tungstosilicic acid hydrate <u>For stock solution C:</u> 500ml Distilled water + 1g Ammonium nitrate (NH_4NO_3) + 1g Silver nitrate ($AgNO_3$) + 5g Tungstosilicic acid hydrate + 3.65ml 37% Formaldehyde solution	them regularly under microscope
Stop of development (1)	1% Acetic acid	see above	1min, 5 dips
Stop of development (2)	1% Acetic acid	see above	4min
Rinsing	Running demineralized water		5min
Fixation	T-MAX	400ml Distilled water + 100ml T-MAX	2min; protected from light
Rinsing	Running demineralized water		5min
Dehydration (1)	70% 2-Propanol	150ml 100% 2-Propanol + 350ml Distilled water	5min
Dehydration (2)	96% 2-Propanol	20ml 100% 2-Propanol + 480ml Distilled water	5min
Dehydration (3)	100% 2-Propanol		5min
Intermedium	Xylene		3 x 5min
Mounting	DPX		

8.1.11. Standard protocols: receptor autoradiography

Table A3: Receptor binding protocols of [^{3}H]ligands, displacers (marked with *), and incubation conditions.

Receptor subtype/ [^{3}H]ligand	Procedure	Incubation buffer	Incubation conditions
AMPA	Pre-incubation	50mM Tris-acetate (pH 7.2)	3 x 10min at 4°C
[^{3}H]AMPA	Main incubation	50mM Tris-acetate (pH 7.2) + 100mM KSCN + 10nM [^{3}H]AMPA + 10µm Quisqualate*	45min at 4°C
	1st rinsing	50mM Tris-acetate (pH 7.2)	4 x 4sec at 4°C
	2nd rinsing	2.5% Glutaraldehyde in acetone	2 x 2sec at 22°C
Kainate	Pre-incubation	50mM Tris-citrate (pH 7.1)	3 x 10min at 4°C
[^{3}H]Kainic acid	Main incubation	50mM Tris-citrate (pH 7.1) + 10mM Calcium acetate + 9.4nM [^{3}H]Kainic acid + 100µM SYM 2081*	45min at 4°C
	1st rinsing	50mM Tris-citrate (pH 7.1)	3 x 4sec at 4°C
	2nd rinsing	2.5% Glutaraldehyde in acetone	2 x 2sec at 22°C
NMDA	Pre-incubation	50mM Tris-HCl (pH 7.2) + 50µM Glutamate	15min at 4°C
[^{3}H]MK-801	Main incubation	50mM Tris-HCl (pH 7.2) + 50µM Glutamate + 30µM Glycine + 50µM Spermidine + 3.3nM [^{3}H]MK-801 + 100µM MK 801	60min at 22°C
	1st rinsing	50mM Tris-HCl (pH 7.2) + 50µM Glutamate	2 x 5min at 4°C
	2nd rinsing	Distilled water	1 dip at 4°C
mGlu2/3	Pre-incubation	Phosphate buffer (pH 7.6) (137mM NaCl; 2.7mM KCl; 4.3mM $Na_2HPO_4x2H_2O$; 1.4mM KH_2PO_4)	2 x 5min at 22°C
[^{3}H]LY 341495	Main incubation	Phosphate buffer (pH 7.6) +100mM KBr + 1nM [^{3}H]LY 341495 + 1mM L-Glutamate*	60min at 4°C
	1st rinsing	Phosphate buffer (pH 7.6)	2 x 5min at 4°C
	2nd rinsing	Distilled water	1 dip at 4°C
$GABA_A$	Pre-incubation	50mM Tris-citrate (pH 7.0)	3 x 5min at 4°C
[^{3}H]Muscimol	Main incubation	50mM Tris-citrate (pH 7.0) + 7.7nM [^{3}H]Muscimol + 10µM GABA*	40min at 4°C
	1st rinsing	50mM Tris-citrate (pH 7.0)	3 x 3sec at 4°C
	2nd rinsing	Distilled water	1 dip at 4°C
$GABA_B$	Pre-incubation	50mM Tris-HCl (pH 7.2) + 2.5mM $CaCl_2$	3 x 5min at 4°C
[^{3}H]CGP 54626	Main incubation	50mM Tris-HCl (pH 7.2) + 2.5mM $CaCl_2$ + 2nM [^{3}H]CGP 54626 + 100µM CGP 55845*	60min at 4°C
	1st rinsing	50mM Tris-HCl (pH 7.2) + 2.5mM $CaCl_2$	3 x 2sec at 4°C
	2nd rinsing	Distilled water	1 dip at 4°C

BZ **[^{3}H]Flumazenil**	Pre-incubation	170mM Tris-HCl (pH 7.4)	15min at 4°C
	Main incubation	170mM Tris-HCl (pH 7.4) + 1nM [^{3}H]Flumazenil + 2µM Clonazepam*	60min at 4°C
	1st rinsing	170mM Tris-HCl (pH 7.4)	2 x 1min at 4°C
	2nd rinsing	Distilled water	1 dip at 4°C
M_1 **[^{3}H]Pirenzepine**	Pre-incubation	Modified Krebs buffer (pH 7.4) (5.6mM KCl; 30.6mM NaCl; 1.2mM $MgSO_4$; 1.4mM KH_2PO_4; 5.6mM D-Glucose; 5.2mM $NaHCO_3$; 2.5mM $CaCl_2$)	15min at 4°C
	Main incubation	Modified Krebs buffer (pH 7.4) + 10nM [^{3}H]Pirenzepine + 2µM Pirenzepine dihydrate*	60min at 22°C
	1st rinsing	Modified Krebs buffer (pH 7.4)	2 x 1min at 4°C
	2nd rinsing	Distilled water	1 dip at 4°C
M_2 **[^{3}H]Oxotremorine-M**	Pre-incubation	20mM HEPES-Tris (pH 7.5) + 10mM $MgCl_2$	20min at 22°C
	Main incubation	20mM HEPES-Tris (pH 7.5) + 10mM $MgCl_2$ + 1.7nM [^{3}H]Oxotremorine-M + 10µM Carbachol*	60min at 22°C
	1st rinsing	20mM HEPES-Tris (pH 7.5) + 10mM $MgCl_2$	2 x 2min at 4°C
	2nd rinsing	Distilled water	1 dip at 4°C
M_3 **[^{3}H]4-DAMP**	Pre-incubation	50 mM Tris-HCl (pH 7.4) + 0.1 mM PMSF + 1 mM EDTA	15min at 22°C
	Main incubation	50 mM Tris-HCl (pH 7.4) + 0.1 mM PMSF + 1 mM EDTA + 1nM [^{3}H]4-DAMP + 10µM Atropine sulphate*	45min at 22°C
	1st rinsing	50 mM Tris-HCl (pH 7.4) + 0.1mM PMSF + 1mM EDTA	2 x 5min at 4°C
	2nd rinsing	Distilled water	1 dip at 4°C
Nicotinic $\alpha_4\beta_2$ **[^{3}H]Epibatidine**	Pre-incubation	15mM HEPES (pH 7.5) + 120mM NaCl, + 5.4mM KCl + 0.8mM $MgCl_2$ + 1.8mM $CaCl_2$	20min at 22°C
	Main incubation	15mM HEPES (pH 7.5) + 120mM NaCl + 5.4mM KCl + 0.8mM $MgCl_2$ + 1.8mM $CaCl_2$ + 0.11nM [^{3}H]Epibatidine + 100µM Nicotine*	90min at 4°C
	1st rinsing	15mM HEPES (pH 7.5) + 120mM NaCl + 5.4mM KCl + 0.8mM $MgCl_2$ + 1.8mM $CaCl_2$	5min at 4°C
	2nd rinsing	Distilled water	1 dip at 4°C

α_1	Pre-incubation	50mM Na/K-phosphate buffer (pH 7.4)	15min at 22°C
[^{3}H]Prazosin	Main incubation	50mM Na/K-phosphate buffer (pH 7.4) + 0.09nM [^{3}H]Prazosin + 10µM Phentolamine mesylate*	60min at 22°C
	1st rinsing	50mM Na/K-phosphate buffer (pH 7.4)	2 x 5min at 4°C
	2nd rinsing	Distilled water	1 dip at 4°C
5-HT$_{1A}$	Pre-incubation	170mM Tris-HCl (pH 7.7)	30min at 22°C
[^{3}H]8-OH-DPAT	Main incubation	170mM Tris-HCl (pH 7.7) + 0.01% Ascorbate + 4mM $CaCl_2$ + 0.3nM [^{3}H]8-OH-DPAT + 1µM 5-HT*	60min at 22°C
	1st rinsing	170mM Tris-HCl (pH 7.7)	5min at 4°C
	2nd rinsing	Distilled water	3 dips at 4°C
5-HT$_2$	Pre-incubation	170mM Tris-HCl (pH 7.7)	30min at 22°C
	Main incubation	170mM Tris-HCl (pH 7.7) + 1.14nM [^{3}H]Ketanserin + 10µM Mianserin*	120min at 22°C
	1st rinsing	170mM Tris-HCl (pH 7.7)	2 x 10min at 4°C
	2nd rinsing	Distilled water	3 dips at 4°C
D_1	Pre-incubation	50mM Tris-HCl (pH 7.4) + 120mM NaCl + 5mM KCl + 2mM $CaCl_2$ + 1mM $MgCl_2$	20min at 22°C
[^{3}H]SCH 23390	Main incubation	50mM Tris-HCl (pH 7.4) + 120mM NaCl + 5mM KCl + 2mM $CaCl_2$ + 1mM $MgCl_2$ + 1µM Mianserin + 1.67nM [^{3}H]SCH 23390 + 1µM SKF 83566*	90min at 22°C
	1st rinsing	50mM Tris-HCl (pH 7.4) + 120mM NaCl + 5mM KCl + 2mM $CaCl_2$ + 1mM $MgCl_2$	2 x 10min at 4°C
	2nd rinsing	Distilled water	1 dip at 4°C
D_2	Pre-incubation	50mM Tris-HCl (pH 7.4) + 150mM NaCl + 0.1% Ascorbate	20min at 22°C
[^{3}H]Raclopride	Main incubation	50mM Tris-HCl (pH 7.4) + 150mM NaCl + 0.1% Ascorbate + 0.55nM [^{3}H]Raclopride + 1µM Butaclamol*	45min at 22°C
	1st rinsing	50mM Tris-HCl (pH 7.4) + 150mM NaCl + 0.1% Ascorbate	6 x 1min at 4°C
	2nd rinsing	Distilled water	1 dip at 4°C
$D_{2/3}$	Pre-incubation	50mM Tris-HCl (pH 7.4) + 5mM KCl + 120mM NaCl	30min at 22°C
[^{3}H]Fallypride	Main incubation	50mM Tris-HCl (pH 7.4) + 5mM KCl + 120mM NaCl + 4nM [^{3}H]Fallypride	60min at 37°C

		+ 10µM Haloperidol*	
	1st rinsing	50mM Tris-HCl (pH 7.4) + 5mM KCl + 120mM NaCl	2 x 2min at 4°C
	2nd rinsing	Distilled water	1 dip at 4°C
A_1 **[^{3}H]DPCPX**	Pre-incubation	170 mM Tris-HCl (pH 7.4) + 2 Units/L Adenosine Deaminase	15min at 4°C
	Main incubation	170 mM Tris-HCl (pH 7.4) + 2 Units/L Adenosine Deaminase + 100µM Gpp(NH)p + 1nM [^{3}H]DPCPX + 100µM R-PIA*	120min at 22°C
	1st rinsing	170 mM Tris-HCl (pH 7.4) + 2 Units/L Adenosine Deaminase	2 x 5min at 4°C
	2nd rinsing	Distilled water	1 dip at 4°C
A_{2A} **[^{3}H]ZM 241385**	Pre-incubation	170mM Tris-HCl (pH 7.4) + 1mM EDTA x 2 H_2O + 2 Units/l Adenosine Deaminase	30min at 37°C
	1st rinsing	170mM Tris-HCl (pH 7.4) + 10mM $MgCl_2$ x 6 H_2O	2 x 10min at 22°C
	Main incubation	170mM Tris-HCl (pH 7.4) + 10mM $MgCl_2$ x 6 H_2O + 2 Units/l Adenosine Deaminase + 0.42nM [^{3}H]ZM 241385 + 20µM 2-Chloro-Adenosine*	120min at 22°C
	2nd rinsing	170mM Tris-HCl (pH 7.4)	2 x 5min at 4°C
	3rd rinsing	Distilled water	1 dip at 4°C

8.1.12. Exposure time

Table A4: Exposure times for [^{3}H]ligands.

[^{3}H]ligand	**Exposure time (weeks)**
[^{3}H]AMPA	15
[^{3}H]CGP 54626	10
[^{3}H]4-DAMP	9
[^{3}H]DPCPX	10
[^{3}H]Epibatidine	15
[^{3}H]Fallypride	15
[^{3}H]Flumazenil	9
[^{3}H]Kainic acid	12
[^{3}H]Ketanserin	15
[^{3}H]LY 341495	10
[^{3}H]MK-801	12
[^{3}H]Muscimol	12
[^{3}H]8-OH-DPAT	15
[^{3}H]Oxotremorine-M	15
[^{3}H]Pirenzepine	12
[^{3}H]Prazosin	15
[^{3}H]Raclopride	15
[^{3}H]SCH 23390	15
[^{3}H]ZM 241385	15

8.2. Supplemental Data

8.2.1. Raw Data

Table A5: $GABA_A$ receptor densities (fmol/mg protein) and mean (MD) ± standard deviation (SD) in brain regions (left and right hemisphere) of control mice. Ligand: [^{3}H]Muscimol

		OB		M1		CPu		CA1		CA2/3		DG		SN	
animal	**group**	**left**	**right**	**left**	**right**	**left**	**right**	**left**	**right**	**left**	**right**	**left**	**right**	**left**	**right**
30189369	**control**	2469	2294	2000	2480	1237	1534	1808	1849	818	716	1650	1613	803	700
30189372	**control**	2446	-	1646	1754	1036	1014	1216	1255	657	604	1402	1373	719	684
30189408	**control**	3620	3555	2189	2566	1359	1330	1837	1949	749	951	1599	1714	1029	1099
30189465	**control**	3329	2992	2110	2620	1345	1368	2232	2101	938	865	2089	2019	1173	879
30190808	**control**	3121	2919	2005	1926	1193	1230	1995	2056	808	877	1796	1866	1005	968
30190809	**control**	2773	2662	2137	1917	1042	1053	1991	1707	805	841	1562	1513	821	761
30190810	**control**	2446	2597	2637	2970	1422	1388	2379	2342	937	974	2214	2173	1293	1176
30190811	**control**	3234	3205	2371	2623	1129	1089	1438	1597	690	762	1490	1428	741	904
30190812	**control**	2392	2051	760	1500	1141	982	1293	1776	783	772	1510	1840	1025	932
30191181	**control**	2445	2131	2833	2220	1292	1113	2342	2529	1041	1050	2005	2183	1253	984
	MD ± SD	2773 ± 471		2163 ± 517		1215 ± 159		1885 ± 386		832 ± 123		1752 ± 280		947 ± 186	

Table A6: $GABA_A$ receptor densities (fmol/mg protein) and mean (MD) ± standard deviation (SD) in brain regions (left and right hemisphere) of *Pink1*$^{-/-}$ mice. Ligand: [^{3}H]Muscimol

		OB		M1		CPu		CA1		CA2/3		DG		SN	
animal	**group**	**left**	**right**	**left**	**right**	**left**	**right**	**left**	**right**	**left**	**right**	**left**	**right**	**left**	**right**
30189346	***Pink1*$^{-/-}$**	2806	2975	2540	2422	1548	1453	1766	2129	859	925	1862	2004	726	641
30189373	***Pink1*$^{-/-}$**	1883	2024	1859	2064	1185	1273	2062	2005	902	842	1944	1944	974	1032
30189376	***Pink1*$^{-/-}$**	3156	3541	2987	2552	1530	1578	-	-	-	-	-	-	1173	1360
30189381	***Pink1*$^{-/-}$**	2612	3030	2079	1897	1116	1217	1592	1820	785	821	1526	1523	948	746
30189387	***Pink1*$^{-/-}$**	2557	2537	2908	2780	1538	1560	2116	2316	853	918	1824	1942	1190	1207
30189407	***Pink1*$^{-/-}$**	3213	3071	2774	2908	1465	1519	2564	2650	1138	1098	2359	2360	1045	895

30189539	***Pink1*$^{-/-}$**	2153	2976	2214	2652	1195	1323	2493	2345	1133	1002	2109	1874	820	713
30189591	***Pink1*$^{-/-}$**	1804	2211	2309	2027	1215	1098	2358	2208	978	867	1979	1902	1250	1083
30189592	***Pink1*$^{-/-}$**	3023	3105	2654	2849	1701	1534	2837	3179	1247	1155	2724	2837	1053	1075
30190641	***Pink1*$^{-/-}$**	2250	1864	1437	1758	1097	1032	2058	1915	956	784	1949	1832	774	493
	MD ± SD	2640 ± 523		2384 ± 447		1359 ± 204		2245 ± 397		959 ± 140		2027 ± 347		960 ± 229	

Table A7: BZ binding site densities (fmol/mg protein) and mean (MD) ± standard deviation (SD) in brain regions (left and right hemisphere) of control mice. Ligand: [^{3}H]Flumazenil

		OB		**M1**		**CPu**		**CA1**		**CA2/3**		**DG**		**SN**	
animal	**group**	**left**	**right**	**left**	**right**	**left**	**right**	**left**	**right**	**left**	**right**	**left**	**right**	**left**	**right**
30189369	**control**	5012	4973	3576	3990	920	1048	4859	5021	2471	2587	4138	4341	3058	3730
30189372	**control**	4687	-	3821	3814	969	915	4589	4493	2378	2144	3861	3863	3199	3284
30189408	**control**	4552	4731	3965	3718	1013	970	4562	4594	2203	2500	3776	3950	5288	5406
30189465	**control**	4860	4876	3806	3895	958	979	5245	5009	2508	2426	4360	4225	4460	4210
30190808	**control**	5045	5183	4206	4027	1130	1100	5008	4904	2837	2824	4517	4407	4796	4688
30190809	**control**	4954	4794	4289	4306	1097	1111	5326	5301	3085	3054	4663	4694	3949	4212
30190810	**control**	4460	4347	3964	3855	1045	960	4990	4862	2935	2745	4555	4533	4960	5084
30190811	**control**	4664	4762	3866	3799	961	986	4412	4403	2333	2426	4147	4081	5255	5192
30190812	**control**	3925	3987	3488	2943	963	941	4711	4567	2594	2416	4149	4225	4201	4095
30191181	**control**	4576	4664	3894	3599	1031	1014	5354	4836	2884	2341	4664	4475	5250	4835
	MD ± SD	4687 ± 332		3841 ± 301		1006 ± 65		4852 ± 306		2585 ± 275		4281 ± 285		4458 ± 739	

Table A8: BZ binding site densities (fmol/mg protein) and mean (MD) ± standard deviation (SD) in brain regions (left and right hemisphere) of *Pink1*$^{-/-}$ mice. Ligand: [^{3}H]Flumazenil

		OB		**M1**		**CPu**		**CA1**		**CA2/3**		**DG**		**SN**	
animal	**group**	**left**	**right**	**left**	**right**	**left**	**right**	**left**	**right**	**left**	**right**	**left**	**right**	**left**	**right**
30189346	***Pink1*$^{-/-}$**	4760	4931	4106	4023	1048	986	4751	5109	2362	2291	4190	4427	4256	4167
30189373	***Pink1*$^{-/-}$**	4404	4198	4058	4286	1061	1043	4765	4848	2464	2480	3983	4067	4565	4639
30189376	***Pink1*$^{-/-}$**	4298	4551	3923	3807	900	914	-	-	-	-	-	-	3684	4105
30189381	***Pink1*$^{-/-}$**	4475	4607	3972	3985	1008	952	5016	5225	2753	2825	4322	4404	4486	4850
30189387	***Pink1*$^{-/-}$**	4640	4542	4139	4236	1024	1002	5094	5112	2596	2618	4569	4527	5237	5058

30189407	***Pink1*$^{-/-}$**	4820	5022	4559	4429	1194	1193	4872	4964	2756	2650	4402	4285	5203	4638
30189539	***Pink1*$^{-/-}$**	4543	4823	4311	4146	1156	1072	5328	5318	2831	2946	4885	4624	4149	4025
30189591	***Pink1*$^{-/-}$**	4551	4750	3986	4177	1053	1124	4994	4970	2698	2841	4383	4470	4593	4276
30189592	***Pink1*$^{-/-}$**	4766	4850	3765	3828	1099	1094	4894	4659	2488	2501	4201	4009	5232	5007
30190641	***Pink1*$^{-/-}$**	4489	4717	3868	3890	1001	1007	4830	4587	2544	2390	4102	3997	3717	3914
	MD ± SD	4637 ± 211		4075 ± 213		1047 ± 82		4963 ± 211		2613 ± 187		4325 ± 246		4490 ± 495	

Table A9: $GABA_B$ receptor densities (fmol/mg protein) and mean (MD) ± standard deviation (SD) in brain regions (left and right hemisphere) of control mice. Ligand: [^{3}H]CGP 54626

		OB		**M1**		**CPu**		**CA1**		**CA2/3**		**DG**		**SN**	
animal	**group**	**left**	**right**	**left**	**right**	**left**	**right**	**left**	**right**	**left**	**right**	**left**	**right**	**left**	**right**
30189369	**control**	531	490	1232	1253	544	652	1137	880	1470	1203	1416	1241	799	667
30189372	**control**	440	-	1299	1232	655	630	996	966	1213	1121	1353	1305	721	640
30189408	**control**	537	516	1060	1054	610	631	944	1068	1321	1363	1231	1262	763	808
30189465	**control**	448	493	1082	1073	570	563	886	843	1107	1016	1152	1074	623	744
30190808	**control**	478	498	1106	1213	640	665	1053	1061	1307	1362	1329	1273	807	727
30190809	**control**	407	445	1136	985	604	561	878	942	1140	1132	1004	1120	756	777
30190810	**control**	334	371	1060	1180	578	602	872	918	1132	1145	1121	1186	526	619
30190811	**control**	470	457	1293	1350	650	635	1101	992	1279	1233	1422	1326	668	723
30190812	**control**	368	325	1049	875	501	419	766	762	1090	1093	1072	959	532	399
30191181	**control**	304	299	972	1027	449	418	773	738	1013	990	1003	991	637	631
	MD ± SD	432 ± 77		1127 ± 125		579 ± 78		929 ± 119		1186 ± 130		1192 ± 145		678 ± 107	

Table A10: $GABA_B$ receptor densities (fmol/mg protein) and mean (MD) ± standard deviation (SD) in brain regions (left and right hemisphere) of *Pink1*$^{-/-}$ mice. Ligand: [^{3}H]CGP 54626

		OB		**M1**		**CPu**		**CA1**		**CA2/3**		**DG**		**SN**	
animal	**group**	**left**	**right**	**left**	**right**	**left**	**right**	**left**	**right**	**left**	**right**	**left**	**right**	**left**	**right**
30189346	***Pink1*$^{-/-}$**	461	482	1270	1372	653	660	1006	917	1229	1068	1312	1299	647	658
30189373	***Pink1*$^{-/-}$**	447	422	1289	1193	584	562	876	838	1187	1091	1209	1164	684	564

30189376	***Pink1*$^{-/-}$**	388	386	1110	1030	542	547	-	-	-	-	-	-	752	739
30189381	***Pink1*$^{-/-}$**	421	437	1158	1116	665	650	842	857	1141	1074	989	1101	753	749
30189387	***Pink1*$^{-/-}$**	453	463	1049	1033	573	523	940	909	1207	1185	1211	1183	748	648
30189407	***Pink1*$^{-/-}$**	480	456	920	1098	592	503	819	766	964	1016	1116	1053	641	612
30189539	***Pink1*$^{-/-}$**	430	458	1153	1247	560	607	918	877	1109	1034	1214	1147	508	546
30189591	***Pink1*$^{-/-}$**	359	374	874	923	429	411	766	730	1075	891	1015	978	594	506
30189592	***Pink1*$^{-/-}$**	331	326	839	985	416	440	679	845	1020	1034	889	1022	544	572
30190641	***Pink1*$^{-/-}$**	274	295	934	960	462	449	595	687	841	865	829	918	548	551
	MD ± SD	407 ± 62		1078 ± 149		541 ± 85		826 ± 105		1057 ± 114		1092 ± 139		628 ± 86	

Table A11: AMPA receptor densities (fmol/mg protein) and mean (MD) ± standard deviation (SD) in brain regions (left and right hemisphere) of control mice. Ligand: [^{3}H]AMPA

		OB		**M1**		**CPu**		**CA1**		**CA2/3**		**DG**		**SN**	
animal	**group**	**left**	**right**	**left**	**right**	**left**	**right**	**left**	**right**	**left**	**right**	**left**	**right**	**left**	**right**
30189369	**control**	1111	1166	1664	1856	1264	1362	5238	5255	3071	3246	3228	3157	350	404
30189372	**control**	1086	-	1953	1899	1698	1610	6011	5924	3115	3423	3891	3927	575	538
30189408	**control**	1160	1343	1882	2053	1651	1674	7334	6666	4701	3708	4690	3826	485	397
30189465	**control**	1207	1259	1432	1571	1177	1225	6319	6815	3326	3827	3759	4276	454	409
30190808	**control**	967	909	1161	1230	985	983	4711	4823	2651	2778	2949	2796	411	428
30190809	**control**	823	892	1304	1432	1116	1130	6360	5623	3540	3242	3529	3084	371	335
30190810	**control**	840	838	1230	1327	1017	1104	5844	6660	3808	3786	3347	3724	392	393
30190811	**control**	912	1034	1650	1721	1285	1369	5140	4456	2584	2437	3174	2623	413	408
30190812	**control**	1404	1393	1740	1723	1571	1475	5858	5748	3331	3536	4082	4271	507	545
30191181	**control**	1279	1387	1853	2066	1567	1714	8009	7883	5488	5058	5372	5426	586	655
	MD ± SD	1106 ± 204		1637 ± 286		1349 ± 254		6034 ± 991		3533 ± 790		3757 ± 777		453 ± 87	

Table A12: AMPA receptor densities (fmol/mg protein) and mean (MD) ± standard deviation (SD) in brain regions (left and right hemisphere) of *Pink1*$^{-/-}$ mice. Ligand: [^{3}H]AMPA

		OB		**M1**		**CPu**		**CA1**		**CA2/3**		**DG**		**SN**	
animal	**group**	**left**	**right**	**left**	**right**	**left**	**right**	**left**	**right**	**left**	**right**	**left**	**right**	**left**	**right**
30189346	***Pink1*$^{-/-}$**	1332	1307	1813	1998	1364	1639	5431	5963	3298	3985	3372	3591	460	514

30189373	***Pink1*$^{-/-}$**	967	994	1518	1660	1144	1330	4146	5312	2478	2878	2672	3494	428	455
30189376	***Pink1*$^{-/-}$**	1660	1445	2110	1964	1620	1592	-	-	-	-	-	-	309	392
30189381	***Pink1*$^{-/-}$**	1190	1274	2141	2137	1721	1748	7906	6932	4115	3880	4835	4642	436	397
30189387	***Pink1*$^{-/-}$**	727	797	1269	1501	1138	1211	5184	5039	2805	2739	2877	2719	324	326
30189407	***Pink1*$^{-/-}$**	832	882	1459	1522	1051	1094	5066	4827	2680	2882	2613	2550	381	350
30189539	***Pink1*$^{-/-}$**	881	1021	1570	1870	1141	1197	5619	5357	2964	2771	3134	2930	411	379
30189591	***Pink1*$^{-/-}$**	948	891	1305	1413	1069	1097	5315	5629	2596	3313	2882	3199	473	484
30189592	***Pink1*$^{-/-}$**	1195	1029	1466	1738	1593	1643	5765	5658	3778	4101	4049	3816	571	616
30190641	***Pink1*$^{-/-}$**	1253	1296	1678	1744	1444	1436	5615	5394	3338	3206	3826	3544	460	497
	MD ± SD	1096 ± 245		1694 ± 273		1364 ± 245		5564 ± 805		3211 ± 546		3375 ± 670		433 ± 81	

Table A13: Kainate receptor densities (fmol/mg protein) and mean (MD) ± standard deviation (SD) in brain regions (left and right hemisphere) of control mice. Ligand: [^{3}H]Kainic acid

		OB		**M1**		**CPu**		**CA1**		**CA2/3**		**DG**		**SN**	
animal	**group**	**left**	**right**	**left**	**right**	**left**	**right**	**left**	**right**	**left**	**right**	**left**	**right**	**left**	**right**
30189369	**control**	1769	1767	1362	1356	1697	1665	527	535	1195	1143	1154	1132	374	377
30189372	**control**	1605	-	1289	1358	1589	1611	447	454	967	928	951	1019	303	262
30189408	**control**	1656	1717	1265	1299	1625	1541	534	480	1123	1098	1109	1093	378	373
30189465	**control**	1815	1892	1227	1287	1486	1523	443	421	1091	1045	1022	1040	315	283
30190808	**control**	1807	1811	1272	1309	1561	1596	484	492	1142	1054	1128	1122	291	320
30190809	**control**	1841	1946	1436	1389	1722	1714	560	577	1256	1198	1142	1235	335	274
30190810	**control**	1595	1615	1276	1244	1547	1517	435	420	1058	953	1003	1009	316	321
30190811	**control**	1908	2021	1552	1497	1796	1680	483	483	1151	1080	1109	1112	289	352
30190812	**control**	1401	1424	1368	1293	1547	1507	499	440	1062	1011	1048	1014	381	278
30191181	**control**	1750	1745	1453	1419	1711	1606	520	499	1192	1011	1116	1093	353	355
	MD ± SD	1741 ± 163		1348 ± 88		1612 ± 86		487 ± 46		1088 ± 89		1083 ± 67		326 ± 39	

Table A14: Kainate receptor densities (fmol/mg protein) and mean (MD) ± standard deviation (SD) in brain regions (left and right hemisphere) of *Pink1*$^{-/-}$ mice. Ligand: [^{3}H]Kainic acid

		OB		M1		CPu		CA1		CA2/3		DG		SN	
animal	**group**	**left**	**right**	**left**	**right**	**left**	**right**	**left**	**right**	**left**	**right**	**left**	**right**	**left**	**right**
30189346	***Pink1*$^{-/-}$**	2212	2256	1639	1718	2092	2011	598	619	1265	1322	1227	1200	357	359
30189373	***Pink1*$^{-/-}$**	1565	1593	1234	1223	1483	1487	482	470	1063	1071	1069	1045	275	253
30189376	***Pink1*$^{-/-}$**	1435	1489	1235	1210	1405	1413	-	-	-	-	-	-	279	349
30189381	***Pink1*$^{-/-}$**	1783	1788	1340	1326	1646	1580	462	450	1102	1073	1043	1065	334	284
30189387	***Pink1*$^{-/-}$**	1869	1870	1322	1253	1569	1652	488	459	1060	1079	1100	1137	315	299
30189407	***Pink1*$^{-/-}$**	2141	2072	1527	1563	1694	1764	531	554	1185	1151	1290	1306	318	332
30189539	***Pink1*$^{-/-}$**	1554	1650	1242	1221	1435	1450	405	416	979	904	1010	996	243	233
30189591	***Pink1*$^{-/-}$**	1535	1541	1085	1078	1299	1207	347	377	866	851	852	871	283	269
30189592	***Pink1*$^{-/-}$**	1893	2048	1575	1409	1903	1825	556	550	1193	1110	1284	1288	320	301
30190641	***Pink1*$^{-/-}$**	1824	1825	1287	1190	1376	1323	467	435	947	913	1000	1009	303	277
	MD ± SD	1797 ± 251		1334 ± 181		1581 ± 242		481 ± 74		1063 ± 134		1100 ± 140		299 ± 36	

Table A15: NMDA receptor densities (fmol/mg protein) and mean (MD) ± standard deviation (SD) in brain regions (left and right hemisphere) of control mice. Ligand: [^{3}H]MK-801

		OB		M1		CPu		CA1		CA2/3		DG		SN	
animal	**group**	**left**	**right**	**left**	**right**	**left**	**right**	**left**	**right**	**left**	**right**	**left**	**right**	**left**	**right**
30189369	**control**	872	867	1329	1388	907	888	4698	4808	1957	2231	3081	3289	263	301
30189372	**control**	855	-	1334	1310	843	781	4562	4845	2028	2022	3176	3167	273	301
30189408	**control**	612	600	1238	1247	726	694	3748	3729	1427	1478	2387	2220	175	183
30189465	**control**	548	527	1110	1016	642	568	3752	3625	1606	1559	2353	2355	129	146
30190808	**control**	620	626	1255	1239	721	689	4660	4515	2005	1830	2760	2705	190	228
30190809	**control**	902	897	1572	1633	1015	1033	4599	4790	2142	2207	2943	3051	383	363
30190810	**control**	743	730	1420	1414	994	942	4226	4153	1882	1728	2741	2739	365	325
30190811	**control**	950	960	1651	1566	1043	1019	4121	3637	1962	1723	2693	2459	332	368
30190812	**control**	837	837	1246	1308	888	843	3920	3751	1814	1781	2476	2439	371	381

30191181	**control**	837	826	1549	1397	1006	961	4327	4120	2166	1851	2848	2661	354	389
	MD ± SD	771 ± 140		1361 ± 169		860 ± 146		4229 ± 432		1870 ± 236		2727 ± 314		291 ± 87	

Table A16: NMDA receptor densities (fmol/mg protein) and mean (MD) ± standard deviation (SD) in brain regions (left and right hemisphere) of *Pink1*$^{-/-}$ mice. Ligand: [^{3}H]MK-801

		OB		**M1**		**CPu**		**CA1**		**CA2/3**		**DG**		**SN**	
animal	**group**	**left**	**right**	**left**	**right**	**left**	**right**	**left**	**right**	**left**	**right**	**left**	**right**	**left**	**right**
30189346	***Pink1*$^{-/-}$**	939	937	1654	1661	1074	1002	4693	4612	2358	2376	3133	3206	372	308
30189373	***Pink1*$^{-/-}$**	807	794	1513	1456	925	943	4193	4558	1946	1940	2924	3086	358	311
30189376	***Pink1*$^{-/-}$**	747	743	1322	1415	881	875	-	-	-	-	-	-	220	287
30189381	***Pink1*$^{-/-}$**	529	508	1004	1117	630	644	4001	3878	1625	1410	2393	2333	145	112
30189387	***Pink1*$^{-/-}$**	585	579	1154	1083	672	647	3867	3729	1553	1493	2442	2257	156	156
30189407	***Pink1*$^{-/-}$**	999	995	1649	1583	1084	1073	4478	4475	1959	2000	3014	3039	375	369
30189539	***Pink1*$^{-/-}$**	714	788	1444	1376	978	926	4197	4056	1934	1937	2812	2759	345	350
30189591	***Pink1*$^{-/-}$**	826	837	1366	1338	982	934	4363	4362	1892	1930	2827	2863	362	342
30189592	***Pink1*$^{-/-}$**	858	860	1391	1385	947	902	4166	4048	1809	1886	2680	2623	357	310
30190641	***Pink1*$^{-/-}$**	782	778	1397	1424	911	905	4090	3984	1799	1795	2491	2419	347	361
	MD ± SD	780 ± 142		1387 ± 185		897 ± 141		4208 ± 279		1869 ± 251		2739 ± 298		297 ± 88	

Table A17: mGlu$_{2/3}$ receptor densities (fmol/mg protein) and mean (MD) ± standard deviation (SD) in brain regions (left and right hemisphere) of control mice. Ligand: [^{3}H]LY 341495

		OB		**M1**		**CPu**		**CA1**		**CA2/3**		**DG**		**SN**	
animal	**group**	**left**	**right**	**left**	**right**	**left**	**right**	**left**	**right**	**left**	**right**	**left**	**right**	**left**	**right**
30189369	**control**	-	-	11556	11900	-	-	-	-	-	-	-	-	-	-
30189372	**control**	2956	-	9125	9151	8959	8245	2896	2959	2302	2200	8389	7897	4432	4433
30189408	**control**	2296	2154	10794	10971	11110	10817	3755	3591	2214	2269	10180	10079	2986	2591
30189465	**control**	2436	2623	9522	9332	8275	8232	3459	3407	2020	2052	9127	8810	3459	3641
30190808	**control**	2773	2665	7349	8230	8061	7820	2850	2708	2288	2123	8477	8293	4367	4149
30190809	**control**	2806	2691	9488	8653	7763	7368	3680	3701	2080	2192	8156	8072	4037	3771
30190810	**control**	2794	2816	8648	8951	7823	7306	2401	2366	1610	1768	7390	7209	3070	3615

30190811	**control**	3038	3197	8401	8969	8654	7952	3581	3345	2491	2547	10039	9697	2970	3187
30190812	**control**	2658	2669	10140	10738	7237	7014	2256	2396	1622	1791	7736	7208	2838	2957
30191181	**control**	2687	2900	7965	8083	7423	7537	3369	3171	2076	2176	8869	8869	3344	3597
	MD ± SD	2715 ± 255		9398 ± 1250		8200 ± 1126		3105 ± 513		2101 ± 263		8583 ± 959		3525 ± 580	

Table A18: $mGlu_{2/3}$ receptor densities (fmol/mg protein) and mean (MD) ± standard deviation (SD) in brain regions (left and right hemisphere) of *Pink1*$^{-/-}$ mice. Ligand: [^{3}H]LY 341495

		OB		**M1**		**CPu**		**CA1**		**CA2/3**		**DG**		**SN**	
animal	**group**	**left**	**right**	**left**	**right**	**left**	**right**	**left**	**right**	**left**	**right**	**left**	**right**	**left**	**right**
30189346	***Pink1*$^{-/-}$**	-	-	10224	9880	9276	8805	4280	4394	2764	2983	10443	10233	5405	5130
30189373	***Pink1*$^{-/-}$**	3405	3616	8663	8908	8719	8620	3991	3801	2465	2507	10686	11185	4145	3592
30189376	***Pink1*$^{-/-}$**	3473	3426	9883	10009	9031	8412	-	-	-	-	-	-	4287	4121
30189381	***Pink1*$^{-/-}$**	2958	2854	9761	10087	9055	8778	2937	2941	2235	2045	8811	8112	4020	4471
30189387	***Pink1*$^{-/-}$**	2667	2645	8361	8712	8466	8078	3546	3194	2312	2307	9356	9028	3561	3268
30189407	***Pink1*$^{-/-}$**	2904	2999	9599	9468	9404	8532	3146	3054	2203	2168	8579	9004	4133	4263
30189539	***Pink1*$^{-/-}$**	2771	2962	8684	8178	8165	7655	3767	3544	2445	2361	9145	8814	4825	4787
30189591	***Pink1*$^{-/-}$**	2948	3105	11180	10432	8354	7578	2905	3093	2077	1999	7830	8007	3920	3564
30189592	***Pink1*$^{-/-}$**	3220	3324	8327	8553	8371	8341	4479	4459	2539	2618	10072	10418	3743	3601
30190641	***Pink1*$^{-/-}$**	2999	2856	12540	11509	10610	10610	3831	3629	2315	2360	10433	10268	3441	3641
	MD ± SD	3063 ± 286		9648 ± 1163		8743 ± 791		3611 ± 551		2372 ± 252		9468 ± 1019		4096 ± 587	

Table A19: M_1 receptor densities (fmol/mg protein) and mean (MD) ± standard deviation (SD) in brain regions (left and right hemisphere) of control mice. Ligand: [^{3}H]Pirenzepine

		OB		**M1**		**CPu**		**CA1**		**CA2/3**		**DG**		**SN**	
animal	**group**	**left**	**right**	**left**	**right**	**left**	**right**	**left**	**right**	**left**	**right**	**left**	**right**	**left**	**right**
30189369	**control**	771	740	1917	1859	4056	3811	3973	3798	1884	2003	4199	4120	274	278
30189372	**control**	850	-	1713	1597	3348	2969	4090	3965	1882	1927	4503	4521	268	297
30189408	**control**	876	876	1866	1674	3612	3336	3515	3199	1713	1602	3908	3551	382	350
30189465	**control**	779	759	1214	1367	2613	2554	2930	2933	1515	1440	3432	3428	272	277
30190808	**control**	804	792	2162	1971	4333	4121	4753	4699	2234	2222	5179	5059	334	327

30190809	**control**	1166	1106	2430	2381	4440	4124	4545	4473	2326	2269	5273	5019	403	312
30190810	**control**	1028	965	2568	2485	4608	4308	5338	4914	2740	2427	6142	5737	384	369
30190811	**control**	1451	1371	3465	3326	6562	6215	6710	6522	3438	3298	7334	7304	569	541
30190812	**control**	1265	1259	3445	3339	5586	5352	5868	5714	3258	3010	6076	6384	457	422
30191181	**control**	1283	1259	3112	3081	6163	5949	6044	5974	3162	3233	6913	6887	457	461
	MD ± SD	1021 ± 238		2349 ± 729		4403 ± 1213		4698 ± 1167		2379 ± 656		5248 ± 1295		372 ± 90	

Table A20: M_1 receptor densities (fmol/mg protein) and mean (MD) ± standard deviation (SD) in brain regions (left and right hemisphere) of *Pink1*$^{-/-}$ mice. Ligand: [^{3}H]Pirenzepine

		OB		**M1**		**CPu**		**CA1**		**CA2/3**		**DG**		**SN**	
animal	**group**	**left**	**right**	**left**	**right**	**left**	**right**	**left**	**right**	**left**	**right**	**left**	**right**	**left**	**right**
30189346	***Pink1*$^{-/-}$**	821	826	1805	1789	3665	3432	2948	2937	1447	1520	3098	3032	291	299
30189373	***Pink1*$^{-/-}$**	639	614	1519	1533	2874	2810	2955	2880	1335	1317	3191	3144	283	297
30189376	***Pink1*$^{-/-}$**	562	524	1378	1600	2986	2911	-	-	-	-	-	-	286	271
30189381	***Pink1*$^{-/-}$**	768	716	1587	1438	3051	2836	2906	2757	1411	1436	3092	3184	283	328
30189387	***Pink1*$^{-/-}$**	912	912	2119	2226	4406	4239	4284	4186	1909	1878	4537	4607	333	367
30189407	***Pink1*$^{-/-}$**	767	732	1710	1822	3564	3407	3485	3394	1720	1860	3664	3885	347	359
30189539	***Pink1*$^{-/-}$**	979	957	2652	2606	4875	4533	5260	5065	2533	2558	5866	5774	294	272
30189591	***Pink1*$^{-/-}$**	1022	962	2510	2333	4639	4309	5282	5129	2538	2462	5728	5964	437	381
30189592	***Pink1*$^{-/-}$**	1432	1486	3703	3728	7342	6909	7194	7449	3539	3641	7805	8163	621	612
30190641	***Pink1*$^{-/-}$**	1023	1025	2392	2334	4561	4239	5262	5005	2455	2438	5729	5734	397	413
	MD ± SD	884 ± 251		2139 ± 676		4079 ± 1252		4354 ± 1458		2111 ± 710		4789 ± 1636		358 ± 101	

Table A21: M_2 receptor densities (fmol/mg protein) and mean (MD) ± standard deviation (SD) in brain regions (left and right hemisphere) of control mice. Ligand: [^{3}H]Oxotremorine-M

		OB		**M1**		**CPu**		**CA1**		**CA2/3**		**DG**		**SN**	
animal	**group**	**left**	**right**	**left**	**right**	**left**	**right**	**left**	**right**	**left**	**right**	**left**	**right**	**left**	**right**
30189369	**control**	1774	1607	781	800	1677	1630	538	545	456	492	364	387	261	269
30189372	**control**	2341	-	1136	1130	3004	2801	649	627	510	507	518	538	256	267
30189408	**control**	1787	1797	984	1000	2880	2633	579	560	515	480	419	392	269	298

30189465	**control**	1204	1192	959	946	2569	2497	534	527	416	454	396	389	205	222
30190808	**control**	2234	2217	1115	1117	3491	3469	638	613	550	558	428	420	317	233
30190809	**control**	1468	1456	912	966	2804	2925	666	689	537	561	485	502	208	201
30190810	**control**	1725	1706	935	998	2322	2483	535	561	467	467	412	422	246	354
30190811	**control**	3082	3063	1328	1454	4516	4512	679	635	555	542	460	419	370	333
30190812	**control**	1027	1071	815	824	2235	2200	414	392	314	309	402	384	90	105
30191181	**control**	1482	1540	894	800	1914	1981	444	468	383	419	307	292	261	217
	MD ± SD	1778 ± 586		995 ± 177		2727 ± 796		565 ± 87		475 ± 75		417 ± 62		249 ± 71	

Table A22: M_2 receptor densities (fmol/mg protein) and mean (MD) ± standard deviation (SD) in brain regions (left and right hemisphere) of *Pink1*$^{-/-}$ mice. Ligand: [^{3}H]Oxotremorine-M

		OB		**M1**		**CPu**		**CA1**		**CA2/3**		**DG**		**SN**	
animal	**group**	**left**	**right**	**left**	**right**	**left**	**right**	**left**	**right**	**left**	**right**	**left**	**right**	**left**	**right**
30189346	***Pink1*$^{-/-}$**	2125	2123	1210	1310	3518	3639	647	620	554	581	425	413	242	265
30189373	***Pink1*$^{-/-}$**	1756	1834	1025	1023	2807	2943	530	486	442	475	354	368	323	312
30189376	***Pink1*$^{-/-}$**	1006	1053	852	819	1500	1723	-	-	-	-	-	-	259	275
30189381	***Pink1*$^{-/-}$**	1484	1508	901	938	2367	2523	623	602	488	487	513	523	249	242
30189387	***Pink1*$^{-/-}$**	2000	2173	917	950	2352	2686	454	483	377	422	326	335	314	325
30189407	***Pink1*$^{-/-}$**	1884	1913	1063	1086	2696	2923	559	582	482	508	427	426	241	251
30189539	***Pink1*$^{-/-}$**	2076	2095	1199	1155	3222	3263	542	580	458	510	389	401	301	312
30189591	***Pink1*$^{-/-}$**	1658	1752	1019	1045	2710	2434	572	548	459	492	393	408	329	279
30189592	***Pink1*$^{-/-}$**	2435	2470	1372	1300	4204	4165	624	638	608	600	474	474	228	219
30190641	***Pink1*$^{-/-}$**	1592	1632	782	797	2151	2249	453	471	352	367	452	475	170	177
	MD ± SD	1828 ± 389		1038 ± 175		2804 ± 714		556 ± 65		481 ± 74		421 ± 57		266 ± 47	

Table A23: M_3 receptor densities (fmol/mg protein) and mean (MD) ± standard deviation (SD) in brain regions (left and right hemisphere) of control mice. Ligand: [^{3}H]4-DAMP

		OB		**M1**		**CPu**		**CA1**		**CA2/3**		**DG**		**SN**	
animal	**group**	**left**	**right**	**left**	**right**	**left**	**right**	**left**	**right**	**left**	**right**	**left**	**right**	**left**	**right**
30189369	**control**	2488	2424	5314	5303	8227	8434	7738	8140	4244	4736	6418	6532	602	604

30189372	**control**	2305	-	5265	5357	8249	8487	7358	7691	4151	4478	5986	6002	601	617
30189408	**control**	2108	2070	5173	5257	9356	8768	7712	7710	4158	4299	6704	6559	670	622
30189465	**control**	2625	2689	5267	5314	8685	8464	7493	7810	3972	3750	6316	6414	575	539
30190808	**control**	2420	2523	5520	5327	8271	8465	8005	8066	4423	4755	6337	6650	683	660
30190809	**control**	2525	2468	5332	5579	8498	8740	7574	7232	4390	4455	6037	6177	601	553
30190810	**control**	2299	2401	5601	5466	8552	8684	7999	7914	4587	4574	6491	6527	659	616
30190811	**control**	2512	2448	5319	5604	8270	8391	7764	7782	4335	4570	6192	6049	729	732
30190812	**control**	1888	1944	4222	4457	8578	8690	7868	7496	3808	3658	6514	6168	591	628
30191181	**control**	2215	2239	5491	5340	8802	9089	7425	7670	4094	4485	6394	6251	733	724
	MD ± SD	2347 ± 222		5276 ± 345		8585 ± 284		7722 ± 242		4296 ± 316		6336 ± 220		637 ± 59	

Table A24: M_3 receptor densities (fmol/mg protein) and mean (MD) ± standard deviation (SD) in brain regions (left and right hemisphere) of *Pink1*$^{-/-}$ mice. Ligand: [^{3}H]4-DAMP

		OB		**M1**		**CPu**		**CA1**		**CA2/3**		**DG**		**SN**	
animal	**group**	**left**	**right**	**left**	**right**	**left**	**right**	**left**	**right**	**left**	**right**	**left**	**right**	**left**	**right**
30189346	***Pink1*$^{-/-}$**	2306	2300	5241	5352	8186	8322	7646	7622	4414	4723	5939	6067	621	624
30189373	***Pink1*$^{-/-}$**	2117	2125	4698	4695	8179	8239	7282	7473	3744	4144	6048	6006	690	617
30189376	***Pink1*$^{-/-}$**	2159	2291	5082	4934	8258	8168	-	-	-	-	-	-	550	632
30189381	***Pink1*$^{-/-}$**	2331	2344	4426	4704	7715	8113	7355	7557	3949	4390	5987	6124	592	643
30189387	***Pink1*$^{-/-}$**	2328	2336	5126	5390	8714	8832	8040	7581	4543	4200	6365	6322	646	639
30189407	***Pink1*$^{-/-}$**	2535	2494	5387	5439	9078	8944	7987	8146	4555	5103	6890	6905	620	532
30189539	***Pink1*$^{-/-}$**	2425	2592	6051	5956	8589	8551	7871	8346	3915	4434	6407	6589	570	576
30189591	***Pink1*$^{-/-}$**	2540	2576	5711	5930	8938	8777	8202	8519	4406	4864	6601	6766	664	601
30189592	***Pink1*$^{-/-}$**	2528	2571	5183	5190	9194	9129	7897	7693	4136	3976	6443	6295	653	633
30190641	***Pink1*$^{-/-}$**	2117	2163	4308	4202	7614	7690	6810	6747	3521	3377	5537	5380	518	509
	MD ± SD	2359 ± 166		5150 ± 535		8462 ± 486		7710 ± 478		4244 ± 451		6259 ± 420		607 ± 50	

Table A25: Nicotinic $\alpha_4\beta_2$ receptor densities (fmol/mg protein) and mean (MD) ± standard deviation (SD) in brain regions (left and right hemisphere) of control mice. Ligand: [^{3}H]Epibatidine

		OB		M1		CPu		CA1		CA2/3		DG		SN	
animal	**group**	**left**	**right**	**left**	**right**	**left**	**right**	**left**	**right**	**left**	**right**	**left**	**right**	**left**	**right**
30189369	**control**	147	142	296	279	359	343	140	146	135	135	190	206	170	160
30189372	**control**	140	-	281	268	350	324	140	142	117	128	205	189	175	176
30189408	**control**	155	148	281	277	343	338	113	120	112	122	211	216	158	171
30189465	**control**	114	113	229	232	308	298	98	93	103	86	156	144	151	142
30190808	**control**	107	114	213	233	310	287	107	112	110	102	179	173	116	144
30190809	**control**	116	120	239	226	297	294	105	103	113	107	170	165	137	144
30190810	**control**	107	106	219	229	291	253	88	84	86	81	152	141	158	128
30190811	**control**	160	156	331	308	377	375	135	133	132	118	212	221	192	196
30190812	**control**	127	124	251	245	338	321	117	124	121	125	183	195	160	173
30191181	**control**	131	130	241	279	336	350	121	110	124	118	214	217	209	162
	MD ± SD	129 ± 18		258 ± 33		325 ± 32		116 ± 19		114 ± 16		187 ± 26		161 ± 23	

Table A26: Nicotinic $\alpha_4\beta_2$ receptor densities (fmol/mg protein) and mean (MD) ± standard deviation (SD) in brain regions (left and right hemisphere) of *Pink1*$^{-/-}$ mice. Ligand: [^{3}H]Epibatidine

		OB		M1		CPu		CA1		CA2/3		DG		SN	
animal	**group**	**left**	**right**	**left**	**right**	**left**	**right**	**left**	**right**	**left**	**right**	**left**	**right**	**left**	**right**
30189346	***Pink1*$^{-/-}$**	139	139	297	305	386	373	145	132	128	125	207	213	196	192
30189373	***Pink1*$^{-/-}$**	139	137	278	271	359	350	145	137	111	118	210	197	183	149
30189376	***Pink1*$^{-/-}$**	150	143	301	289	366	363	-	-	-	-	-	-	172	162
30189381	***Pink1*$^{-/-}$**	109	105	231	252	301	303	97	105	105	95	172	144	146	131
30189387	***Pink1*$^{-/-}$**	101	98	197	207	271	261	93	96	88	85	150	140	172	126
30189407	***Pink1*$^{-/-}$**	123	124	251	257	310	304	116	114	112	97	183	164	162	136
30189539	***Pink1*$^{-/-}$**	104	100	194	198	281	264	82	84	86	87	142	143	127	126
30189591	***Pink1*$^{-/-}$**	104	101	195	199	263	262	94	86	88	84	156	147	120	140
30189592	***Pink1*$^{-/-}$**	144	146	291	292	353	362	129	139	141	130	230	216	180	170

30190641	***Pink1*$^{-/-}$**	124	120	279	268	333	335	115	114	120	103	187	191	168	179
	MD ± SD	123 ± 19		253 ± 41		320 ± 43		112 ± 21		106 ± 18		177 ± 30		157 ± 24	

Table A27: α_1 receptor densities (fmol/mg protein) and mean (MD) ± standard deviation (SD) in brain regions (left and right hemisphere) of control mice. Ligand: [^{3}H]Prazosin

		OB		**M1**		**CPu**		**CA1**		**CA2/3**		**DG**		**SN**	
animal	**group**	**left**	**right**	**left**	**right**	**left**	**right**	**left**	**right**	**left**	**right**	**left**	**right**	**left**	**right**
30189369	**control**	515	493	746	741	115	109	103	100	89	84	135	133	130	101
30189372	**control**	502	-	670	604	94	87	109	101	91	85	128	126	108	101
30189408	**control**	635	612	723	723	188	174	175	173	162	164	216	209	212	192
30189465	**control**	605	601	753	742	171	167	158	149	143	147	181	178	176	175
30190808	**control**	599	617	739	758	172	166	170	154	160	148	201	194	209	197
30190809	**control**	517	500	812	764	139	134	124	125	122	119	146	147	147	138
30190810	**control**	565	537	802	791	119	114	124	127	125	111	165	161	167	126
30190811	**control**	651	628	966	937	152	149	157	147	143	128	184	184	146	162
30190812	**control**	488	489	810	786	136	130	126	128	114	125	151	148	168	109
30191181	**control**	521	516	789	739	116	118	123	128	131	114	165	151	133	106
	MD ± SD	557 ± 57		770 ± 79		137 ± 29		135 ± 24		125 ± 25		165 ± 27		150 ± 36	

Table A28: α_1 receptor densities (fmol/mg protein) and mean (MD) ± standard deviation (SD) in brain regions (left and right hemisphere of *Pink1*$^{-/-}$ mice. Ligand: [^{3}H]Prazosin

		OB		**M1**		**CPu**		**CA1**		**CA2/3**		**DG**		**SN**	
animal	**group**	**left**	**right**	**left**	**right**	**left**	**right**	**left**	**right**	**left**	**right**	**left**	**right**	**left**	**right**
30189346	***Pink1*$^{-/-}$**	821	793	1071	1147	142	134	140	126	128	115	175	153	154	129
30189373	***Pink1*$^{-/-}$**	484	474	733	668	101	98	104	103	94	87	121	122	121	100
30189376	***Pink1*$^{-/-}$**	396	386	575	604	90	95	-	-	-	-	-	-	135	123
30189381	***Pink1*$^{-/-}$**	564	549	788	779	167	163	170	160	160	137	200	186	189	187
30189387	***Pink1*$^{-/-}$**	637	632	828	832	170	171	157	160	163	145	189	196	212	194
30189407	***Pink1*$^{-/-}$**	553	573	831	862	134	127	126	130	123	123	170	163	159	145
30189539	***Pink1*$^{-/-}$**	533	572	806	778	127	122	115	110	110	100	133	143	147	122
30189591	***Pink1*$^{-/-}$**	575	551	912	823	119	110	126	121	112	105	159	154	136	124

30189592	***Pink1*$^{-/-}$**	569	618	712	686	138	144	136	139	116	130	164	161	158	140
30190641	***Pink1*$^{-/-}$**	523	542	821	894	125	126	131	124	134	109	156	149	144	117
	MD ± SD	567 ± 105		807 ± 137		130 ± 25		132 ± 20		122 ± 21		161 ± 23		147 ± 29	

Table A29: D_1 receptor densities (fmol/mg protein) and mean (MD) ± standard deviation (SD) in brain regions (left and right hemisphere) of control mice. Ligand: [^{3}H]SCH 23390

		OB		**M1**		**CPu**		**SN**	
animal	**group**	**left**	**right**	**left**	**right**	**left**	**right**	**left**	**right**
30189369	**control**	98	93	186	183	5922	6143	2758	2970
30189372	**control**	79	-	145	155	6135	5791	2037	2350
30189408	**control**	173	174	276	287	6936	6533	2353	2367
30189465	**control**	122	116	176	187	5153	4864	2030	1860
30190808	**control**	115	118	209	214	5603	5374	2721	2711
30190809	**control**	109	103	188	196	5345	5038	2014	2011
30190810	**control**	104	101	213	218	6068	5710	1575	1342
30190811	**control**	95	88	175	190	6296	5891	2039	2479
30190812	**control**	58	63	136	138	4958	4837	2651	3383
30191181	**control**	77	74	167	162	6053	5556	2104	2089
	MD ± SD	103 ± 31		190 ± 40		5710 ± 576		2292 ± 483	

Table A30: D_1 receptor densities (fmol/mg protein) and mean (MD) ± standard deviation (SD) in brain regions (left and right hemisphere) of *Pink1*$^{-/-}$ mice. Ligand: [^{3}H]SCH 23390

		OB		**M1**		**CPu**		**SN**	
animal	**group**	**left**	**right**	**left**	**right**	**left**	**right**	**left**	**right**
30189346	***Pink1*$^{-/-}$**	153	144	273	269	8957	8547	2383	2698
30189373	***Pink1*$^{-/-}$**	79	82	150	168	6353	6116	1889	2050
30189376	***Pink1*$^{-/-}$**	69	71	119	125	5137	4987	1955	1984
30189381	***Pink1*$^{-/-}$**	129	131	209	202	5235	5155	1761	1690
30189387	***Pink1*$^{-/-}$**	124	117	211	231	5969	5561	2465	2385
30189407	***Pink1*$^{-/-}$**	122	121	185	186	5385	5431	1922	1784
30189539	***Pink1*$^{-/-}$**	92	96	196	199	5691	5708	1908	2092

30189591	***Pink1*$^{-/-}$**	121	115	207	191	5728	5349	1797	1996
30189592	***Pink1*$^{-/-}$**	86	83	208	193	6956	6817	1824	2234
30190641	***Pink1*$^{-/-}$**	83	80	138	147	5345	5458	1514	1193
	MD ± SD	105 ± 26		190 ± 41		5994 ± 1084		1976 ± 344	

Table A31: D_2 receptor densities (fmol/mg protein) and mean (MD) ± standard deviation (SD) in brain regions (left and right hemisphere) of control mice. Ligand: [^{3}H]Raclopride

		CPu	
animal	**group**	**left**	**right**
30189369	**control**	346	362
30189372	**control**	403	402
30189408	**control**	433	427
30189465	**control**	482	496
30190808	**control**	477	456
30190809	**control**	432	421
30190810	**control**	367	370
30190811	**control**	436	434
30190812	**control**	394	383
30191181	**control**	406	385
	MD ± SD	416 ± 42	

Table A32: D_2 receptor densities (fmol/mg protein) and mean (MD) ± standard deviation (SD) in brain regions (left and right hemisphere) of *Pink1*$^{-/-}$ mice. Ligand: [^{3}H]Raclopride

		CPu	
animal	**group**	**left**	**right**
30189346	***Pink1*$^{-/-}$**	432	414
30189373	***Pink1*$^{-/-}$**	413	379
30189376	***Pink1*$^{-/-}$**	398	391
30189381	***Pink1*$^{-/-}$**	402	388
30189387	***Pink1*$^{-/-}$**	414	472
30189407	***Pink1*$^{-/-}$**	403	411

30189539	***Pink1*$^{-/-}$**	361	347
30189591	***Pink1*$^{-/-}$**	389	402
30189592	***Pink1*$^{-/-}$**	449	447
30190641	***Pink1*$^{-/-}$**	419	422
	MD ± SD	408 ± 29	

Table A33: $D_{2/3}$ receptor densities (fmol/mg protein) and mean (MD) ± standard deviation (SD) in brain regions (left and right hemisphere) of control mice. Ligand: [^{3}H]Fallypride

		OB		**M1**		**CPu**	
animal	**group**	**left**	**right**	**left**	**right**	**left**	**right**
30189369	**control**	403	394	121	127	2534	2496
30189372	**control**	303	-	125	109	2279	2230
30189408	**control**	448	431	136	127	2705	2626
30189465	**control**	370	412	107	118	2375	2255
30190808	**control**	339	399	111	104	2549	2311
30190809	**control**	297	314	100	97	2351	2202
30190810	**control**	282	219	87	90	2133	1911
30190811	**control**	525	465	179	160	2841	2699
30190812	**control**	421	362	135	132	2174	2169
30191181	**control**	440	472	147	142	2755	2616
	MD ± SD	384 ± 77		123 ± 23		2411 ± 249	

Table A34: $D_{2/3}$ receptor densities (fmol/mg protein) and mean (MD) ± standard deviation (SD) in brain regions (left and right hemisphere) of *Pink1*$^{-/-}$ mice. Ligand: [^{3}H]Fallypride

		OB		**M1**		**S1**		**CPu**	
animal	**group**	**left**	**right**	**left**	**right**	**left**	**right**	**left**	**right**
30189346	***Pink1*$^{-/-}$**	387	453	146	152	142	131	2838	2505
30189373	***Pink1*$^{-/-}$**	306	228	117	134	140	134	2518	2351
30189376	***Pink1*$^{-/-}$**	402	421	99	107	118	108	2447	2314
30189381	***Pink1*$^{-/-}$**	323	333	125	132	140	133	2511	2539
30189387	***Pink1*$^{-/-}$**	373	348	96	104	122	107	2403	2225

30189407	***Pink1*$^{-/-}$**	372	303	118	120	122	123	2750	2664
30189539	***Pink1*$^{-/-}$**	373	277	83	86	97	85	2369	2211
30189591	***Pink1*$^{-/-}$**	321	337	90	92	105	93	2352	2305
30189592	***Pink1*$^{-/-}$**	433	411	165	168	174	161	2742	2723
30190641	***Pink1*$^{-/-}$**	370	337	134	135	142	154	2199	2272
	MD ± SD	355 ± 55		120 ± 26		127 ± 23		2462 ± 196	

Table A35: 5-HT$_{1A}$ receptor densities (fmol/mg protein) and mean (MD) ± standard deviation (SD) in brain regions (left and right hemisphere) of control mice. Ligand: [^{3}H]8-OH-DPAT

		M1		**CPu**		**CA1**		**CA2/3**		**DG**		**SN**	
animal	**group**	**left**	**right**	**left**	**right**	**left**	**right**	**left**	**right**	**left**	**right**	**left**	**right**
30189369	**control**	86	83	39	37	388	401	69	84	77	76	38	48
30189372	**control**	87	88	38	38	436	412	67	77	77	76	39	46
30189408	**control**	65	64	30	29	308	301	60	70	59	58	32	34
30189465	**control**	61	58	25	24	320	326	66	61	58	54	26	25
30190808	**control**	59	66	25	23	345	337	58	54	61	59	20	23
30190809	**control**	88	88	39	35	386	374	108	115	85	82	35	36
30190810	**control**	76	79	35	33	436	423	75	85	76	75	36	38
30190811	**control**	93	90	42	40	434	413	69	71	72	73	40	43
30190812	**control**	70	72	33	34	385	367	66	62	70	72	36	32
30191181	**control**	90	94	33	33	421	440	104	95	90	92	37	35
	MD ± SD	78 ± 12		33 ± 6		383 ± 46		76 ± 17		72 ± 11		35 ± 7	

Table A36: 5-HT$_{1A}$ receptor densities (fmol/mg protein) and mean (MD) ± standard deviation (SD) in brain regions (left and right hemisphere) of *Pink1*$^{-/-}$ mice. Ligand: [^{3}H]8-OH-DPAT

		M1		**CPu**		**CA1**		**CA2/3**		**DG**		**SN**	
animal	**group**	**left**	**right**	**left**	**right**	**left**	**right**	**left**	**right**	**left**	**right**	**left**	**right**
30189346	***Pink1*$^{-/-}$**	92	93	43	41	459	448	60	61	80	82	42	41
30189373	***Pink1*$^{-/-}$**	87	87	37	39	369	359	57	65	82	71	36	42

30189376	***Pink1*$^{-/-}$**	92	93	41	42	-	-	-	-	-	-	48	49
30189381	***Pink1*$^{-/-}$**	71	69	26	24	362	377	49	49	67	57	29	26
30189387	***Pink1*$^{-/-}$**	65	55	27	27	265	269	55	58	46	45	27	28
30189407	***Pink1*$^{-/-}$**	96	98	45	44	475	495	101	100	91	92	38	40
30189539	***Pink1*$^{-/-}$**	75	72	36	33	428	443	79	67	80	83	39	35
30189591	***Pink1*$^{-/-}$**	-	-	-	-	434	420	107	112	75	74	34	34
30189592	***Pink1*$^{-/-}$**	103	102	38	36	513	549	120	122	85	94	36	34
30190641	***Pink1*$^{-/-}$**	78	70	34	32	301	295	82	82	67	74	35	31
	MD ± SD	83 ± 14		36 ± 7		403 ± 84		79 ± 25		75 ± 14		36 ± 6	

Table A37: 5-HT$_2$ receptor densities (fmol/mg protein) and mean (MD) ± standard deviation (SD) in brain regions (left and right hemisphere) of control mice. Ligand: [^{3}H]Ketanserin

		OB		**M1**		**CPu**		**CA1**		**CA2/3**		**DG**		**SN**	
animal	**group**	**left**	**right**	**left**	**right**	**left**	**right**	**left**	**right**	**left**	**right**	**left**	**right**	**left**	**right**
30189369	**control**	180	189	404	402	691	682	236	236	199	197	205	197	180	196
30189372	**control**	154	-	345	346	543	581	230	233	188	211	202	202	186	192
30189408	**control**	143	144	282	290	440	445	149	163	116	123	143	142	128	109
30189465	**control**	99	103	241	274	408	376	140	145	115	134	140	138	115	106
30190808	**control**	115	116	256	282	446	444	152	163	140	143	138	139	123	122
30190809	**control**	225	228	429	473	572	625	295	297	254	271	291	272	213	220
30190810	**control**	233	227	468	463	721	759	302	297	256	259	280	281	289	302
30190811	**control**	170	163	415	428	608	627	189	207	172	172	184	198	175	162
30190812	**control**	114	120	233	235	404	428	138	140	128	126	136	139	135	125
30191181	**control**	129	135	329	337	502	533	163	161	128	145	165	163	162	146
	MD ± SD	157 ± 45		347 ± 83		542 ± 117		202 ± 59		174 ± 53		188 ± 54		169 ± 55	

Table A38: 5-HT$_2$ receptor densities (fmol/mg protein) and mean (MD) ± standard deviation (SD) in brain regions (left and right hemisphere) of *Pink1*$^{-/-}$ mice. Ligand: [^{3}H]Ketanserin

		OB		**M1**		**CPu**		**CA1**		**CA2/3**		**DG**		**SN**	
animal	**group**	**left**	**right**	**left**	**right**	**left**	**right**	**left**	**right**	**left**	**right**	**left**	**right**	**left**	**right**
30189346	***Pink1*$^{-/-}$**	220	221	490	518	768	759	232	241	215	238	223	212	196	189

30189373	***Pink1*$^{-/-}$**	172	167	352	392	564	584	206	206	154	194	170	181	158	158
30189376	***Pink1*$^{-/-}$**	154	164	347	356	535	529	-	-	-	-	-	-	209	210
30189381	***Pink1*$^{-/-}$**	117	117	233	231	325	323	146	171	135	119	120	139	100	109
30189387	***Pink1*$^{-/-}$**	121	120	260	276	443	441	142	143	117	102	111	120	107	109
30189407	***Pink1*$^{-/-}$**	228	227	442	442	678	647	280	287	252	282	282	260	261	234
30189539	***Pink1*$^{-/-}$**	206	213	402	446	744	766	291	306	210	240	257	269	230	231
30189591	***Pink1*$^{-/-}$**	234	244	455	468	655	643	274	286	236	234	242	261	253	225
30189592	***Pink1*$^{-/-}$**	151	146	309	320	612	624	173	176	141	141	136	136	123	141
30190641	***Pink1*$^{-/-}$**	129	127	257	253	364	395	152	158	137	149	148	140	126	119
	MD ± SD	174 ± 46		362 ± 92		570 ± 147		215 ± 60		183 ± 56		189 ± 61		174 ± 55	

Table A39: A_1 receptor densities (fmol/mg protein) and mean (MD) ± standard deviation (SD) in brain regions (left and right hemisphere) of control mice. Ligand: [^{3}H]DPCPX

		OB		**M1**		**CPu**		**CA1**		**CA2/3**		**DG**		**SN**	
animal	**group**	**left**	**right**	**left**	**right**	**left**	**right**	**left**	**right**	**left**	**right**	**left**	**right**	**left**	**right**
30189369	**control**	1007	998	3141	3098	3351	3395	6319	6206	5127	5225	3923	3828	3145	3110
30189372	**control**	910	-	3111	3231	3196	3114	6654	6593	5479	5397	4114	4066	2848	2968
30189408	**control**	957	975	3813	3844	3901	3847	7501	7446	6118	5692	4853	4851	3562	3709
30189465	**control**	925	924	3774	3816	3916	4082	7319	7285	5794	5726	4655	4599	4389	4140
30190808	**control**	1064	1074	3413	3377	3675	3526	7831	7851	6218	6185	4664	4751	3765	3752
30190809	**control**	1008	1005	3686	3801	3828	3469	7341	7680	5946	5897	4815	4848	3246	2933
30190810	**control**	976	1015	3162	3586	3601	3709	6748	7148	6041	6008	4409	4425	3312	3179
30190811	**control**	831	899	3387	3498	3249	3354	6966	7121	5566	6112	4019	4367	3264	3331
30190812	**control**	997	1035	3610	3483	3683	3510	7817	7509	6203	6341	4390	4554	3725	4062
30191181	**control**	981	956	3432	3537	3673	3426	6490	6719	5476	5458	4596	4623	3602	3459
	MD ± SD	976 ± 59		3490 ± 252		3575 ± 262		7127 ± 516		5800 ± 359		4468 ± 324		3475 ± 419	

Table A40: A_1 receptor densities (fmol/mg protein) and mean (MD) ± standard deviation (SD) in brain regions (left and right hemisphere) of *Pink1*$^{-/-}$ mice. Ligand: [^{3}H]DPCPX

		OB		**M1**		**CPu**		**CA1**		**CA2/3**		**DG**		**SN**	
animal	**group**	**left**	**right**	**left**	**right**	**left**	**right**	**left**	**right**	**left**	**right**	**left**	**right**	**left**	**right**

30189346	***Pink1*$^{-/-}$**	994	1046	3444	3485	3369	3595	6933	6964	5995	5933	4259	4249	3329	3307
30189373	***Pink1*$^{-/-}$**	909	965	3145	3122	3331	3328	6491	6577	5179	5691	4103	4124	3144	3156
30189376	***Pink1*$^{-/-}$**	1011	1028	3821	3832	3735	3756	-	-	-	-	-	-	3301	2815
30189381	***Pink1*$^{-/-}$**	1037	1088	3693	3418	3490	3281	6644	6603	5372	5398	4333	4124	3433	3265
30189387	***Pink1*$^{-/-}$**	1064	1106	3754	2970	3398	3390	6631	6865	5521	6290	4368	4310	3538	3637
30189407	***Pink1*$^{-/-}$**	1114	1149	3676	4005	3828	4128	7450	7408	6477	6323	4864	4729	3545	3318
30189539	***Pink1*$^{-/-}$**	1026	935	3398	3495	3522	3492	7793	7708	6331	6372	4569	4482	3126	2968
30189591	***Pink1*$^{-/-}$**	950	928	3464	3363	3535	3668	7355	7337	6380	5931	4344	4307	3062	3041
30189592	***Pink1*$^{-/-}$**	1338	1334	4232	4297	4193	4143	8362	8474	6490	6252	5453	5344	4244	-
30190641	***Pink1*$^{-/-}$**	945	955	3470	3683	3597	3734	7011	7303	5555	6018	4530	4689	3299	3323
	MD ± SD	1046 ± 120		3588 ± 343		3626 ± 276		7217 ± 589		5973 ± 424		4510 ± 387		3308 ± 306	

Table A41: A_{2A} receptor densities (fmol/mg protein) and mean (MD) ± standard deviation (SD) in brain regions (left and right hemisphere) of control mice. Ligand: [^{3}H]ZM 241385

		CPu	
animal	**group**	**left**	**right**
30189369	**control**	2428	2371
30189372	**control**	1894	1872
30189408	**control**	2800	2843
30189465	**control**	2422	2476
30190808	**control**	2786	2373
30190809	**control**	2366	2428
30190810	**control**	2623	2409
30190811	**control**	2299	2431
30190812	**control**	2419	2340
30191181	**control**	2429	2384
	MD ± SD	2420 ± 242	

Table A42: A_{2A} receptor densities (fmol/mg protein) and mean (MD) ± standard deviation (SD) in brain regions (left and right hemisphere) of *Pink1*$^{-/-}$ mice. Ligand: [^{3}H]ZM 241385

		CPu	
animal	**group**	**left**	**right**
30189346	***Pink1*$^{-/-}$**	2932	2413
30189373	***Pink1*$^{-/-}$**	2415	2436
30189376	***Pink1*$^{-/-}$**	2655	2848
30189381	***Pink1*$^{-/-}$**	2319	2289
30189387	***Pink1*$^{-/-}$**	2366	2407
30189407	***Pink1*$^{-/-}$**	2625	2615
30189539	***Pink1*$^{-/-}$**	2577	2310
30189591	***Pink1*$^{-/-}$**	2316	2350
30189592	***Pink1*$^{-/-}$**	2680	2735
30190641	***Pink1*$^{-/-}$**	2565	2493
	MD ± SD	2517 ± 187	

8.2.2. Immunohistochemical staining

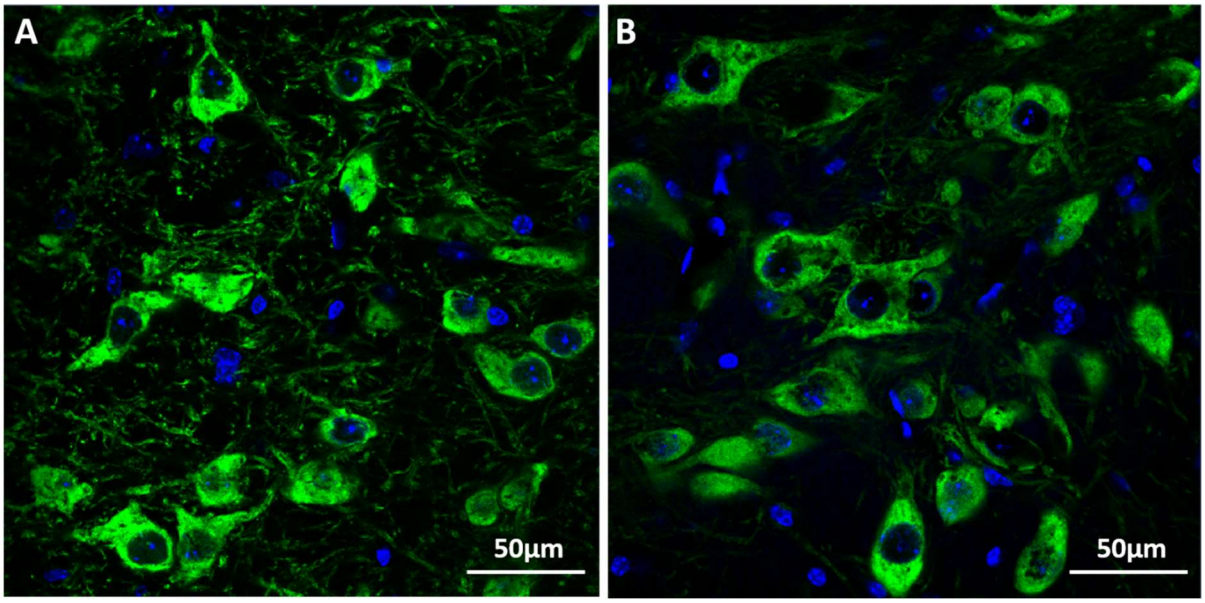

Fig. A1: Exemplary immunohistochemical staining against TH (green) in the SN of control mice (A) and *Pink1*$^{-/-}$ mice (B) indicating no differences in TH-positive neurons. Cell nuclei are stained blue. Magnification: 40x objective at a final resolution of 0.221µm/pixel. Scale bar = 50µm

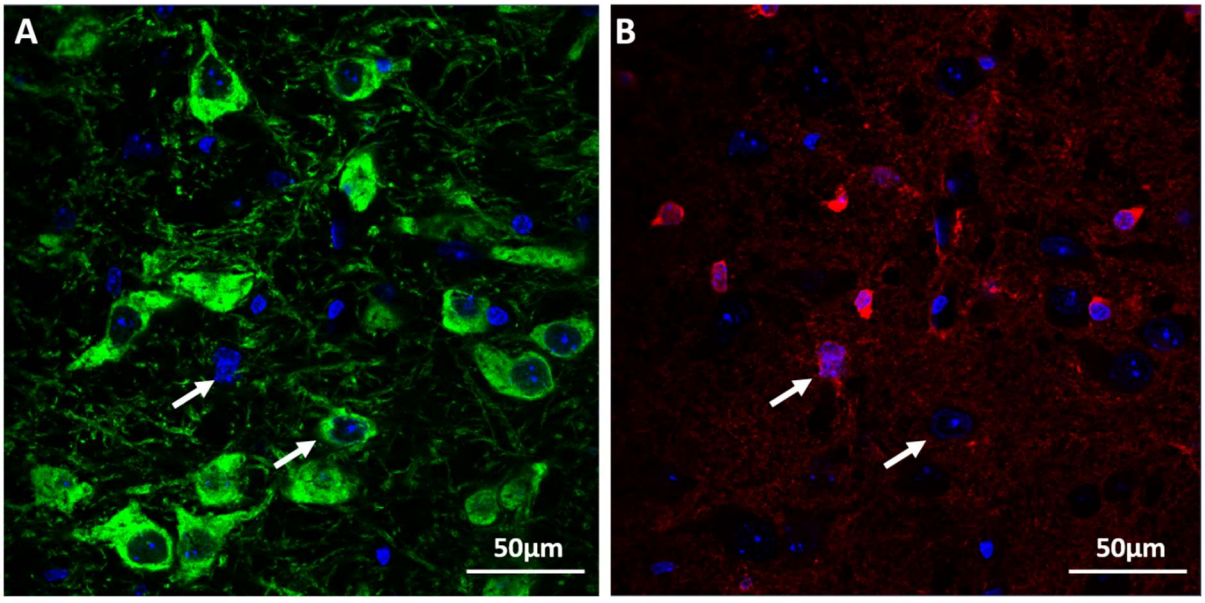

Fig. A2: Exemplary immunohistochemical staining against TH (A; green) and GS (B; red) of control mice indicating that there is no co-localization of TH and GS in neurons of the SN. Arrows mark examples of TH-positive neurons and GS-positive astrocytes. Cell nuclei are stained blue. Magnification: 40x objective at a final resolution of 0.221µm/pixel. Scale bar = 50µm

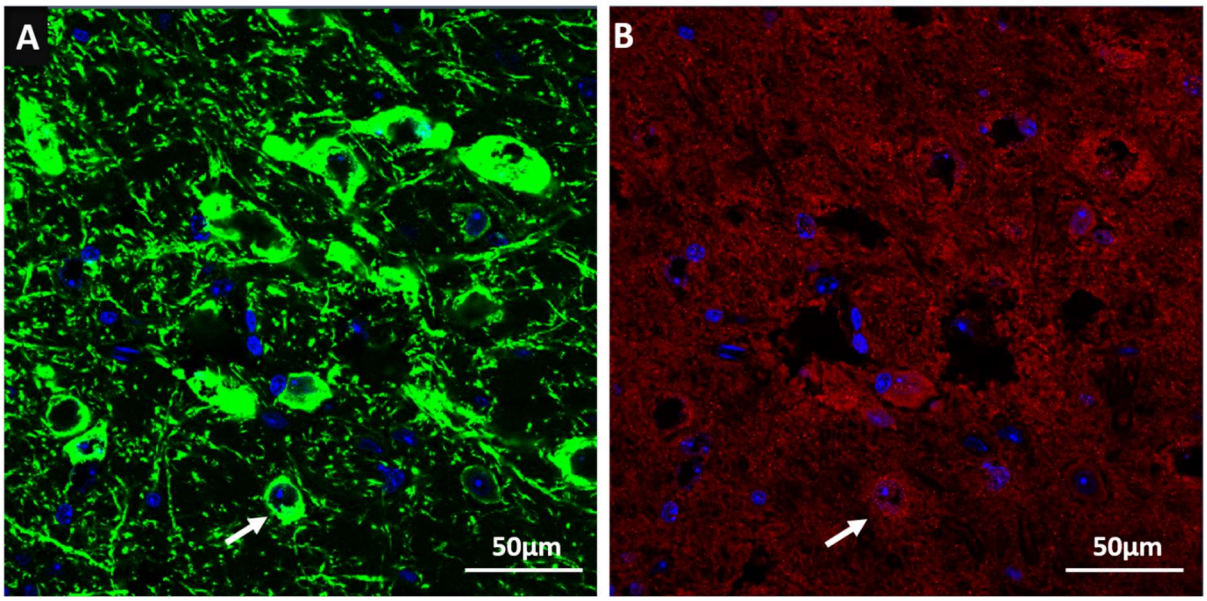

Fig. A3: Exemplary immunohistochemical staining against TH (A; green) and GABA (B; red) of control mice indicating that GABA immunoreactivity was co-localized with TH-positive neurons in the SN. Note that the arrows marks the same neuron with co-localized TH (A) and GABA (B). Cell nuclei are stained blue. Magnification: 40x objective at a final resolution of 0.221µm/pixel. Scale bar = 50µm

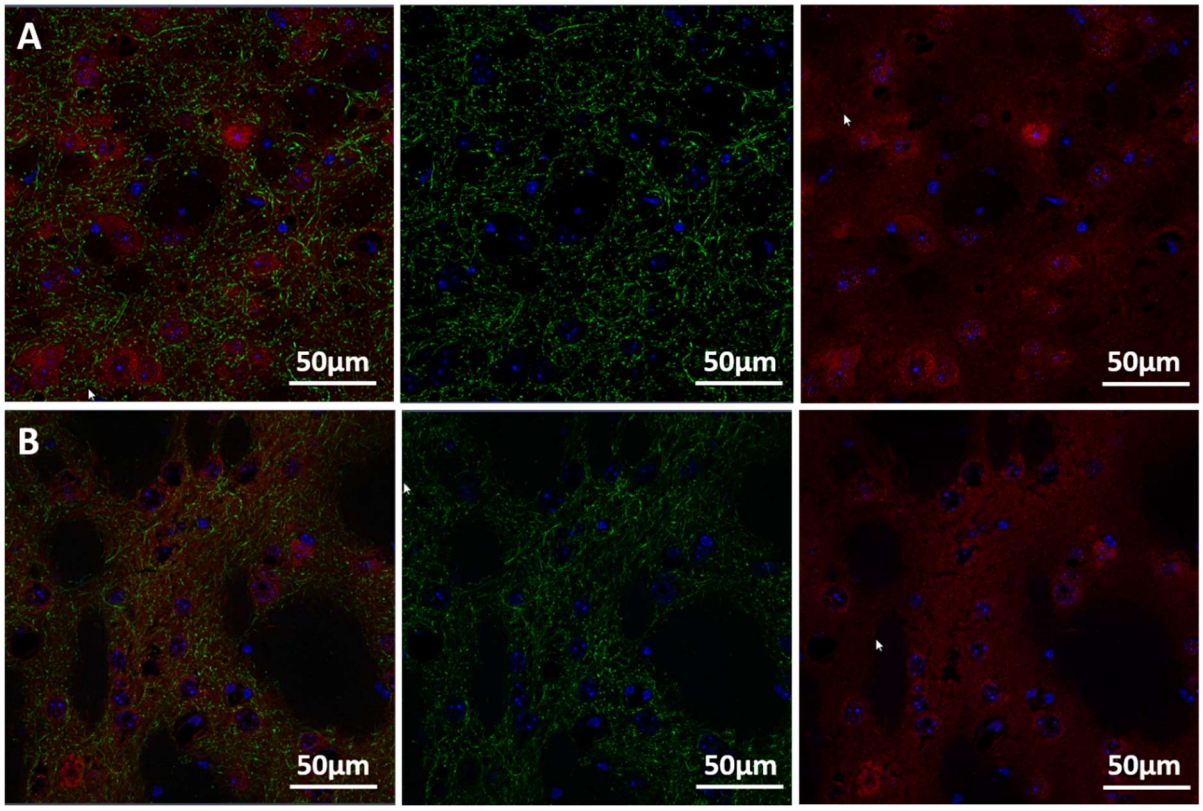

Fig. A4: Exemplary immunohistochemical staining against GABA (red) and TH (green) in the striatum of control mice (A) and *Pink1*$^{-/-}$ mice (B) indicating that the staining intensity of GABA-positive neurons was slightly reduced in *Pink1*$^{-/-}$ mice. Cell nuclei are stained blue. Left images indicate GABA, TH and cell nuclei staining. Middle images indicate TH and cell nuclei staining. Right images indicate GABA and cell nuclei staining. Magnification: 40x objective at a final resolution of 0.221µm/pixel. Scale bar = 50µm

8.2.3. Quantification of neurotransmitter receptor densities

GABA receptors

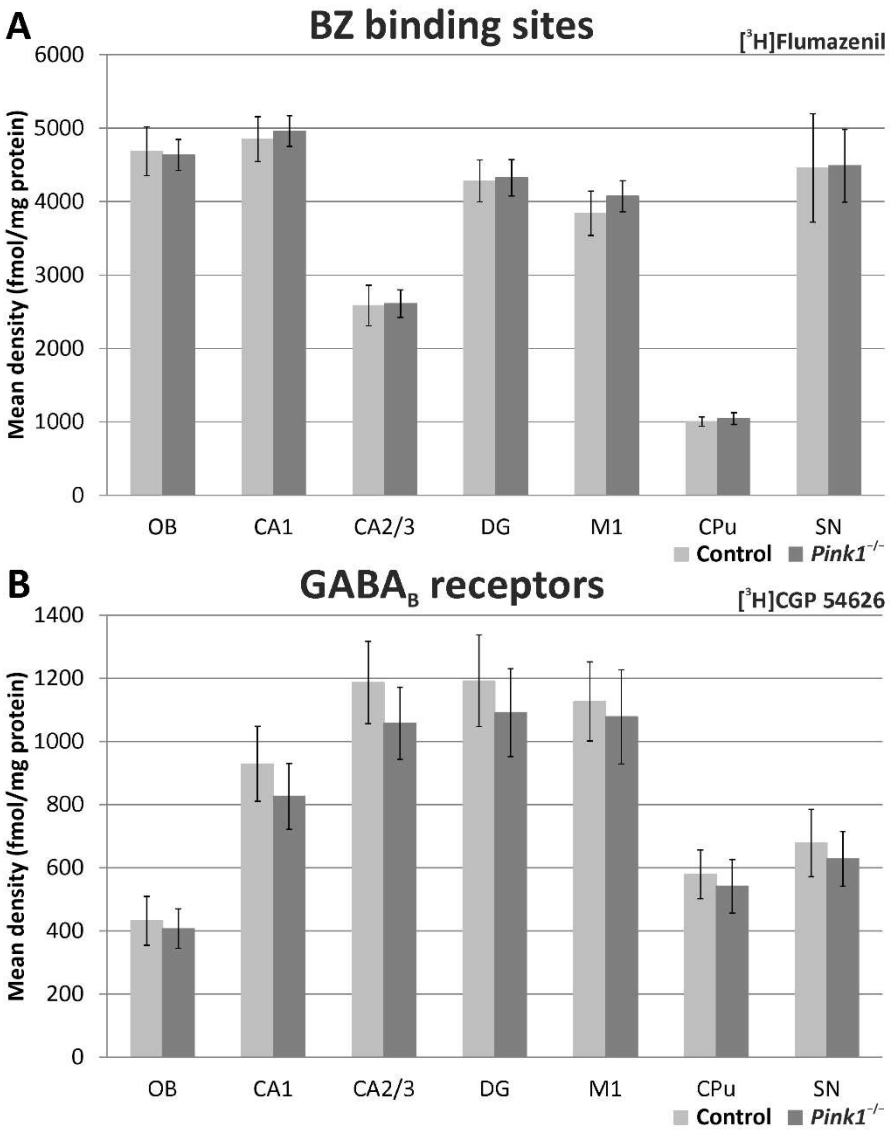

Fig. A5: Bar charts of mean GABAergic receptor densities (fmol/mg protein) including standard deviation in brain regions of the limbic (OB, hippocampal regions CA1, CA2/3, and DG) and motor systems (M1, CPu, SN) of control (light gray) and *Pink1*$^{-/-}$ mice (dark gray). **A**: Ligand: [^{3}H]Flumazenil; **B**: Ligand: [^{3}H]CGP 54626

Glutamate receptors

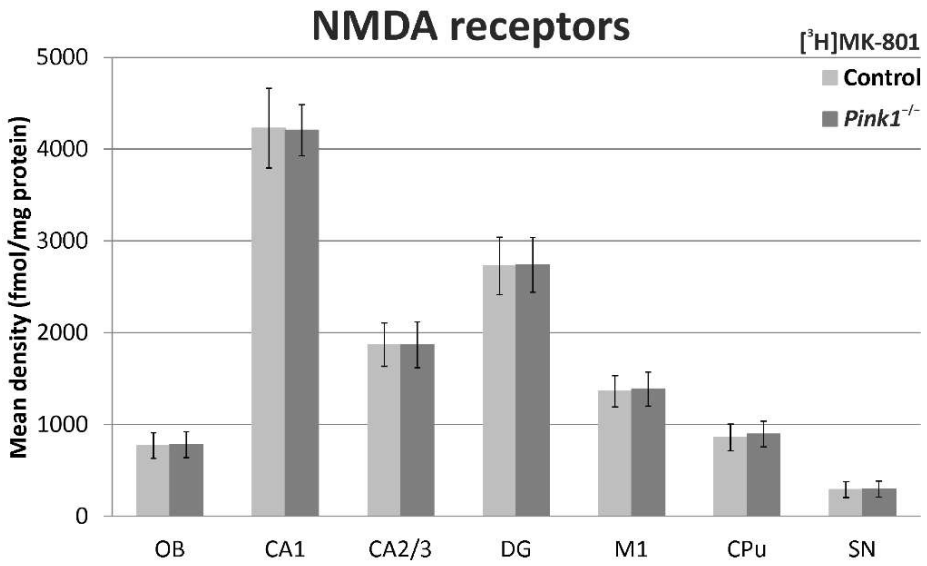

Fig. A6: Bar charts of mean NMDA receptor densities (fmol/mg protein) including standard deviation in brain regions of the limbic (OB, hippocampal regions CA1, CA2/3, and DG) and motor systems (M1, CPu, SN) of control (light gray) and *Pink1*$^{-/-}$ mice (dark gray). Ligand: [^{3}H]MK-801

Acetylcholine receptors

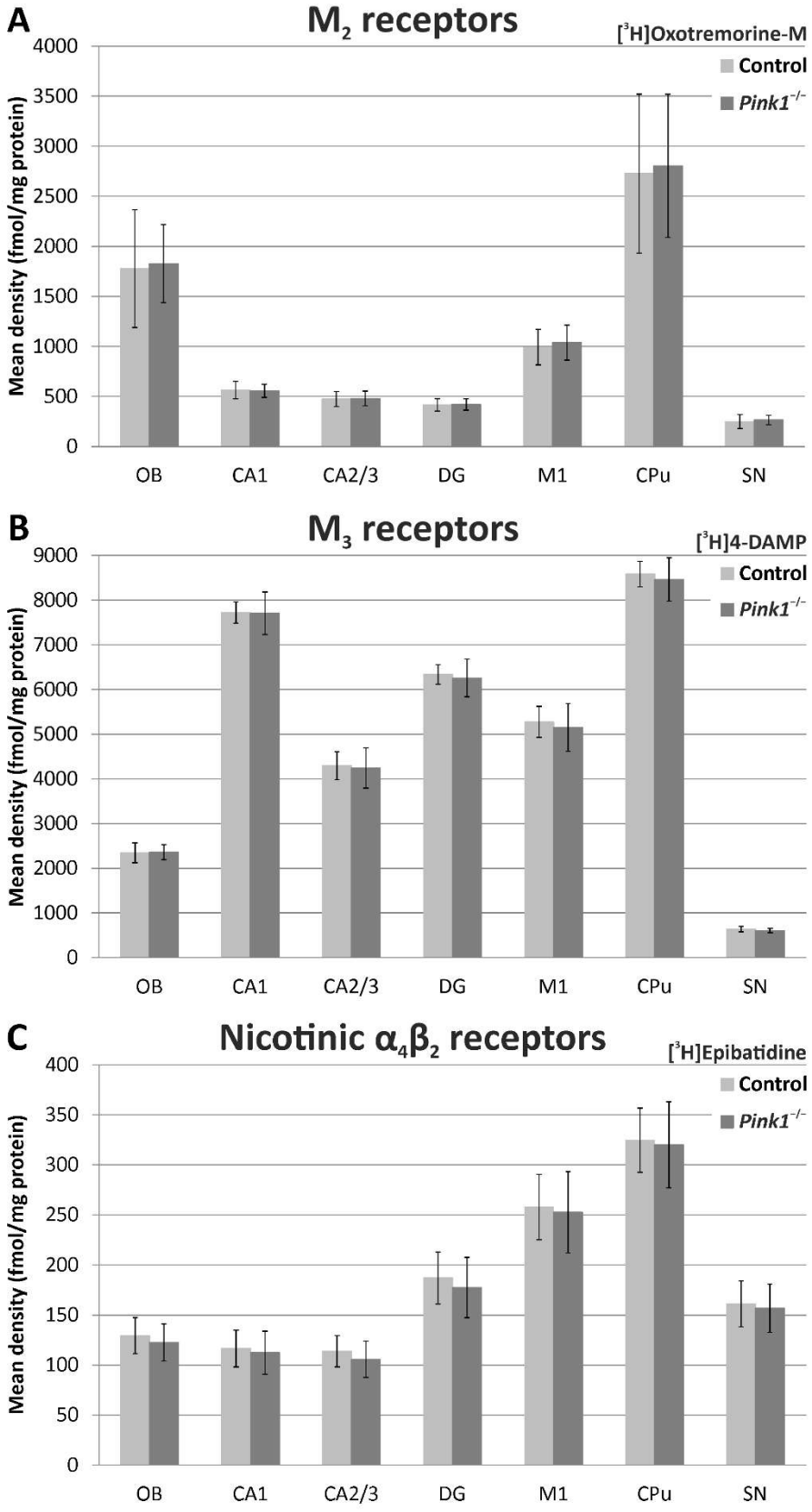

Fig. A7: Bar charts of mean cholinergic receptor densities (fmol/mg protein) including standard deviation in brain regions of the limbic (OB, hippocampal regions CA1, CA2/3, and DG) and motor systems (M1, CPu, SN) of control (light gray) and *Pink1*$^{-/-}$ mice (dark gray). **A**: Ligand: [^{3}H]Oxotremorine-M; **B:** Ligand: [^{3}H]4-DAMP; **C:** Ligand: [^{3}H]Epibatidine

Adrenaline receptors

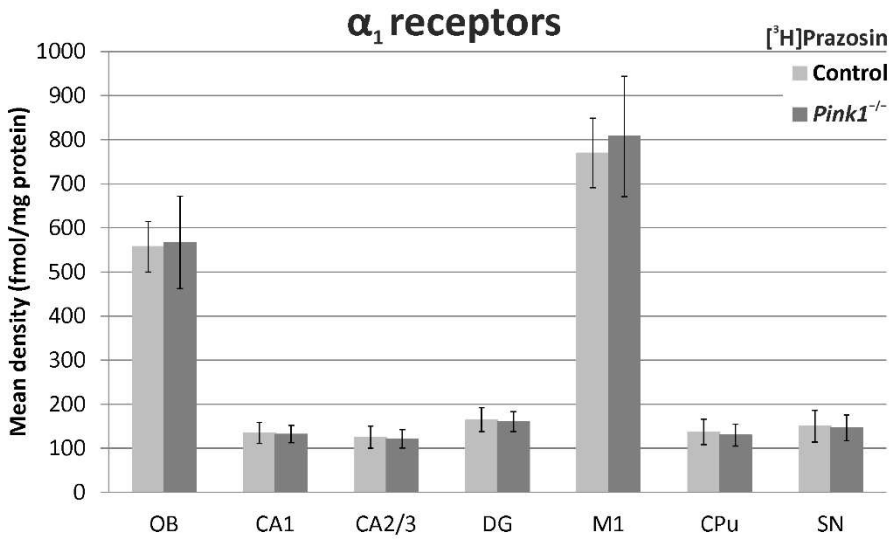

Fig. A8: Bar chart of mean α_1 receptor densities (fmol/mg protein) including standard deviation in brain regions of the limbic (OB, hippocampal regions CA1, CA2/3, and DG) and motor systems (M1, CPu, SN) of control (light gray) and *Pink1*$^{-/-}$ mice (dark gray). Ligand: [^{3}H]Prazosin

Dopamine receptors

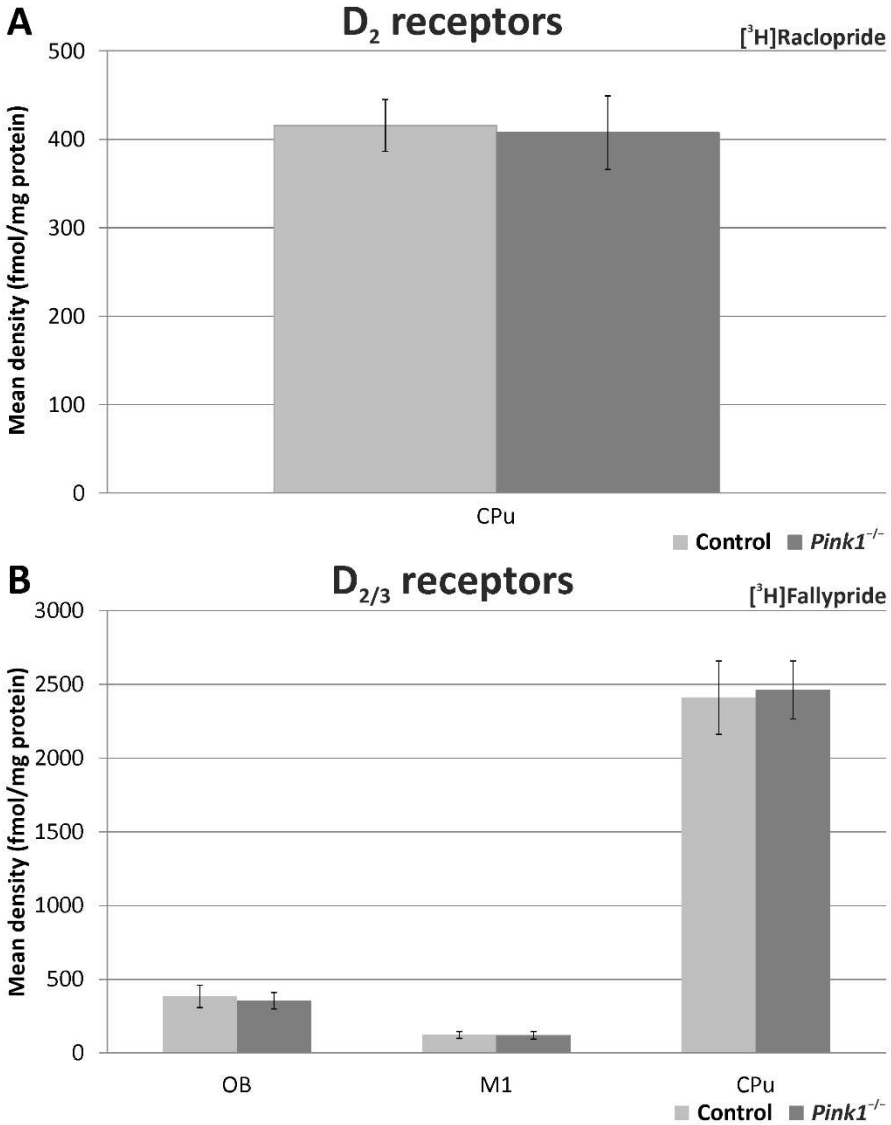

Fig. A9: Bar charts of mean dopaminergic receptor densities (fmol/mg protein) including standard deviation in brain areas OB, CPu, and SN of control (light gray) and *Pink1*$^{-/-}$ mice (dark gray). **A**: Ligand: [^{3}H]Raclopride; **B:** Ligand: [^{3}H]Fallypride

Serotonin receptors

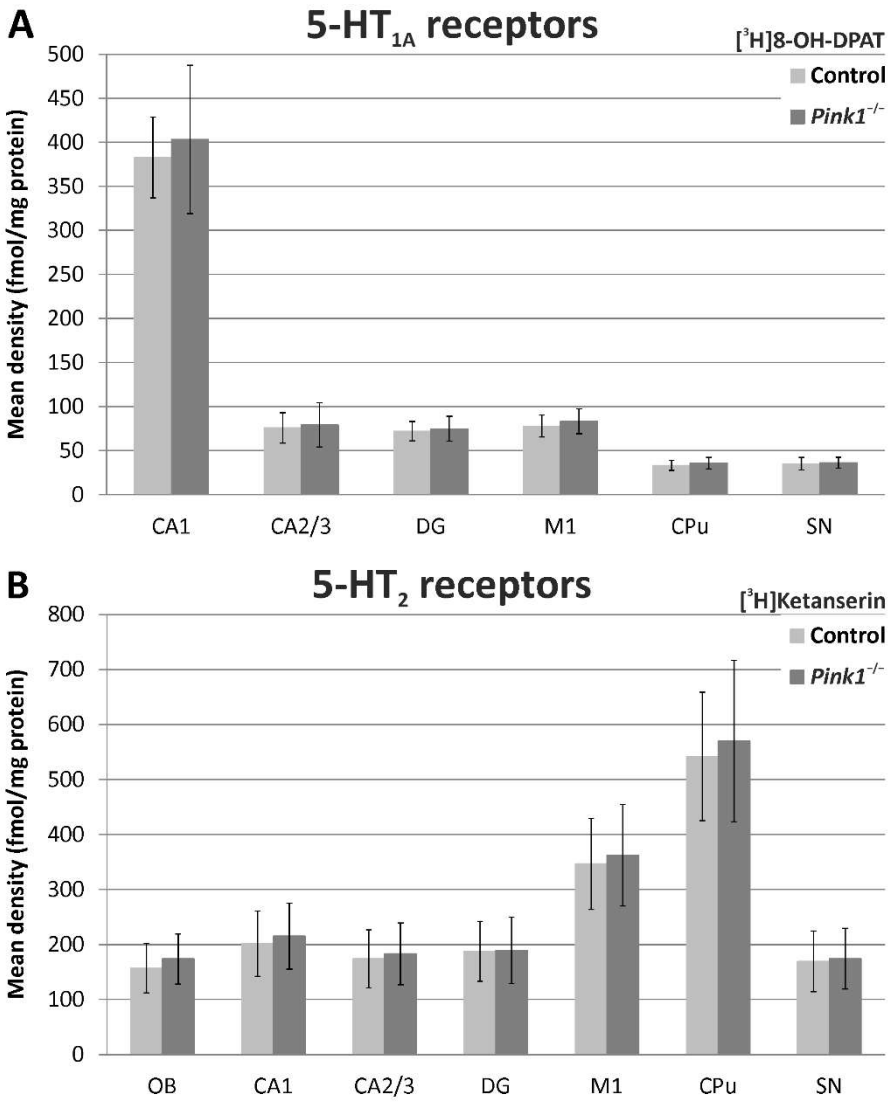

Fig. A10: Bar charts of mean serotonergic receptor densities (fmol/mg protein) including standard deviation in brain regions of the limbic (OB, hippocampal regions CA1, CA2/3, and DG) and motor systems (M1, CPu, SN) of control (light gray) and *Pink1*$^{-/-}$ mice (dark gray). **A**: Ligand: [^{3}H]8-OH-DPAT; **B:** Ligand: [^{3}H]Ketanserin

Adenosine receptors

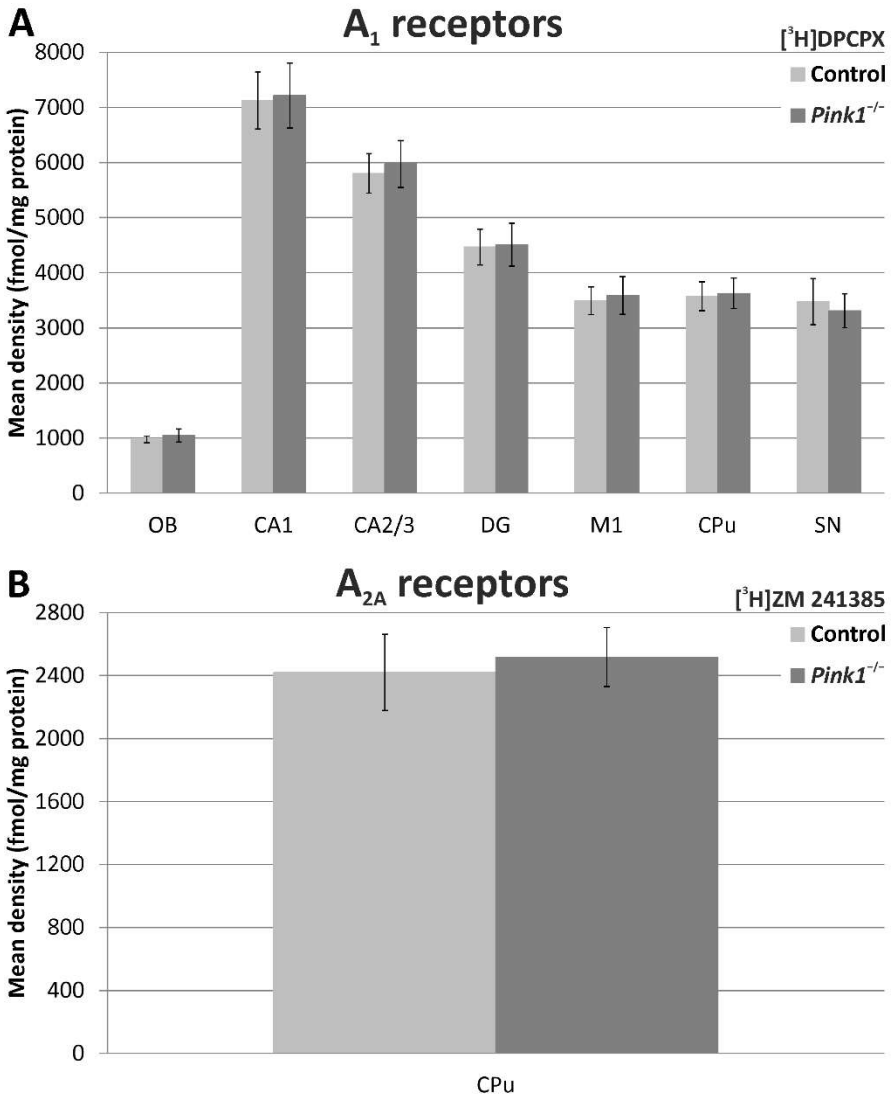

Fig. A11: Bar charts of mean adenosinergic receptor densities (fmol/mg protein) including standard deviation in brain regions of the limbic (OB, hippocampal regions CA1, CA2/3, and DG) and motor systems (M1, CPu, SN) of control (light gray) and *Pink1*$^{-/-}$ mice (dark gray). **A**: Ligand: [^{3}H]DPCPX; **B:** Ligand: [^{3}H]ZM 241385

Acknowledgments

In erster Linie möchte ich mich bei Frau Prof. Dr. Katrin Amunts bedanken, die mir die Aufnahme eines Vollzeitstudiums bei gleichzeitiger Vollzeitbeschäftigung ermöglicht und mich von Anfang an in jeder Hinsicht unterstützt hat. Weiterhin möchte ich mich bei ihr für die Bereitstellung des Themas bedanken.

A sincerely thank you to my UM supervisors Prof. Dr. Pilar Martinez-Martinez and MSc. Daan van Kruining. Thank you for your excellent supervision and for your helpful reflections and comments on my Master's thesis.

Auch bei meinen Institutsbetreuern Dr. Hans-Jürgen Bidmon und PD Dr. Nicola Palomero-Gallagher möchte ich mich ganz herzlich für die hervorragende Betreuung bedanken. Vielen Dank für eure Unterstützung, für die sehr hilfreichen Diskussionen zur Interpretation meiner Daten und dafür, dass ihr euch wirklich immer Zeit für mich genommen habt.

Ein herzliches Dankeschön an Dr. Florian Giesert und sein Team für die Bereitstellung und Präparation der untersuchten Mausgehirne.

I would also like to thank PD Dr. Nicola Palomero-Gallagher and Ling Zhao for their support with statistical analysis.

Ein besonderer Dank geht an meine lieben Kollegen Dr. Jennifer Cremer, Markus Cremer, Dominique Hilger, Anika Kuckertz, Patrick Nysten, Jessica Teske-Bausch, Beatrice Thevis, Steffen Werner und Vanessa Wölfer. Danke für euer stets offenes Ohr, eure motivierenden und aufbauenden Worte, das herzliche Klima am Arbeitsplatz und für stets humorvolle Gespräche bei Kaffee und Kuchen. Ich bin wirklich sehr dankbar so ein tolles Team an meiner Seite zu haben.

Ich bedanke mich ganz herzlich bei meinen Eltern und meiner Schwester für ihre liebevolle und nie nachlassende Unterstützung.

Ohne die Unterstützung, Geduld und vor allem Liebe von meinem Mann Jean-Baptiste, wäre weder das Masterstudium, noch diese Masterarbeit möglich gewesen. Danke, dass du mir wirklich immer den Rücken freihältst, immer für mich da bist und immer an mich glaubst.